Modeling Freshwater Inflows, Nutrient Dynamics and their Relationships to Algal Bloom in Nueces Bay, Texas

S M Shaheeq Mahmood Rony[1], Jianhong Ren[1], Edward Buskey[2], Tushar Sinha[1], and Thomas Lynn[1]

[1]Department of Environmental Engineering, Texas A&M University-Kingsville
Kingsville, TX 78363
[2]The University of Texas at Austin Marine Science Institute
750 Channel View Drive, Port Aransas, TX 78373

A Report Funded by A Texas Coastal Management Program Grant Approved by The Texas Land Commissioner Pursuant to National Oceanic and Atmospheric Administration Award No. NA18NOS4190153.

TABLE OF CONTENTS

Page

TABLE OF CONTENTS (contd.)

Page

PROJECT SUMMARY

The Gulf of Mexico coastal zone has suffered significant degradation of water quality and freshwater inputs due to coastal population and industrial growth, excess nutrient inputs, emerging environmental crises, and changes in regional climate and land use. Excessive nutrient loading is among the top environmental concerns since they can cause hypoxia and lead to excessive phytoplankton blooms. Harmful algal blooms (HABs) and eutrophication are increasing worldwide in frequencies in coastal waterbodies including estuaries and bays. Estuaries are vital components to ecosystems, and economics including tourism, fishing, hotels, industries, ports, and other developments which are dependent on the health of these estuaries. Freshwater inflows are essential to the function and productivity of these estuaries. Excessive nutrient discharges that come with these freshwater inflows can degrade the health and causing HABs in their receiving estuaries and bays. Eutrophication, hypoxia and/or HABs lead to negative impacts such as respiratory illnesses, fish kills and economic disruptions.

This project focused on the development of reliable and site-specific decision support tools that can be used by coastal resources managers for developing state-of-the-art freshwater inflow and nutrient criteria and by the scientific community for an enhanced quantitative understanding of the controlling factors for hypoxia or HAB occurrence. This report presents the modeling effort and data collection conducted for elucidating the controlling factors related to nutrient dynamics and algal blooms in Nueces Bay, Texas and the nutrient loading from Nueces River Basin (NRB) to the Nueces Bay (NB). Delft3D, an open source software that is widely used around the world, was employed to simulate hydrodynamics, nutrient dynamics and algal growth within Nueces Bay. The Soil and Water Assessment Tool (SWAT) was used to simulate freshwater inflows and nutrients loading from the NRB. Nitrogen, the limiting nutrient for coastal eutrophication, was focused. Delft3D Flow-Wave coupled model was used to simulate hydrodynamics and wave growth. The results from the coupled model were integrated in Delft3D WAQ to simulate phytoplankton growth. The models were calibrated and validated for freshwater inflows, water levels, total nitrogen (TN) and chlorophyll-a (algal biomass concentration).

The model successfully simulated HABs observed in October 2016, where chlorophyll-a > 20 µg/L. Simulation results indicated that wave growth in the NB was dominated by wind (> 1-foot wave-height). High inflow rates (80 m^3/s) increased hydrodynamics and mixing, which yielded in lower chlorophyll-a (< 20 µg/L) concentration, and vice versa. Nueces Bay exhibited

uniform hydrodynamics throughout the bay except at the confluences. Lower algal growth (< 10 µg/L) was observed at high winds (60 mph). During HABs, TN decreased while chlorophyll-a increased. Sensitivity analyses showed water temperature and maximum production rate parameter had the most impact (sensitivity > 50) on the algal growths. Hypothetical scenarios indicated that high TN (> 3.0 mg/L) and chlorophyll-a (> 100 µg/L) inflows from Nueces River significantly increased algal growth and can potentially induce blooms. The SWAT model was successfully used to simulate the freshwater inflow and total nitrogen loadings from the NRB. Model results show that total nitrogen transported through the Nueces River increases with total freshwater flow and vice versa (r^2 = 0.72). The models provided an analysis tool for better understanding the mechanisms and dynamics of algal growth/blooms, and this kind of tools can be an effective means to manage other similar estuaries or coastal waters.

PART I. MODELING NUTRIENT DYNAMICS AND ALGAL BLOOMS USING DELFT3D – FLOW, WAVE AND WAQ, IN NUECES BAY, TEXAS

1. INTRODUCTION

Eutrophication, which can result in harmful algal blooms, is becoming a common phenomenon around the globe increasing in frequencies and sizes, both locally and globally (Dodds et al., 2009; Smith, 2003). Eutrophication is the excessive growth of aquatic plants, including algae in the presence of excess nutrients. Although eutrophication is a common natural phenomenon, it can be accelerated by increasing nutrient discharges from anthropogenic activities (Khan and Ansari, 2005). Harmful algal 'blooms' or HABs can lead to a variety of problems posed to the environment and humans, such as toxins released in both water and air, difficulty in breathing, respiratory diseases, fish die offs, reduced tourism and bird kills. HABs can also increase turbidity of water bodies reducing the light penetration for other aquatic organisms. They are responsible in disrupting economic growth and degrade the water qualities of bays, lakes and coasts (Dodds et al., 2009; Ferreira et al., 2011; Khan and Ansari, 2005; NOAA, 2016; Roelke et al., 1997; Smayda, 1997; Zhang et al., 2020).

Understanding eutrophication and harmful algal blooms dynamics and the effects of climate change and anthropogenic activities on these ecological processes is becoming more and more vital for better management practices. Research conducted by Cloern et. al. (2001) in the coastal estuaries have led to the understanding that harmful algal blooms, hypoxia, degraded water quality and fish die-offs are related to nutrient loads to estuaries. Zhang et. al. (2020) studied the effects of microplastics loads and resuspension, linking to accelerated eutrophication and algal blooms. Studies conducted by Turner et. al. (2015) linked nutrients and chlorophyll-a measurements (an indicator for algal biomass) with seasonal trends for hypoxia and HABs. Multiple studies, using laboratory analysis, empirical solutions, statistical analysis and numerical methods, were prevalent in past years to correlate eutrophication to nutrient loads (Begin et al., 1988; Ferreira et al., 2011; Longley et al., 2019; Zhang et al., 2020).

Numerical modeling of the aquatic systems can help identify the root causes, processes, factors and can help predict the formation of, or evaluate the management options to mitigate harmful algal blooms (Jian et al., 2014). Numerical models have been developed and employed to analyze

and simulate environmental conditions for water bodies across the globe. Researchers have used numerical models to define hydrologic relationships, establish baselines for nutrients and define freshwater inflow requirements to maintain healthy ecosystems (Brock, 2001; Turner, 2014; Turner et al., 2015). Numerical modeling can integrate multiple processes in a single model and in different phases. It can be used to simulate 'worst-case' scenarios and to predict and forecast environmental disasters. Model sensitivity analysis can identify key parameters to which the model is most responsive to and can be translated to environmental situations for remediation or preventive measures. It can also be used as a guideline to legislate management practices and regulations (Brock, 2001; Felip and Catalan, 2000; Jian et al., 2014; Schoenbaechler and Guthrie, 2011; Turner et al., 2015; Xu et al., 2017).

A three-dimensional modeling study (Chen et al., 2019) conducted using Delft3D examined the impact of carbon dioxide (a greenhouse gas) and eutrophication in a drinking water reservoir. Anthropogenic activities have increased carbon dioxide concentration in the atmosphere which has simultaneously increased the chances of eutrophication in a nutrient rich environment (Chen et al., 2019). Vaz et al. (2019) developed a model using the Delft3D suite and studied different factors including water temperature, salinity, pH and chlorophyll–a concentration to relate to eutrophication of the coastal mesotidal lagoon, Ria de Aveiro. A numerical model using fuzzy cell automata techniques and limited observed data was developed and applied on Dutch coastal waters in predicting possible algal blooms (Chen and Mynett, 2006). A data-driven statistical model was developed by Shen et al. (2019) using long-term observed data and Least-Squares Support Vector Machine (LS-SVM) to simulate and predict algal blooms in relation to nutrient loads and environmental conditions, such as, solar radiation, temperature, dissolved oxygen and suspended solids.

In these previous studies, models were developed using process algorithms and statistical approaches (Chen and Mynett, 2006), data-driven statistical models (Shen et al., 2019), and Delft3D–Flow, Wave and WAQ (Alosairi and Alsulaiman, 2019; Chen et al., 2019; Mao et al., 2015; Vaz et al., 2019; Xu et al., 2017) to simulate hydrodynamics and water qualities including water levels, salinity, temperature, emerging contaminants, dissolved oxygen, etc. The performance of the models was evaluated and determined using criteria and objective functions set for each individual study. Delft3D models (Alosairi and Alsulaiman, 2019; Chen et al., 2019; Mao et al., 2015; Vaz et al., 2019; Xu et al., 2017) performed "well" for salinity and temperature

simulations for Qingcaosha Reservoirs (Xu et al., 2017), hypoxia simulation in Kuwait Bay (Alosairi and Alsulaiman, 2019), nitrate and phosphate (Chen and Mynett, 2006) and spatial and temporal distribution of nutrients and phytoplankton (Mao et al., 2015). The data-driven model developed by Shen et al. (2019) performed 'well' in simulating temperature dependency of algal blooms but the model failed to accurately compute the effects of nutrient reduction and nutrient limitation on algal growth. This is because the model used observed data for training and did not incorporate the growth processes or mechanisms of algal blooms. The algal concentration decreased with decreased nutrient concentrations and vice versa. Thus, this model is likely to simulate lower algal concentrations during algal blooms, when the nutrient concentrations are reduced due to nutrient uptake, instead of higher algal concentrations. The model showed satisfactory results in predicting algal concentration but is limited in its application because the model requires training data for its predictive capabilities (Shen et al., 2019). In general, Delft3D model studies (Alosairi and Alsulaiman, 2019; Chen et al., 2019; Mao et al., 2015; Vaz et al., 2019) showed the effect of hydrodynamics on algal growth, but none of the studies included the impacts of hydro-nutrient dynamics relating to mechanisms and biological factors underlying algal growth.

Delft3D models (Alosairi and Alsulaiman, 2019; Mao et al., 2015; Vaz et al., 2019) have been employed in predicting seasonal variations, hypoxia, water quality and hydrodynamics. Various processes are integrated with the modeling tool and thus the model provides a great flexibility to analyze the effect of each process in individual study and model applications (Alosairi and Alsulaiman, 2019; Mao et al., 2015; Vaz et al., 2019). However, Delft3D models failed to perform 'well' in the absence of consistent data and presented large discrepancies when data measurements with large uncertainties were used (Vaz et al., 2019). Delft3D is process sensitive, that is, all governing parameters must be evaluated for accurate results. For example, in the study of hypoxia in Kuwait Bay (Alosairi and Alsulaiman, 2019), algal mortality and respiration, which stress dissolved oxygen, were not considered (Alosairi and Alsulaiman, 2019; Mao et al., 2015, 2015; Xu et al., 2017). Furthermore, a calibrated model designed for a specific estuary would be difficult to implement and calibrate for another estuary due to different geographical location, bathymetry, population, temperature and nutrient inputs (Turner, 2014; Turner and Chislock, 2010).

Studies using Delft3D models conducted by Xu et. al (2017) showed that wind drag coefficient, astronomic forcing components and bottom roughness have been the key parameters

in simulating the wind stress on the free water surface that is responsible for intermixing, hydrodynamics and nutrient distributions (Xu et al., 2017). During a hypoxia and fish kill study of Kuwait Bay, the reaeration transfer coefficient, which is dependent on wind speed, water velocity and temperature, was found to be the key parameter in hypoxia modeling (Alosairi and Alsulaiman, 2019). Nutrient levels, limitation functions, nutrient kinetics, reaction rates, light attenuation coefficient and water temperature have been identified as the key parameters when considering algal growth, especially in deep waters where light penetration becomes limited and vertical temperature gradient is observed (Glé et al., 2008; Jian et al., 2014). The analyses of the parameters, that is, wind drag coefficient, bottom roughness, temperature, etc., have established that water qualities and HABs are affected by the inflows to, and hydrodynamics of, a waterbody (Alosairi and Alsulaiman, 2019; Xu et al., 2017).

The water quality, temperature and nutrient dynamics, in turn, impacts the algal dynamics of estuaries. Studies conducted by Vaz et al. (2019) pointed out that during winter the freshwater inflow from rivers with lower temperature and nutrient concentration and reduced solar radiations on estuaries could potentially reduce the phytoplankton growth and biomass of estuaries. The study also concluded that high inflow rates of around 50 m^3/s, having a constant nutrient concentration, can yield lower algal growth, even under favorable conditions due to a high magnitude of hydrodynamic activities. Studies conducted by Paudel et al. (2019) showed that inflow affects the dynamics of total suspended solid concentrations (TSS), nutrients and salinity regimes. The study also found that limited inflow resulted in the curtailing of inorganic nitrogen and TSS transport (Paudel et al., 2019). During algal blooms, nutrient concentrations decreased due to nutrient uptakes by algae (Vaz et al., 2019). At the same time, it has also been observed that nutrient concentrations were lower in the absence of algal blooms (Turner et al., 2015). The study accounted this phenomenon to be the result of fast denitrification. The denitrification rates can vary inconsistently both temporally and spatially (Turner et al., 2015). The nutrients tend to accumulate in the shallow areas of lagoons with lower hydrodynamic processes and thus can yield in higher algal biomass especially during spring and summer. The dissolved oxygen decreases during these periods which can lead to hypoxia with persisting algal formations, even with freshwater inflows to water bodies (Vaz et al., 2019).

Nueces Bay, the second largest bay of the Nueces Estuary, which is connected to the Nueces River, receives intermittent flow carrying nutrients, from Nueces River. This intermittent flow can

act as a pulsed nutrient input (Glé et al., 2008; Longley, 1994) to Nueces Bay. Pulsed nutrient input has shown to promote phytoplankton diversity and growth, which is vital to the health of the estuarine system over a short period of time (Yamamoto and Hatta, 2004). Nueces estuary is surrounded by large urban development and is expanding both in size and economy (Ritter and Montagna, 1999). Over the past decades, Nueces estuary has observed seasonal hypoxia, fish kills, respiratory illnesses and algal blooms (NOAA, 2016; TPWD, 2019a; Turner et al., 2015). Understanding the interplay among the freshwater inflow, nutrient dynamics and algal blooms can help prevent economic losses and environmental disasters, promote urban and economic growth, tourism, fishing, healthy aquatic system and healthy estuary.

Various studies have been conducted to characterize hydro-morpho-dynamics and water quality in assessing environmental pollution, groundwater-river exchange, suspended solids and nutrient concentrations (Murgulet et al., 2016; Paudel et al., 2019) for Nueces River and Nueces Bay; however, few studies exist on Nueces Bay (Turner et al., 2015) in relation to harmful algal blooms. Studies conducted by Paudel et al. (2019) established relation between nutrients with suspended solids (Paudel et al., 2019). In another study, Murgulet et al. (2016) quantified the impact of variable groundwater-surface water interactions due to anthropogenic activities, for example, multiple dams on water quality in the Nueces River and Nueces Estuary. Studies on the relationships between algal blooms, hydrodynamics, and nutrient dynamics of Nueces Bay to help understand the underlying factors affecting HABs have been very limited.

This study focused on evaluating the relationships between freshwater inflows, nutrients loading, and algal blooms in Nueces Bay. A Delft3D–Flow and Wave (hyrdro-morpho-dynamics) coupled model was used to simulate the hydrodynamics of the bay. The coupled model incorporated the effects of wind, wind-induced waves, currents, swell conditions and tides on the intermixing in the bay. Current and historic data were used to calibrate and validate the coupled Delft3D -Flow-Wave model. The hydrodynamic results were used as inputs to the Delft3D WAQ model to simulate nutrient distribution and algal formations, along with other parameters and processes such as water temperature, nutrient loading, salinity, nutrient limitation factors. The outputs of Delft3D WAQ were compared with the current and historical events for algal blooms. The integrated calibrated model can be used to predict and forecast the effects of climate changes or anthropogenic activities on nutrient dynamics and algal blooms. It can also be used to simulate and ‘foresee’ environmental disasters and provide baselines for establishing guidelines or

preventive or remedial measures and for proper management practices to coastal managers, municipalities, communities, and states. This study could also facilitate management practices for freshwater inflow and nutrients to maintain a healthy ecosystem.

2. STUDY AREA

Nueces River Basin is a large semi-arid watershed located in South Texas, which serves as the main source of freshwater inflows to Nueces Estuary and the Nueces Delta (Hill et al., 2011). Waters from the Nueces River are used in industries and urban developments as well as in agriculture by City of Corpus Christi and its adjacent regions (Anderson, 1960). The Nueces Estuary consists of a primary bay, the Corpus Christi Bay which opens to the Gulf of Mexico with a confining barrier island running at an offset and in parallel to the coastline (Figure I-1). Nueces Bay is a large shallow secondary bay having an average depth of about 2.40 m (Buskey, 1993).

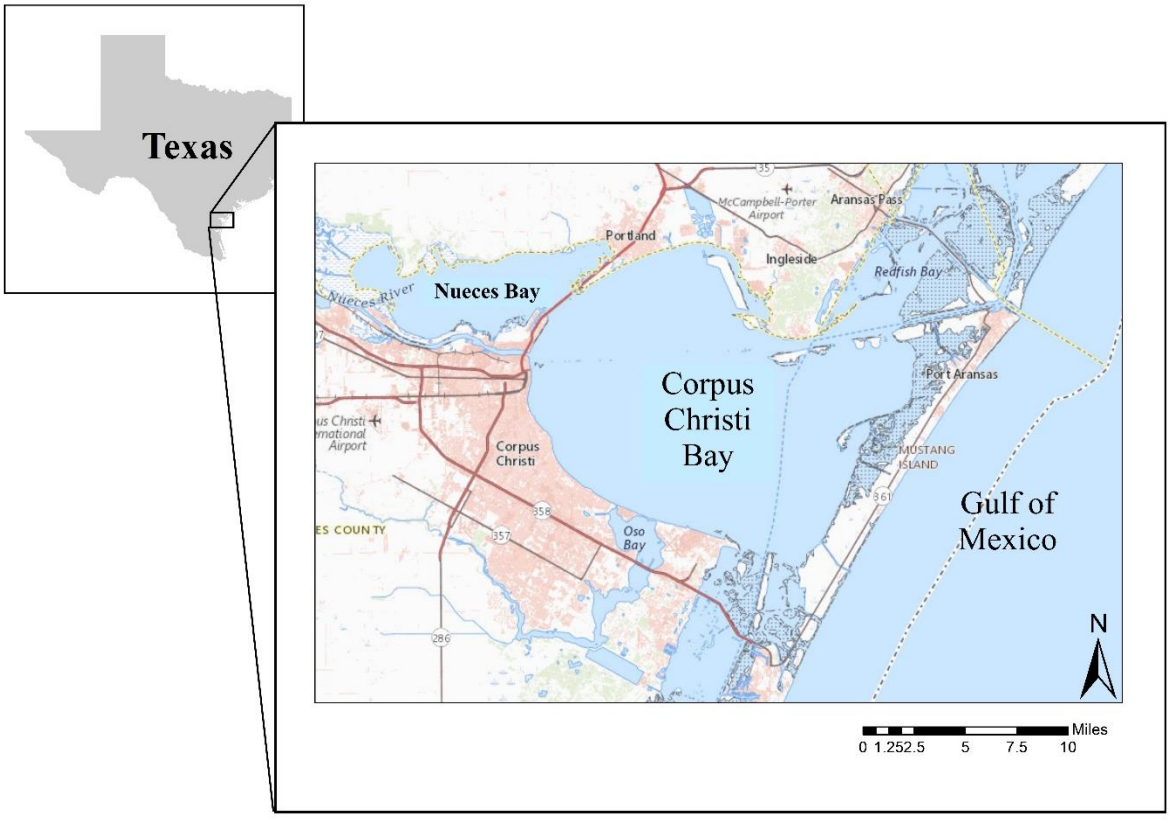

Figure I-1. Geographical location of Nueces Bay, Corpus Christi Bay along the Gulf of Mexico.

Nueces Bay, like other estuaries, requires freshwater inflows of varying degree to support its flora and fauna (Ritter, 2005). Over the years, there has been a reduced freshwater inflow into the

bay (Cunningham, 1999; Hill et al., 2011). Reduced freshwater inflow from the semi-arid Nueces River Basin (NRB) coupled with urban and industrial discharges carrying excess nutrients leads to an imbalanced ecosystem which can jeopardize the health of the aquatic system and environmental health of the Nueces Bay (Hill et al., 2011; Ritter and Montagna, 1999). With increased nutrient loadings and reduced flow, the Nueces Bay has experienced eutrophication and harmful algal blooms (red tides) over the past decades (TPWD, 2019a). Harmful algal blooms (HABs) are often referred to as 'red tide' but the HABs do not necessarily result only in red color. It can come in blue, blue-green, green or brown colors as well, depending on the type of dominant species (NOAA, 2016). The term 'harmful' refers to release of toxins by certain species of algae which is responsible for fish die-off, bird kills, respiratory illnesses and economic losses (Dodds et al., 2009; NOAA, 2016). The losses are not just limited to communities, they are also a national concern as it affects the economic health, health of people, fishing, tourism and jobs especially in the coastal communities (Brock, 2001; Buskey, 1998; Cunningham, 1999; Dodds et al., 2009; Hill et al., 2011).

Apart from the nutrient loadings from the Nueces River, the Nueces Bay also receives and/or exchanges materials due to tidal exchanges with Corpus Christi and adjacent bays, along the Gulf of Mexico (Brock, 2001). The adjacent bays of the Nueces Estuary contribute about 25-33 % of the net tidal entrainments and inflows. 8% of the total nitrogen is deposited through atmospheric deposition in the Nueces Estuary (Brock, 2001). The Nueces estuary has a restricted tidal mixing with the Corpus Christi Bay and the Gulf of Mexico due to a bottle neck resulting in microtidal amplitudes (Figure I-2). Despite these conditions, the main loss of nutrients is through tidal exchange of entrainments and denitrification, where the later accounts for almost 40% of nitrogen losses (Brock, 2001).

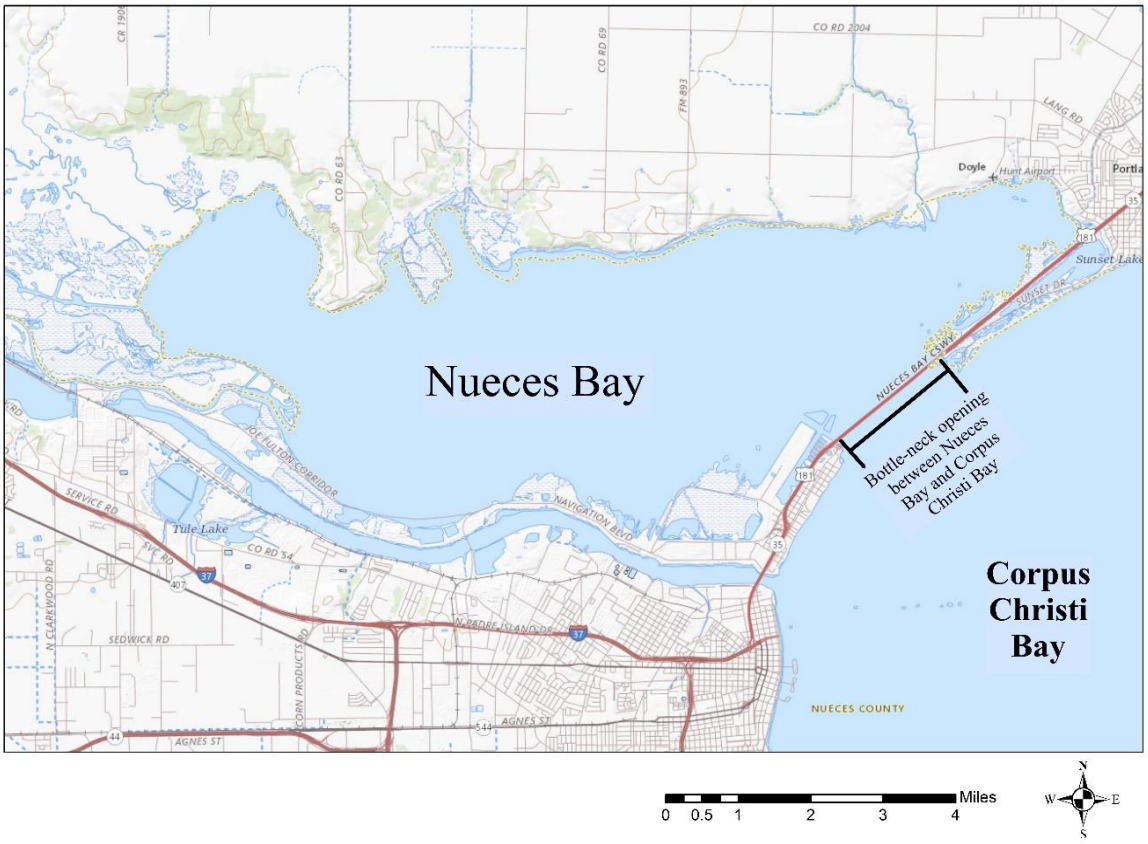

Figure I-2. Map of Nueces Bay and Corpus Christi Bay with a bottleneck opening connecting the two bays.

Nueces River Basin (NRB) covers approximately 16,600 square miles at an elevation of 730 m with the Nueces River travelling around 320 miles in the southeast direction before discharging into Nueces Bay (TPWD, 1974). Reservoirs and dams on the NRB were built to meet water demands with increasing population and developments, further decreasing the inflow to Nueces Bay and changing water quality into the bay (Cunningham, 1999). Since the 1980s, these impoundments in the watershed have reduced the flow to the coastal bay by more than 50%, changing the water quality and nutrient loads into the bay, coast and the Nueces Delta (Hill et al., 2011). Choke Canyon Reservoir and Lake Corpus Christi serve as the main water sources for over 600 thousand people stretching over seven counties (Cunningham, 1999). With increase in population and water demands, more water needs to be stored upstream of the river in the reservoirs. The major recharge to this semi-arid basin is thus through precipitation and rainfall.

Water demand is likely to increase with the development and regional growth coupled with climate changes and the amount of freshwater flowing through the Nueces River and into the Nueces Bay is challenged by these events (Anderson, 1960; Cunningham, 1999; Hill et al., 2011; Powell et al., 2002; TCEQ, 2014).

3. BACKGROUND

Freshwater inflows have positive impacts in terms of water circulation in estuaries, supplies of nutrients for the ecosystem, and sediment transport which contribute to the valuable production of coastal fisheries. It can also have negative impacts including toxic compound transport and diseases through bacteria (Powell et al., 2002). Prolonged hypersaline conditions of Nueces Bay from reduced freshwater inflow impact the vegetation cover, marine species diversity and richness and biological productivity (Hill et al., 2011). Hill et al. (2011) also showed that prevailing conditions have affected the productivity of shrimp and recreational faunal species. Mitigation efforts were undertaken for the Nueces Delta, through freshwater inflows from the Choke Canyon reservoir, but were soon challenged, due to the dilemma between meeting population water demands and restoring environmental health during droughts (Hill et al., 2011).

At the same time, the economic development, growth, and climate change contribute to the sources of the nutrients responsible for eutrophication (Kiedrzyńska et al., 2014; Novotny, 1994). The sources of the nutrients consist of two parts: point and non-point sources. Section 502 of the Clean Water Act has defined and classified the point and non-point sources of nutrient loads. Point sources for nutrient loads, includes runoff from various farms, mining operations, oil and gas fields, constructions, and domestic sewers. While non-point source, for example, includes agricultural land runoffs, leachates, unchanneled runoffs from urban areas, runoffs from abandoned and active mines and construction sites, atmospheric deposition and leachates from septic tanks and others (EPA, 2015; Kiedrzyńska et al., 2014).

One of the major sources of point and non-point nutrients is the runoff from the use and overuse of chemical fertilizers in agricultural and farm applications. According to studies conducted by Cao et al. (2018), to promote and achieve a better yield of crops, a large amount of anthropogenic fertilizers (N-fertilizers) have been used in the US since the latter half of 1900s. Poor use efficiency and management, rather than the use of the fertilizers, have been cited for the resulting environmental and ecological problems from this use of fertilizers. From 1940 to 2015,

the use of nitrogen (N) fertilizers increased from 0.2 g N m^{-2} yr^{-1} to 9.0 g N m^{-2} yr^{-1} (Cao et al., 2018). Increased application has increased the agricultural production and N fertilizer use efficiency about 25% and 30%, respectively. Since only about 50% of the N fertilizers are utilized by the crops, most of the unused N fertilizers are carried by the runoff into waterbodies including streams, rivers, and bays (Smil, 1999). Smil (1999) also revealed that N fertilizers applied are lost to the environment through denitrification, nitrification, volatilization, and leaching causing numerous environmental and ecological problems. As such, acidification of soil, biodiversity reduction, emission of greenhouse gases and eutrophication were the end results and are some of the examples of the problems encountered (Bowman et al., 2008; Brock, 2001; Smil, 1999).

In research conducted by Alexandratos and Bruinsma (2012), it was predicted that by 2050, to meet the demand of the growing population, the agricultural production would need to be doubled. This implies that the application of N fertilizer would increase leading to higher N loss and higher stress to the environment and ecology including excessive phytoplankton growth and eutrophication. Phytoplankton including algae are micro- and macroscopic plants without roots and branches, residing and growing in water across continents around the globe. They are the primary producers in the aquatic systems (Deltares, 2018c; Glé et al., 2008). They can live and grow, both in freshwater and in saltwater and contain about thirty-thousand known species. They can grow at different degrees of salinity, organic matter, temperatures and pH (O'Neil, 2011). With the versatility and adaptivity to different conditions for growth, phytoplankton require the macronutrients namely, nitrogen and phosphorous, to grow. When these macronutrients are available in excess, phytoplankton including algae can have excessive growth resulting in eutrophication leading to a variety of problems posed to the environment and society (NOAA, 2016; Roelke et al., 1997; Smayda, 1997).

Algal blooms are the significant increase of algae in the ecosystem, growing out of control, due to the excessive supply of nutrients. Although phytoplankton are the primary producers of an aquatic ecosystem, eutrophication being a natural phenomenon can be accelerated by anthropogenic nutrients and can be harmful to the environment and to humans. Harmful algal blooms produce toxins which are harmful to humans, shellfish, marine mammals and birds resulting in fish kills, respiratory diseases, hypoxia (deficiency of dissolved oxygen for marine plants and animals, especially, when DO < 3 mg O_2 /L at the bottom (Kristin, 2011)) and sometimes even death in fishes, plants, birds, animals and humans. Other types of non-harmful algae are

present in aquatic system but they assert a certain amount of demand for dissolved oxygen in water which can also lead to fatal results for marine aquatic system (NOAA, 2016; Roelke et al., 1997; Smayda, 1997). Equation 1 represents typical algal photosynthesis (Powley et al., 2017a):

$$16\ NO_3^- + HPO_4^{2-} + 16\ CO_2 + 122\ H_2O + 18\ H^+ + \left(\frac{\text{photon, or}}{\text{light}}\right) \rightarrow C_{106}H_{263}O_{110}N_{16}P + 138\ O_2 \quad (1)$$

Equation 1 shows that nitrogen (nitrate as N) and phosphorous (hypophosphate as P) are the macronutrients required for the algal growth. Although both nitrogen and phosphorous are essential nutrients, they are usually not limiting at the same time. Study of Turner (2014) showed that in freshwater systems, phosphorous is normally the limiting nutrient and in saline or coastal areas, nitrogen is normally the limiting nutrient for algal growth (Turner, 2014). In the event of deficient inorganic carbon in the water bodies during eutrophication, the required CO_2 is drawn from the atmosphere which is also responsible for the increase in pH during day time (Schindler, 1974; Turner and Chislock, 2010). With excessive growth, the turbidity of the water increases, reducing the transparency and light availability for other aquatic plants. Other marine plants, vegetation and fishes die due to deficiency of light, inorganic carbon, and hypoxia (Chai et al., 2020; EPA, 2000; Fondriest, 2014).

Decomposition of dead marine plants, vegetation and fishes further increases the oxygen demand in the water. The toxins that are produced by HABs and hypoxia result in adverse effects to aquatic systems, plants and birds (Ferreira et al., 2011). The overall effect is the increased cost of water treatment for potable water, economic losses and human and environmental health hazards (Kristin, 2011). Studies conducted by Dodds et al. (2009) found that in the past decade, the US had encountered a loss of about 2 billion US dollars to eutrophication. In a report published by NOAA (NOAA, 2016), Texas alone has suffered a loss of about $10 million in oyster landings from a red tide in 2011, while around 500,000 people in Ohio did not have access to clean drinking water as HABs were present near the treatment plant in Lake Erie in 2014. In Washington state, closure for razor clam recreational harvesting due to algal blooms has resulted in an estimated loss of $40 million in 2015 (Dodds et al., 2009; NOAA, 2016).

4. LITERATURE REVIEW

Algal blooms are spreading globally from ongoing climate changes and anthropogenic activities causing excessive nutrient loads to lakes, estuaries, and coasts (Griffith and Gobler, 2019; Raven et al., 2020). To predict and forecast these algal blooms, numerical models can act as

a vital tool for management practices, locally and globally (Janssen et al., 2019). Literature review of previous research on hydrodynamics, water quality, and modeling have been conducted and briefed below.

4.1 Nutrients dynamics and algal blooms in coastal bays and knowledge gaps

Algal blooms and their relations to different environmental factors have been studied around the globe by numerous researchers. Studies by Bricker et al. (1999) showed that majority of the studied estuaries exhibited high eutrophic conditions stemming from anthropogenic nutrient inputs. The elevated nutrient concentrations can spur algal blooms. During phytoplankton blooms, Assmy et al. (2019) found that diatoms are generally the dominating species in phytoplankton community. Kumar et al. (2018) reported that high silicon flux and total nitrogen, and low sea-surface temperatures of water bodies played a prominent role in inducing harmful algal blooms in southeastern coastal waters of the Arabian Sea. Apart from nutrients and hydrodynamics, carbon content can also contribute to the flora-fauna of algal dynamics (Raven et al., 2020). Global warming and increase in carbon dioxide levels in the atmosphere has shifted the equilibrium in the carbon cycle and participated in the increase of dissolved carbon contents in water bodies and estuaries (Raven et al., 2020). Atmospheric transport and deposition of nutrients, through dusts, prior to algal blooms had been observed in the coastal water of east China (Tian et al., 2020). Algal blooms are also responsible for the reduction of resources-use efficiency for other plankton communities (Chai et al., 2020). Although nutrient dynamics, anthropogenic activities and climate change play important role in inducing algal blooms, biotic factors for each species of phytoplankton and/or specific abiotic factors of individual estuary also take part in algal dynamics (Bricker et al., 1999; Chai et al., 2020; Kumar et al., 2018; Raven et al., 2020; Tian et al., 2020).

Studies conducted by Kumar et al. (2018) showed the seasonal variation of the nutrient fluxes and their correlation with the phytoplankton growth and HABs in Arabian Sea. Data for dissolved oxygen, chlorophyll-a, salinity, ammonia, nitrite, nitrate, phosphate, and silicate were collected and analyzed. Statistical analyses were performed to establish relationship between phytoplankton growth and water qualities using multivariate regression analysis. The study found that diatoms dominated the phytoplankton community, and the HABs were induced primarily due to total nitrogen. No fish kill events were observed, which might be due to the hydrodynamic mixing and/or tidal effects and runoffs. The study concluded that high total nitrogen was the predominant

HABs driver. The study also concluded that during high monsoon, there would be greater runoffs and greater amount of nutrients would be carried with it, which in turn would induce a greater amount of HABs (Kumar et al., 2018). The studies conducted by Kumar et al. (2018) and Wang et al. (2020) used statistical tools to examine the correlation between studied factors and HABs but did not evaluate HABs in terms of process mechanisms and underlying factors controlling those mechanisms.

A study conducted by Vybernaite-Lubiene et al. (2017) used statistical and laboratory data to establish annual budget for nutrient and understand the effect of hydrologic loading rates on algal blooms and nutrient transformations of a hyper-eutrophic Curonian Lagoon. The study also focused on the mass balance and nutrient retention during algal blooms in determining whether estuaries serve as a nutrient sink or source during algal blooms. The study showed that changes in nutrient loadings influenced phytoplankton composition and algal blooms which in turn changed the transformation of nutrients in the estuary. The study focused on mass balances of nutrients using nutrient cycles and the corresponding chemical transformations, but the relationship between the species of nutrient during retentions, nutrient transformations and biological processes and their influence on algal growth were not evaluated. Also, the study did not address the nutrient dynamics relating to algal growth and the limiting factors and nutrients responsible for algal blooms (Vybernaite-Lubiene et al., 2017).

4.2 Modeling efforts conducted, findings and knowledge gaps

Vaz et al. (2019) used Delft3D Flexible Mesh Suite (D-Flow and D-WAQ) to assess spatiotemporal evolution of chlorophyll a, nutrients, water temperature, salinity, and pH in the coastal waters of Portugal. D-Flow was used to simulate three-dimensional hydrodynamics of the waterbody and D-WAQ was used to simulate for water quality and ecological conditions in the same computational grid. The study also evaluated light availability and nutrient limitation factors in relation to phytoplankton growth. The study found seasonal variations of algal biomass during blooms occurring in spring and summer, while algal concentrations decreased from late summer to winter. The study concluded that algal blooms were principally governed by temperature and nutrient availability, which in turn were strongly influenced by tidal mixing and hydrodynamics. It was observed that, during blooms, the nutrient concentrations were high during low algal concentrations and vice versa. The study found the geomorphological characteristic of the water

body also played an important role in water quality and ecology simulations. The study focused on abiotic factors, that is, water temperature, salinity, pH, and light availability to simulate algal blooms but the biotic factors, for example, nutrient limitation, light limitation, and kinetics, were not evaluated for algal growth mechanisms (Vaz et al., 2019).

A data-driven model was developed for James River estuary using Least Square Support Vector Machine (LS-SVM) and Empirical Orthogonal Function (EOF) model (Shen et al., 2019), to predict algal blooms and nutrient dynamics using consistent and continuous observed data. The study showed that zones with high hydrodynamic processes, which induced high mixing, had a lower algal concentration. The hydrodynamics and distribution of nutrients were similar for observation stations with similar geomorphological characteristics. Larger segments of the water bodies with higher retention time were more susceptible to algal growth than segments with lower retention times. The model was able to predict algal blooms with 'training data' which did not include other abiotic and biotic factors controlling algal blooms, for example, competition of light availability and nutrients, which potentially resulted in discrepancies in the model for algal blooms prediction. Lower data frequency and resolution were also considered to be the potential cause for the discrepancies. The model did not recognize other controlling factors, such as biotic and abiotic factors, but is capable of simulating interannual blooms responding to nutrient loading changes. For predictive skills, the model required training data, which might limit hydrodynamics and water quality studies for many areas where data availability is limited (Shen et al., 2019).

Jian et al. (2014) used Euler-Lagrange Circulation (ELCIRC) model with unstructured mesh to simulate interactions of hydrodynamic conditions, nutrients, temperature, dissolved oxygen, light intensity, and phytoplankton on Xiangxi river (XXR). The study conducted nutrient analyses based on statistical results and the model showed discrepancies in accurately determining the nutrient dynamics, water quality (focusing on pH, phytoplankton, temperature. and dissolved oxygen) and nutrient mass transport in XXR. The model results showed a lower simulation efficiency when compared against a structured grid mesh model. To accurately evaluate the effect of hydrodynamics and algal blooms, further refinements of the model were cited but was not included in the study. The model did not include the biotic factors and driving mechanism of algal growth, which potentially led to the discrepancies in simulated water quality data when compared with observed data (Jian et al., 2014).

Chen and Mynett (2006) used fuzzy cellular automata approach to predict algal blooms on coastal waters based on the hydrodynamics and nutrient dynamics. The study used limited observed data combined with empirical knowledge on algal blooms to predict algal blooms. Detailed biological processes and mechanisms were circumvented; thus, many parameters involving algal growth mechanism and processes were not evaluated. The study showed that nitrate and phosphate concentrations were much higher in winter, during low algal concentrations, than in late spring and early summer when the algal concentrations were high. The study also showed that nutrient concentrations in estuaries were higher than in coastal waters and thus estuaries had a higher algal blooms potential than coastal waters. The complex algal growth mechanisms were not considered in the model (Chen and Mynett, 2006).

4.3 Current available models and their advantages/disadvantages

The data-driven model developed by Shen et al. (2019) used the least-square support vector machine (LS-SVM) and empirical orthogonal function (EOF). The EOF used in this data-driven model reduced the data dimensions thus simplified the model. The EOF performs this by transforming variables of the model into empirical functions and fitting them on all observed stations. The EOF model was also used to separate the temporal and spatial variations for the principle component, that is, chlorophyll -a. The LS-SVM is a powerful learning machine used in time-varying simulations. The LS-SVM and temporal vectors of EOF were coupled to generate one single model for all observation stations and 'fitting' it with the observed data. The single model used flow, total suspended solids, total nitrogen, total phosphorous and chlorophyll–a as independent variables for simulations (Shen et al., 2019). Since the model does not compute processes, rather uses data for its simulations and predictions, the model thus requires training data which might limit the model application in many areas due to the lack of consistent data.

The statistical analysis performed by Vybernaite-Lubiene et al. (2017) was to establish annual budget for nutrient and to understand the effect of hydrologic loading rates on algal blooms and nutrient transformations. The study used mass balances to quantify the water body as source/sink for phytoplankton during algal blooms. The model attributed algal growth to the nutrient concentration in the waterbody without considering any nutrient transformation or algal growth mechanisms. This aided in the advantage that in-depth processes were not considered, and algal blooms were only correlated to the nutrient concentrations. At the same time, it posed the

disadvantage of not understanding what processes affected the algal growth and whether the nutrient concentration as the only parameter that was factored in the algal growth was enough. This also made it difficult to ascertain which nutrient components or which key factors played the vital role(s) during algal blooms (Vybernaite-Lubiene et al., 2017).

The Euler-Lagrange Circulation (ELCIRC) model mentioned above allows user to incorporate complex boundary conditions (Jian et. al. 2014). The model is principally used in three dimensional baroclinic (fluid density depending on temperature and pressure) circulation in oceans and river using algorithms to address physical processes and forcing in oceans and rivers. The ELCIRC model effectively simulates the baroclinic circulations from river to ocean scales and does not require high resolution grid for its simulations. The model integrated separate algorithms for hydrodynamics, tidal forces, and water quality constituents, that is, suspended solids, dissolved oxygen, and chlorophyll a. To accurately evaluate the effect of hydrodynamics and algal blooms, need for further refinements of the model was cited by Jian et. al. (2014). Refinements to study the effects of hydrodynamics and HAB would potentially require inclusion of separate algorithms for complex mechanisms of water quality in the model (Jian et al., 2014).

The fuzzy cellular automata model developed by Chen and Mynett (2006) circumvented complex mechanism calculations for algal blooms and performed simulations using limited observed data and empirical formula. The model thus did not require the calibration and optimization of biotic factors affecting algal blooms. This presents an advantage and a disadvantage. The model does not require large number of parameters to be evaluated/calibrated, at the same time, the model would not evaluate which process parameter(s) is/are responsible in HABs (Chen and Mynett, 2006).

SPAtially Referenced Regressions of Water Quality (SPARROW) (Rebich et al., 2011) model uses process-based hybrid statistical approach to estimate nutrient loads. The nutrient load estimation relates to different upstream sources and landscape characteristics that influence stream loss and nutrient transport. It estimates the nutrient load by considering landscape characteristics, that is, surface and groundwater flow, surface and groundwater velocity, and slope of landscape as independent variable for the river. The model used least squares regression analysis for calibration and validation. The model's capacity is limited in estimating nutrient loads for estuaries and bays and is restricted to reaches only.

The models mentioned above (Chen and Mynett, 2006; Jian et al., 2014; Rebich et al., 2011; Shen et al., 2019) have been implemented to budget for freshwater inflows to maintain a healthy estuary, provide baselines to avoid nutrient pollution and environmental disasters, and establish relationships between nutrient loads and algal blooms. But there is, still, an absence in studying the relationships of the nutrient dynamics with biotic and abiotic factors causing the algal blooms, which was the primary focus of this research.

D-Flow and D-Water Quality modules are parts of the Delft3D modeling tool that have been used to simulate hydrodynamics and water quality, respectively (Alosairi and Alsulaiman, 2019; Bastidas et al., 2015; Chen and Mynett, 2006; Luijendijk, 2001; Rahman and Venugopal, 2017; Roelvink and Banning, 1995; Vaz et al., 2019; Xu et al., 2017). The two modules, D-Flow and D-WAQ, can be integrated into a single model where each module can communicate the results to act as a single model. D-Flow can be used to simulate three-dimensional hydrodynamics of the waterbody and D-WAQ can be used to simulate the water quality and ecological conditions in the same computational grid. D-WAQ model uses Process Library Configuration Tool (PLTC) to simulate water quality for different functional groups including dissolved oxygen, particulate inorganic matter, organics matter, algae, bacterial pollutants, trace metals, vegetation, and higher trophic level. Each functional group includes biotic and abiotic processes in its simulations. D-Flow and D-WAQ are also part of the latest developed Delft3D Flexible Mesh Suite (Delft3D FM). Delft3D–Flow, Wave and WAQ simulate for structured computational grids, whereas the latest version, Delft3D Flexible Mesh Suite, can compute for unstructured flexible mesh.

Vaz et al. (2019) studied the algal growth in relation to water quality and ecological conditions, along the coastal waters of Portugal. Xu et. al. (2017) used Delft3D Flow and WAQ to assess emerging contaminants, atrazine and bisphenol A (BPA), of a reservoir which was responsible for around 50% of Shanghai's water supply. A model employed for Kuwait Bay for hydrodynamics and water quality modeling used Delft3D to simulate dissolved oxygen (DO) for understanding the fish kill events in the bay (Alosairi and Alsulaiman, 2019).

As mentioned above, Delft3D uses structured grid system and Delft3D FM can compute unstructured meshed grids. Each module provides the versatility in using coarse and fine grid systems and uses bilinear interpolation in discretization for grid solutions both in temporal and spatial dimensions. The versatility in computing large number of simultaneous processes requires calibration of large number of parameters. Delft3D requires high resolution temporal input data

for accurate computation, that it, it is data intensive. In case of multiple domain systems, the boundary conditions for smaller domain can be derived from a larger domain which needs to be nested. In such case, multiple domains can be nested together, but with restricted modeling capacities (Alosairi and Alsulaiman, 2019; Deltare, 2018; Deltares, 2018; Vaz et al., 2019; Xu et al., 2017).

Understanding the governing factors, processes and mechanisms in hydrodynamics and algal blooms is the key in modeling, management practices and remediation of blooms. Studies conducted by Garcia et al. (2015), Vaz et al. (2019), and Xu et al. (2017) show that hydrodynamics played an important role in tracer and nutrient dynamics in coastal estuaries and bays. Manning's roughness and bed friction were identified as key parameters in energy transfers in hydrodynamics and wave mixing. Vaz et al. (2019) concluded that temperature and nutrient limitations governed the algal growth kinetics in coastal lagoon of Portugal. Studies using fuzzy logic model (Chen and Mynett, 2006) found that first-order kinetic denitrification and nitrification rates, adsorption rates and mineralization rates in sediments were the most relevant in Dutch coastal waters. Jian et. al. (2014) showed that nutrient availability and nutrient limitation were the most relevant factor in algal blooms (Jian et al., 2014). Alosairi and Alsulaiman (2019) concluded that hypoxia resulted from complex interactions between hydrodynamics, basin flushing time and nutrient loadings, and that further studies were required to understand the effects of individual components in the complex interactions between hydrodynamics and nutrient loading.

4.4 Nutrient dynamics and algal blooms studies in the coastal bend

Studies of the Texas Coastal Bend systems, including the Corpus Christi and Nueces Bay, suggested that freshwater inflows and hypersaline conditions have been the key factors in inducing algal blooms (Buskey, 1998; Wetz et al., 2017). Turner et al. (2015) established baseline nutrient dynamics with HABs and hypoxia formation using sampled data for inorganic nutrients, chlorophyll-a (an indicator for algae) and dissolved oxygen (DO) in Corpus Christi Bay, Texas. The study collected samples and performed statistical analysis for a dry year (October 2011 to September 2012). Phosphate had a mean concentration of 1.07 μmol/L with a maximum of 7.08 and minimum of 0.00 μmol/L. Nitrate and nitrite had a mean of 0.89 μmol/L with maximum and minimum concentrations of 7.08 and 0.00 μmol/L, respectively. Ammonia had a mean of 1.07 μmol/L with a maximum of 3.23 μmol/L and minimum of 0.00 μmol/L. Chlorophyll-a had a mean

of 5.35 µg/L concentration with a maximum of 18.11 and a minimum of 0.32 µg/L. Studies relating to salinity and algal blooms in Baffin Bay, Texas, showed that algal blooms were not restricted only by hyper-salinity, as was previously perceived. The temporal-spatial distributions of the algal blooms were also affected by precipitation and rainfall, and were not limited only to salinity (Cira and Wetz, 2019). Another study showed that high nitrogen concentrations in Baffin Bay linked to its susceptibility to algal blooms (Wetz et al., 2017).

These previous studies (Cira and Wetz, 2019; Wetz et al., 2017) related algal blooms with hypersalinity, freshwater inflows, nutrient dynamics and precipitation but identifying the root causes underlying the blooms has seldomly been conducted. Since a variety of physical, biological, and chemical factors can affect the algal growth, further studies to pinpoint the root causes in the mechanisms of algal blooms are required as indicated by Cira et al. (2019)**.**

5. MODEL THEORY

Delft3D is a two- and three-dimensional multi-disciplinary simulation tool developed by Deltares and is in use for over 30 years (Roelvink and Banning, 1995). It has several modules that can be used to simulate flow, wave, sediment transport, water quality, ecology and morphological developments (Deltare, 2018). Delft3D-Flow, Delft3D-Wave and Delft3D-WAQ modules were used to simulate hydrodynamics and water quality, simultaneously communicating between each module in this study. Delft3D–Flow and Wave were used for two- and three-dimensional hydro-morpho-dynamic simulations. While Delft3D-WAQ was used to simulate nutrient dynamics and algal growth. A brief theoretical model background is presented below.

5.1 Delft3D–Flow

Delft3D-Flow module simulates the hydrodynamics and transport incorporating non-steady flow and transport phenomenon resulting from tidal and meteorological forcing on a fitted grid. Delft3D Flow includes features such as tidal forcing, density driven flows for thermal discharges and Earth's rotation effect (i.e., Coriollis force). The hydrodynamic conditions obtained from Delft3D Flow, for example, water elevations, densities, velocities, salinity, vertical eddy viscosity and diffusivity, can be communicated and interacted with other modules like Delft3D Wave and WAQ (Deltare, 2018).

Delft3D-Flow modeling system numerically solves for unsteady flow equations in two-dimension for depth-averaged grids, and in three dimensions in all other cases. The equations of motion (in the horizontal directions), the continuity equation and transport equations are used. Further details can be found in the Delft3D- Flow manual (Deltare, 2018). In the Flow model, tidal forces and wind forces were accounted, at the open boundaries (water-water boundary). The differential equations solved by Delft3D-Flow, that is, Navier-Stokes equation, is given by Equations 2-4 (Broomans, 2003):

$$\frac{\partial u}{\partial t}+u\frac{\partial u}{\partial x}+v\frac{\partial u}{\partial y}+w\frac{\partial u}{\partial z}=-\frac{1}{\rho_0}\frac{\partial p}{\partial x}+\nu\Delta u-f_x \quad (2)$$

$$\frac{\partial v}{\partial t}+u\frac{\partial v}{\partial x}+v\frac{\partial v}{\partial y}+w\frac{\partial v}{\partial z}=-\frac{1}{\rho_0}\frac{\partial p}{\partial y}+\nu\Delta v-f_y \quad (3)$$

$$\frac{\partial w}{\partial t}+u\frac{\partial w}{\partial x}+v\frac{\partial w}{\partial y}+w\frac{\partial w}{\partial z}=-\frac{1}{\rho_0}\frac{\partial p}{\partial z}+\nu\Delta w-f_z-\frac{\rho}{\rho_0}g \quad (4)$$

where u, v and w represents the velocity components in the x-, y- and z directions, respectively, ρ and ρ_0 are the density and reference density, respectively, p is pressure, g is gravitational acceleration, ν is the the kinematic viscosity, f_x, f_y and f_z are the Coriolis force per unit mass components in the x, y and z directions, respectively and t is time. The Coriolis force components are defined by $(f_x, f_y \text{ and } f_z)^T = -2\Omega * (u,v,w)^T$, where Ω is the Earth's rotation vector (Broomans, 2003; Deltare, 2018). For depth averaged continuity, the equation solved by Delft3D for incompressible fluids over the total depth is expressed by Equation 5 (Deltare, 2018):

$$\frac{\partial \zeta}{\partial t}+\frac{1}{\sqrt{G_{\xi\xi}}\sqrt{G\eta\eta}}\left(\frac{\partial(d+\zeta)U\sqrt{G\eta\eta}}{d\xi}\right)+\frac{1}{\sqrt{G_{\xi\xi}}\sqrt{G\eta\eta}}\left(\frac{\partial(d+\zeta)\,V\sqrt{G\eta\eta}}{d\eta}\right)=(d+\zeta).Q \quad (5)$$

where U and V are depth averaged velocities in the horizontal directions, d is the depth below datum (horizontal plane of reference), ζ is water level with respect to datum, $\sqrt{G\eta\eta}$ and $\sqrt{G_{\xi\xi}}$ are the coefficients to transform curvilinear to rectangular coordinates, ξ, η are the curvilinear coordinates, and Q is source or sink per unit cross-sectional area due to discharge/ withdrawal contributions. U and V are calculated using Equations 6 and 7 (Deltares, 2018c):

$$U=\frac{1}{d+\zeta}\int_{d}^{c} u\,dz=\int_{-1}^{0} u\,d\sigma \quad (6)$$

$$V=\frac{1}{d+\zeta}\int_{d}^{c} v\,dz=\int_{-1}^{0} v\,d\sigma \quad (7)$$

where u and v are the velocities in the horizontal x- and y- directions, respectively, c and d are the integral limits and σ is the vertical scaled coordinates. σ is calculated by Equation 8 (Deltare, 2018):

$$\sigma=\frac{z-\zeta}{H} \quad (8)$$

where z is cartesian coordinate in vertical direction and H is the depth at that point. σ has a value of 0 at the water surface and σ = -1 at the bed level. Q is calculated by Equation 9 (Deltare, 2018):

$$Q=\int_{-1}^{0}(q_{in}-q_{out})\,d\sigma+P-E \quad (9)$$

where q_{in} and q_{out} are the sources (into the grid) and sinks (out of grid), respectively, P is precipitation and E is evaporation. Further details can be found in conceptual and theoretical documentation of Delft3D Flow (Deltare, 2018).

5.2 Delft3D-Wave

Delft3D Wave uses third generation Simulated Waves Nearshore (SWAN) model (Deltares, 2018b) for simulation. The SWAN model incorporates the discrete spectral balance equation which accommodates the random short-crested waves propagating simultaneously at different directions. The model also incorporates the wave propagations from refraction (due to variable depth), dissipation from white-capping (a specific type of wave breaking from steepness induced wave dissipation during which some air is entrained with the near-surface wave layer), bottom friction, non-linear wave-wave interactions and depth-induced wave breaking (Deltares, 2018b, 2016)

SWAN calculates two-dimensional wave action spectrum density for depth averaged models. SWAN uses the relative frequency and wave direction, in its processes. The action density is equal to the energy density over the relative frequency. The spectral action balance equation is defined by Hasselmann et al. (1973) and Whitham (1974) and shown in Equation (10) (Deltares, 2018b):

$$\frac{\partial}{\partial t}N+\frac{\partial}{\partial x}c_x N+\frac{\partial}{\partial y}c_y N+\frac{\partial}{\partial \sigma}c_\sigma N+\frac{\partial}{\partial \theta}c_\theta N=\frac{S}{\sigma} \quad (10)$$

where x, y and z are the Cartesian co-ordinates, t is time, c_x and c_y are the propagation velocities in the x- and y- directions, respectively, N is action density, c_σ and c_θ are the frequency and refraction propagation velocity in σ- & θ- spatial dimensions, and S is the source.

In Equation 10, the term $\frac{\partial}{\partial t}N$ corresponds to the time rate of change of action density, the terms $\frac{\partial}{\partial x}c_x N$, $\frac{\partial}{\partial y}c_y N$, $\frac{\partial}{\partial \sigma}c_\sigma N$, $\frac{\partial}{\partial \theta}c_\theta N$ represent the propagation of action in x-,y- space, and relative frequency & refraction in the σ- & θ- space, respectively. The term $\frac{S}{\sigma}$ represents the source term for the action balance equation with respect to energy density and non-linear wave-wave interactions and dissipation (Dingemans, 1997; Hasselmann et al., 1973; Mei, 1983; Whitham, 1974). SWAN uses the empirical JONSWAP (Joint North Sea Wave Project) model for bottom friction (Hasselmann et al., 1973). Studies conducted by Hasselmann et al. (1973) found that the bottom friction coefficients for swell conditions is C_{jon} = 0.038 m^2s^{-3}. For fully developed wave conditions, Komen and Bouws (Bouws & Komen, 1983) suggested that C_{jon} = 0.068 m^2s^{-3} can be used.

5.3 Delft3D-WAQ

Water quality modeling is a growing tool supporting integrated water management, water policies, alternative management approaches and for evaluating effective management and preventions (Janssen et al., 2019). Delft3D WAQ uses its integrated Process Library Configuration Tool (PLCT) from which substances and processes can be activated for simulations. Delft3D WAQ uses theoretical water quality and advection-dispersion transport equations to simulate the processes in natural systems. Figure I-4 shows the workflow schematics of Delft3D WAQ (Deltares, 2018c).

Delft3D WAQ or D-Water Quality solves advection-diffusion reaction equations on predefined computational grids which can be used for modeling conservative substances like salinity, chloride, temperature, nutrients like ammonia, nitrate, phosphate etc., phytoplankton biomasses and sediments. The advection-diffusion equation solved for the transport of the conservative substances is shown in Equation 11 (Li et al., 2015):

$$\frac{\partial C}{\partial t} = D_x\left(\frac{\partial^2 C}{\partial x^2}\right) - v_x\left(\frac{\partial C}{\partial x}\right) + D_y\left(\frac{\partial^2 C}{\partial y^2}\right) - v_y\left(\frac{\partial C}{\partial y}\right) + S + fR(C,t) \qquad (11)$$

where C is the concentration (kgm^{-3}); fR(C,t) is the reaction term; D_x, D_y are dispersion coefficients in x- and y- directions, respectively (m^2s^{-1}); S is source term, ν_x, ν_y are eddy viscosities (m^2s^{-1}) (due to horizontal turbulences).

Delft3D WAQ can also be used to simulate for settling and resuspension of sediments, nitrification, and denitrification. More details can be found in the conceptual description in Delft3D-WAQ manual (Deltares, 2018c). D–Water Quality (Delft3D-WAQ) implements mass balances for state variables, for example, dissolved oxygen, nitrates and/or heavy metals in multi-dimensions. Equation 12 represents a mass balance equation for advection-diffusion reaction (Deltares, 2018c):

$$M_i^{t+\Delta t}=M_i^t+\Delta t*\left(\frac{\Delta M}{\Delta t}\right)_{Tr}+\Delta t*\left(\frac{\Delta M}{\Delta t}\right)_P+\Delta t*\left(\frac{\Delta M}{\Delta t}\right)_S \quad (12)$$

where M_i^t and $M_i^{t+\Delta t}$ are the initial and final mass at the beginning and end of time step; the third term, $\Delta t*\left(\frac{\Delta M}{\Delta t}\right)_{Tr}$, is the changes of mass by transport, the fourth term, $\Delta t*\left(\frac{\Delta M}{\Delta t}\right)_P$, represents the physical, biochemical or biological changes and the last term, $\Delta t*\left(\frac{\Delta M}{\Delta t}\right)_S$, represents the changes by source or sink. Physical, biochemical or biological processes include aeration, denitrification and/or primary production of phytoplankton. Change by source includes addition of mass, for example, inflows and other contributing sources to the computational grid system.

Delft3D–WAQ also incorporates the advective transport across any sink or sources using Equation 13 (Deltares, 2018c):

$$T_{x_o}^A=v_{x_o}*A*C \quad (13)$$

where T_{xo}^A is the advective transport across boundary $x = x_o$ (g/s), x, x_o are the boundaries during transfer and initial conditions, v_{xo} is the velocity at $x = x_o$ (m/s), A is the surface area across the boundary at $x=x_o$ (m^2) and C is the concentration at $x = x_o$ (g/m^3) and For dispersive transport, Delft3D WAQ assumes that the substance exchange is proportional to the surface area and concentration gradient. The dispersive transport equation, adapted from the Fick's diffusion law, used is Equation 14 (Deltares, 2018c):

$$T_{x_o}^D=-D_{x_o}*A*\left(\frac{\partial C}{\partial x}\right)|_{x=x_0} \quad (14)$$

where T_{xo}^D is the dispersive transport (g/s), D_{xo} is the dispersion coefficient (m^2/s), A is the surface area (m^2) along the open boundaries for depth averaged water bodies, and $\partial C/\partial x$ is the concentration gradient (g/m^4). The negative sign indicates that dispersion results in a net change

in transport from higher concentration to lower concentration. The transport equation for pollutants or nutrients from the source is expressed by Equation 15 (Deltares, 2018c):

$$T_{src} = Q_{src} * C_{src} \quad (15)$$

where T_{src} is the transport of nutrients (g/s), Q_{src} is the discharge from the source (m^3/s) and C_{src} is the concentration of nutrients (g/m^3).

The model also incorporates the effect of temperatures on the rates of biochemical and biological processes. The rate constant is adjusted for first-order reaction rates according to Equation 16 (Deltares, 2018c):

$$k=k^{20}*k_T^{T-20} \quad (16)$$

where k is the rate constant at temperature T (d^{-1}), k^{20} is the rate constant at reference temperature 20°C (d^{-1}), k_T is the temperature coefficient and T is the water temperature (°C). k_T ranges between 1.01 and 1.10 with a value of 1.04 at 10°C. Further details can be found in the Delft3D WAQ manual (Deltares, 2018c)

The major components of the nutrient cycle in the model are dissolved inorganic nutrients, living organic matter (biomass), particulate inorganic nutrients and detrital organic matter. Dissolved inorganic nutrients, like nitrogen and carbon dioxide, are utilized by the primary producers for growth. Nitrogen, not being a conservative substance, is subjected to different transformation throughout the process. Nitrates (NO_3^-) undergoes denitrification in anaerobic zones of the water system. Nitrate is reduced to elementary nitrogen, which can escape as nitrogen gas, through microbial processes. Elemental nitrogen can undergo nitrogen fixation by algae and specific bacterial species. When phytoplankton and other primary producers die, natural detrital organic matters can be produced and consumed by grazers, resulting in dissolved organic mater and particulates. The process produces easily degradable organic substance that are converted to inorganic species in a very short time range. This process is called autolysis. During modeling, the measured parameter used in the model, of particular interest, is Kjeldahl-Nitrogen which is the sum of ammonium and organic nitrogen (Equation 17). It can also be expressed as nitrate and nitrite substracted from total nitrogen (Deltares, 2018c).

$$\text{Kjeldahl-N} = \text{ammonium} + \text{organic nitrogen} \quad (17)$$

Phytoplankton, being a primary producer, uses solar energy or light and organic matter for growth. Nitrogen is an esstential nutrient for growth and primary productions of phytoplankton to form cell proteins like enzymes, genetic material and chlorophyll-a (which utilizes light as well).

Nutrients, due to anthropogenic activities, can have increased presence in water which can accelerate the growth of these phytoplanktons and create a nuissance, like deficit in dissolved oxygen and light penetrating capabilities limiting the sustainability of other aquaitc plants and organisms resulting in eutrophication. Eutrophicaiton can cause low oxygen levels even below the minimum oxygen required by the the respiration of the increased phytoplanktons, and increased biodegradation process from deaths of other aquatic species. Cyano bacteria, a certain type of phytoplankton, can release toxins which have detremental effects to primary and secondary consumers and to humans (respiratory diseases) (Deltares, 2018c; Fasham et al., 1990; Kim and Montagna, 2012; Kingsford, 2000; Steele and Henderson, 1981).

A portion of the nutrients stays as dissolved inorganic nutrients through autolysis and the other part stays as dissolved or particulate detrital organic matter. The autolysis is followed by microbial decomposition, during phytoplankton death and decomposition, which releases nutrients and carbon back into their inorganic (dissolved) forms. Oxygen, nitrates, sulfates and iron (III) are used as electron-acceptors and result in pH variation as alkalinity and carbon dioxide are consumed during autolysis and phytoplankton growth (Deltares, 2018c).

The Delft3D WAQ model incorporates BLOOM and DYNAMO modules. The BLOOM model simulates multi-algal species whereas DYNAMO model simulates the primary production of the phytoplanktons. In the DYNAMO model, two types of algae are considered, that is, diatoms and all non-diatoms, also known as ‘greens’, not to be confused with green algae. The diatoms use silica as its essential element whereas non-diatoms do not. DYNAMO can be used to study eutrophication focusing on mass balances of nutrients, nutrient dynamics and the primary effects of the change of nutrient loads on algal growth (Deltares, 2018c; Jian et al., 2014; Vaz et al., 2019). The mass balance used in the DYNAMO model is given by Equation 18 (Deltares, 2018c):

$$\frac{\Delta \text{Phytoplankton}}{\Delta t} = \text{loads} + \text{transport} - \text{settling} + \text{resuspension} + \\ + \text{gross primary production} - \text{respiration} - \text{mortality} \quad (18)$$

where $\frac{\Delta \text{Phytoplankton}}{\Delta t}$ is the rate of change of phytoplankton biomass, loads is the inflow algal mass into the model, ‘transport’ is the algal mass transport out of the modeling boundary, ‘settling’ and ‘resuspension’ is the settling and resuspension of the algal biomass due to intermixing and swell conditions, and ‘gross primary production’ is the mass increase/decrease of algae. The oxygen produced by the phytoplanktons is proportional to the gross production of organic matter. The

algae, during ‘respiration’, consumes dissolved oxygen and can deplete it rapidly during eutrophication. Respiration is the sum of respiration during growth and maintenance which is proportional to the algal biomass. The mortality of algae is proportional to its biomass concentration and its overall mortality rate, both of which are dependant on temperature and salinity.

In the DYNAMO model, the gross primary production is calculated using Equation 19 (Deltares, 2018a):

$$R_{gp_i} = f_{nut_i} * f_{lt_i} * k_{gp_i} * C_{alg_i} \quad (19)$$

where C_{algi} is the algal biomass concentration (gC m^{-3}), f_{lti} is the light limitation factor, f_{nuti} is the nutrient limitation factor according to Monod kinetics, k_{gpi} is the potential gross primary production rate (day^{-1}), R_{gpi} is the gross primary production rate (gC m^{-3} d^{-1}) and i is the index for species group, that is, diatoms or algae. The nutient limitation factor for the DYNAMO considers the most limiting nutrient according to Equation 20 (Deltares, 2018a):

$$f_{nut_i} = \left(\frac{C_n}{K_{sn}+C_n}\right), \left(\frac{C_{ph}}{K_{sph}+C_{ph}}\right), \left(\frac{C_{si}}{K_{ssi}+C_{si}}\right) \quad (20)$$

where C_n is the ammonium plus nitrate concentration (gN m^{-3}), C_{ph} is the phosphate concentration (gP m^{-3}), C_{si} is the dissolved inorganic silicate concentration (gS m^{-3}), and K_{sn}, K_{sph} and K_{ssi} are the half-saturation constants for nitrogen, phosphate and silicon (g m^{-3}), respectively.

6. MODEL SETUP

Delft3D–Flow-Wave coupled model and Delft3D WAQ were used to simulate hydrodynamics and nutrient transport phenomenon. To simulate the phytoplankton growth, the DYNAMO module of Delft3D WAQ was used. Algal (non-diatoms) growth was simulated using DYNAMO module of Delft3D-WAQ, which used the hydrodynamic results obtained from the Delft3D Flow and Wave to simulate the overall primary production of total algal biomass. For this study, nitrogen as the limiting nutrient for eutrophication in coastal estuaries (Turner et al., 2014, 2015; Vaz et al., 2019), was focused.

6.1 Study Area

The study area, Nueces Bay, is located in the City of Corpus Christi, Nueces County, South Texas. Nueces Bay is a large shallow estuary, with large dimensions in the horizontal x- and y-dimensions in comparison to the depth of the bay. It is bounded by land in three directions, that is North, West and South, with a small open boundary with Corpus Christi Bay to the East. Nueces bay receives freshwater inflows, sediments, and nutrients through Nueces River from the South-West direction of the bay. Nueces Bay is surrounded by the urban developments, industries, agricultural farms, and recreational facilities. Nueces Bay (NB) receives its flow, sediments and nutrients from the large semi-arid Nueces River Basin (NRB) through the point of confluence between Nueces River (NR) and NB (Figure I-3). Over the past few decades, Nueces Bay and Corpus Christi Bay have observed harmful algal blooms, fish kills and economic disruptions which have impacted the economic growth, human and environmental health (NOAA, 2016; TPWD, 2019b). Excessive nutrients due to anthropogenic activities and climate change are cited to be the potential cause for the environmental disasters (Dodds et al., 2009; EPA, 2015).

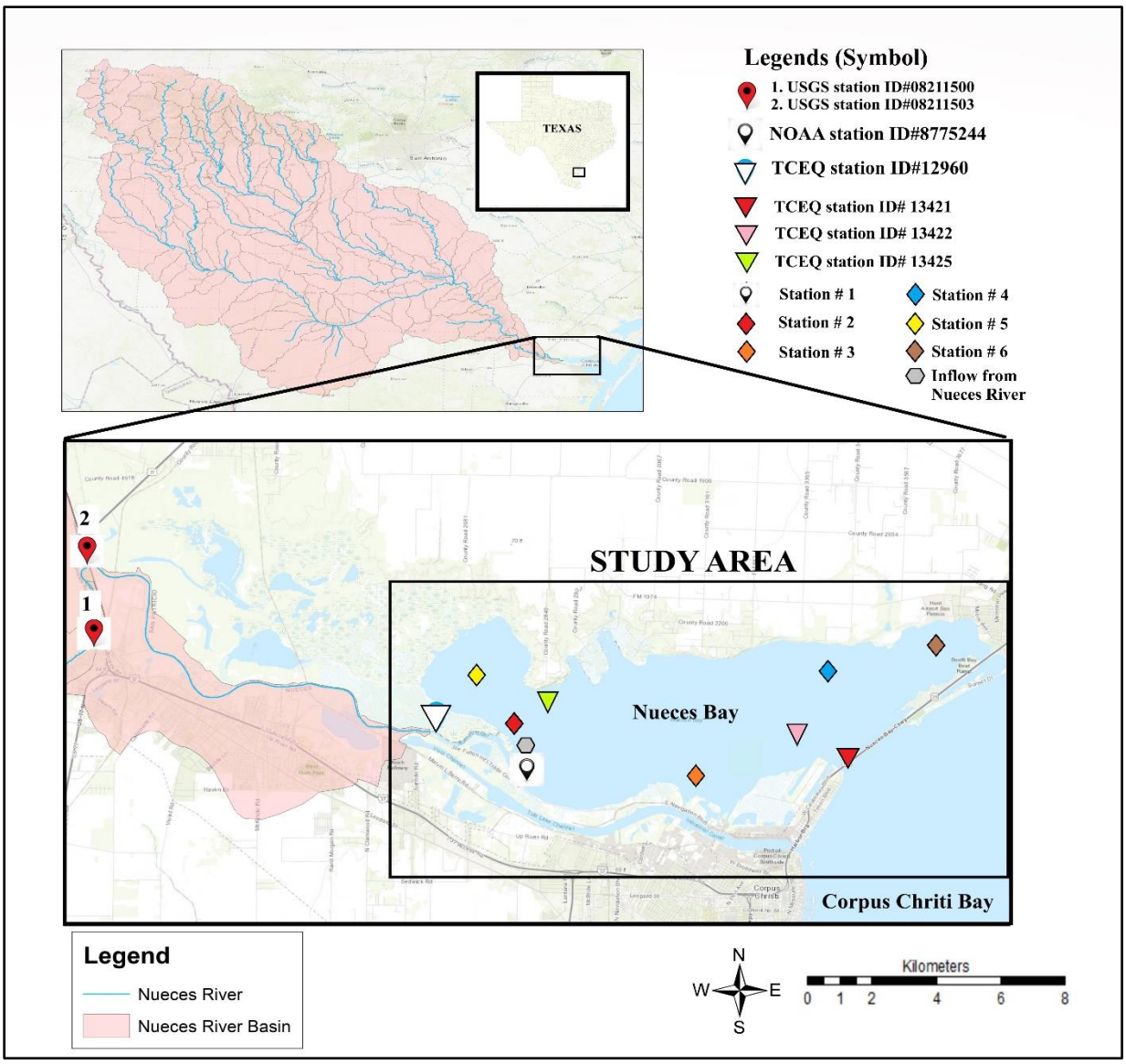

Figure I-3. Study area and geographical locations of stations to be used for model input, calibration and validation.

6.2 Model Input

In this study a depth averaged three-dimensional grids were used since Nueces Bay is a large shallow well mixed estuary with an average depth of 2.40 m (Buskey, 1998; Islam et al., 2014). Table I-1 lists the input parameters and its corresponding values that were used in the calibration of Delft3D–Flow-Wave model. The threshold depth, that is the minimum depth above which a grid cell would be considered to be 'wet' for discretization, peak enhancement factor for waves, the bottom friction coefficient (C_{jon}), wave breaking parameter (α), Manning's roughness

coefficient (n) and horizontal Eddy viscosity and diffusivity were used to simulate wave growth due to wind and/or tidal forces. The wind speed, wind direction and temperature data were collected from NOAA station (ID#8775244) and the salinity data was collected from USGS station (ID#08211503) (Figure I-3). Linear interpolation method was employed in the model to fill any missing data in the input datasets.

Table I-1. Input parameters and values used during calibration for Delft3D–Flow & Wave model.

Parameters	**Values used during calibration**	**Sources and references***
Threshold depth, m	0.1	Deltares (2018)
Peak enhancement factors	3.3	Deltares (2018)
Bottom friction coefficient, C_{jon} (m^2/s^3)	0.067	Deltares (2018)
Wave breaking parameter, α	1.0	Deltares (2018)
Horizontal Eddy viscosity and diffusivity (m^2/s)	1	Deltares (2018)
Manning's coefficient, n	0.02	Deltares (2018)
Wind speed, m/s	From field data	NOAA, station ID#8775244
Wind direction, degree	From field data	NOAA, station ID#8775244
Salinity, ppt	From field data	USGS, station ID#08211503
Temperature, ^oC	From field data	USGS, station ID#08211503

* Sources and references used for initial parameters' values used during calibration.

Table I-2 lists the parameters and their values used to calibrate Delft3D WAQ model. The hydrodynamics results from Delft3D Flow-Wave model (Table I-1), for example, salinity, bathymetry, wind speed and direction, change in depths, wave growths etc., were integrated as inputs to Delft3D WAQ model. Temperature functions for growth and mortality were employed to simulate the growth of algae as many reaction kinetics are dependent on temperature (Deltares, 2018c). The algal respiration factor, growth respiration factor, mortality rate, primary production rate, maximum production rate, half-saturation constants for nitrogen and phosphorous, and temperature coefficient for growth and respiration were initially adopted from sources as tabulated below in Table I-2 (Jian et al., 2014; Schladow and Hamilton, 1997) and adjusted to the calibrated values.

Table I-2. Input parameters and values used during calibration for Delft3D-WAQ model.

Input parameters	Code Names	Value Range	Values Used*	Sources and References[1]
Salinity, ppt			model***	Delft3D-Flow-Wave
maintenance respiration Green temp, 1/d	MRespGreen	0.05-0.17**	0.05	Schladow et al. 1997
growth respiration factor Green, 1/d	GRespGreen	0.05-0.17**	0.085	Schladow et al. 1998
mortality rate Greens, d^{-1}	RcMrtGreen	0.005-0.5**	0.35	Delft3D WAQ
wind speed	Vwind		model***	Delft3D-Flow-Wave
maximum production rate Green (1/d)	PPMaxGreen	1.3-3.6**	1.2	Schladow et al. 1997
half-saturation value N Greens, gN/m^3	KMDINgreen	0.020-0.20**	0.03	Schladow et al. 1997
half-saturation value P Greens, gP/m^3	KMPgreen	0.001-0.025**	0.002	Schladow et al. 1997
temperature coefficient for growth	TcGroGreen	1.02-1.14**	1.04	Schladow et al. 1997
temperature coefficient for respiration	TcDecGreen	1.02-1.14**	1.07	Schladow et al. 1997

Note: * Values used during calibration. ** Ranges of values used during calibration (Deltares, 2018c; Jian et al., 2014; Schladow and Hamilton, 1997). *** Values obtained from Delft3D-Flow-Wave model. [1]Sources and references for initial parameter values used during calibration.

Bathymetric data was obtained from General Bathymetric Chart of the Oceans (GEBCO 08 datum) gridded data. The GEBCO 08 database was integrated with Delft3D Dashboard (DDB), which was used to generate the bathymetry for Nueces Bay. Figure I-4 shows the depth of Nueces Bay using GEBCO 08 datum in WGS 84/UTM zone 14-N Projected cartesian coordinate system with Easting in the x-axis and Northing in the y-axis. Easting and Northing are measured in meters with respect to central meridian and equator as their datum.

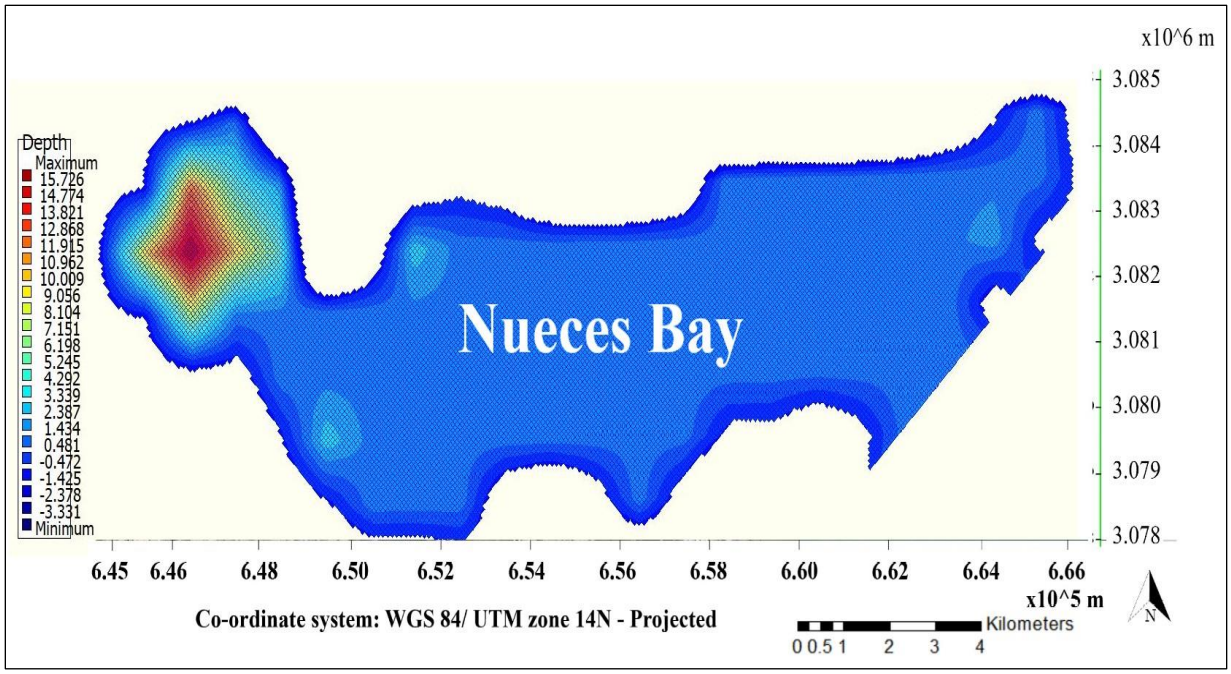

Figure I-4. Coordinate grid showing bathymetry of Nueces Bay (GEBCO 08 datum). Negative values indicate land boundary.

6.3 Model Grid, Boundaries, Initial and Boundary Conditions

Delft3D Dashboard (DDB) was used to generate the Delft3D–Flow-Wave model using World Geodetic System 84 - Universal Transverse Mercator Zone 14 (WGS 84/ UTM Zone – 14 Projected) coordinate system (WGS 84 / UTM Zone 14N, 2020). A grid of 182 x 72, which results in approximately 75 m x 75 m grids, was used to model the study area (Figure I-5). The gridded model has open boundaries to the east and south of the model domain, and closed boundaries on the north, north-west and southwest regions of the gridded model domain. The confluence at the Nueces River and Nueces Bay to the south-west of the model domain was modeled as open (water-water) boundary for nutrient transport. The depth of the bay is represented by elevation levels, that is, from zero meters (0 m) to negative fifteen meters (-15 m) (Figure I-5).

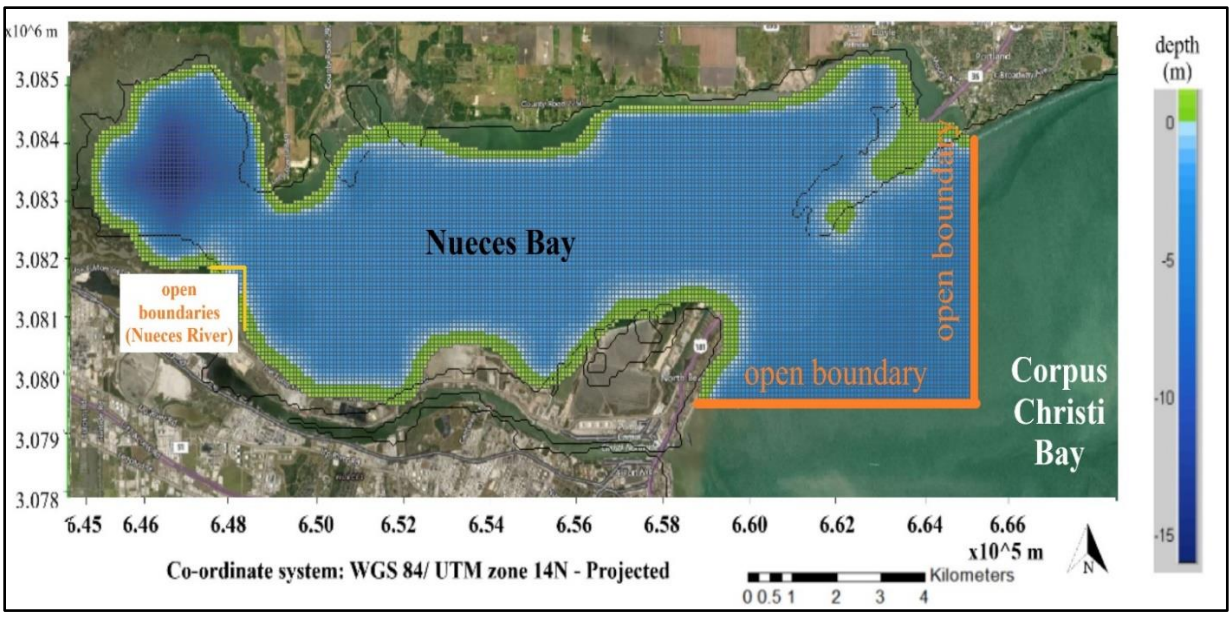

Figure I-5. Map showing the depth (bathymetry), open (water-water) boundaries and closed (land-water) boundaries of Nueces Bay.

The open boundaries at the south and east of the gridded model domain represent the water-water interaction boundary. The closed boundaries on the north, north-west and south-west direction of the simulated area represents the land-water boundaries. The harmonic components for the inputs to open boundary conditions (east and south of model domain) were used from the harmonic constituent data obtained from NOAA Station ID # 8775244 (NOAA, 2019) and TPXO 8.0 Global inverse model which is integrated with DDB (Delft3D Dashboard). Nutrient data from TCEQ 13422 station (Figure I-3) were used for nutrient transport and exchanges at the open boundaries (east and south of model domain). Time series forcing, nutrient, chlorophyll-a and water level data were used at the open boundary (south-west of model domain). At the lateral boundaries, Reimann boundary conditions were imposed so that waves do not reflect back into the model domain (Wang et al., 2019). In coastal areas, the tidal forcing along the open boundaries suffices in generating the accurate and appropriate tidal motion (Mao et al., 2015; Powell et al., 2002; Ritter, 2005; Roelke et al., 1997). Table I-3 shows the initial conditions used in the model at the simulation start time, i.e., August 05th, 2016. Astronomic forcing used at the open boundaries to the east and south of the model domain was defined in terms of the harmonic constituents, as listed in Table I-4.

.

For vertical boundary, a maximum vertical height of zero meters, corresponding to mean sea level, was used (Figure I-5). For Delft3D WAQ, the boundary condition was the algal concentration along the open boundary which was the same as the concentration for Corpus Christi Bay and/or at TCEQ 13422 (Figure I-3), with Thatcher-Harlem time lag of zero.

Delft3D uses the initial conditions, boundary conditions, transport across boundaries, grid, model forcing and input parameters, to numerically solve for finite difference grid systems using finite volume methods. A simple approximation of implicit finite difference is calculated using Crank-Nicholson method. Delft3D then solves for tri-diagonal systems of equations for $t+\Delta t$, where Δt is the time step used. Using continuity equations, mass-balance, and implicit time integration methods, Delft3D simulates and produces outputs at integer multiples of time intervals for concentrations, velocities, etc. Further details are available in the Delft3D-Flow, Wave and WAQ theoretical and conceptual documentation (Deltare, 2018, p. 3; Deltares, 2018b, 2018c).

Table I-3. Initial input used for Delft3D-Flow-Wave simulations at simulation start time.

Description	Value	Units	Source
Water level	0.35	M	NOAA St ID# 8775244
Salinity	1.7	ppt	USGS St ID# 08211503
Temperature	32.9	C	NOAA St ID# 8775244
Total N	0.0009	kg/m^3	TCEQ St ID #12960

Table I-4. Boundary conditions defined by astronomical components and their values at the water-water open boundaries of the model domain for Delft3D Flow-Wave model.

Constituent Name*	Amplitude m*	Phase deg*	Speed deg /hr*	Description
M2	0.02	65.50	28.98	Principal lunar semidiurnal constituent
S2	0.00	5.90	30.00	Principal solar semidiurnal constituent
N2	0.00	38.60	28.44	Larger lunar elliptic semidiurnal constituent
K1	0.06	137.20	15.04	Lunar diurnal constituent
M4	0.00	345.30	57.97	Shallow water over tides of principal lunar constituent
O1	0.07	116.60	13.94	Lunar diurnal constituent
MN4	0.00	316.80	57.42	Shallow water quarter diurnal constituent
MM	0.00	0.00	0.54	Lunar monthly constituent
MF	0.00	0.00	1.10	Lunisolar fortnightly constituent
Q1	0.01	96.90	13.40	Larger lunar elliptic diurnal constituent
P1	0.03	139.30	14.96	Solar diurnal constituent
K2	0.01	56.10	30.08	Lunisolar semidiurnal constituent
MS4	0.00	0.00	58.98	Shallow water quarter diurnal constituent

*Source: TPXO 8.0 Global Inverse Tide model, Delft3D Dashboard and NOAA 8775255 Station harmonic constituents (Deltare, 2018; NOAA, 2019).

6.4 Simulation Time Steps

The period of simulation for the study selected was from August 05th, 2016 to November 30th, 2019. The reference date (simulation start time) was August 05th, 2016. The time step for simulation was determined based on the CFL (Courant-Friedrichs-Lewy number) using Equation 21 (Deltare, 2018):

$$CFL=\frac{\Delta t\sqrt{gH}}{\{\Delta x,\Delta y\}} \quad (21)$$

where Δt = simulation time steps (min), g is gravitation acceleration (m/s^2), H is maximum water depth (m), Δx, Δy = characteristic value, that is, minimum of grid spacing values in either of the x- or y-directions. Rearranging Equation 21, Equation 22 was obtained,

$$\Delta t = \frac{CFL * \{\Delta x, \Delta y\}}{\sqrt{gH}} \quad (22)$$

Using Equation 22 with a maximum CFL value of 10, as suggested by Delft 3D model developers for smooth discretization (Deltare, 2018), a minimum characteristic value (the minimum of $\{\Delta x, \Delta y = 182, 72\}$ which is 72), 9.81 m/s^2 for g and a maximum value of 15 m for H (obtained from bathymetric data using DDB and GEBCO 08), yielded a maximum time step of 60 minutes. In order to achieve a smooth discretization, a time step of 5 minutes was used in this study.

7. MODEL SIMULATION, CALIBRATION, VALIDATION AND SENSITIVITY ANALYSIS

7.1 Simulating effects of wind on wave growth (significant wave height generation)

To evaluate the impacts of wind on wave growth and to determine the type of forcing, Delft3D–Wave standalone model was used to simulate short-crested random wind generated waves. Wave actions were studied for both swell and the fully developed wave conditions (Deltares, 2018b). Wind speeds were applied uniformly throughout the Nueces Bay ranging from 0 to 20 m/s or 0 to 45 mph (approximately) to generate for swell and high wind conditions reflecting wind speeds during rainfall and level 1 hurricanes (20 m/s) ("Hurricanes." World Book Encyclopedia., 1998). Previous researches have shown that at high hydrodynamic mixing conditions, there was no/low algal growth (Shen et al., 2019). Thus, higher level hurricane and wind conditions were not simulated. Wind directions were applied uniformly on the bay in the north and south (nautical) directions. The north and south wind forcing were used to observe the wave generations when the wind was moving South for colder seasons and when the wind was moving North for warmer seasons, respectively. The wind speeds and directions used are tabulated below in Table I-5.

Table I-5. Wind speed and direction used in Delft3D–Wave standalone model to simulate wave growth.

Wind speeds, m/s	Wind speeds, mph	Wind directions, Nautical
0	0	0, 180
5	11	0, 180
20	45	0, 180

7.2 Model calibration and validation

Delft3D Flow-Wave coupled model was calibrated using simulated water level at station point #1 which has the same coordinates as NOAA station ID # 8775244 Nueces Bay, TX (Figure I-3). Studies conducted by Williams and Esteves (2017) showed that for wave modeling, one or two tidal cycles, is enough to assess the performance of the model and the necessary corrections that might be required. Thus, the water level and tidal data were calibrated using one or two tidal cycles for Delft3D-Flow-Wave coupled model using the parameters listed in Table I-1. For Delft3D WAQ model, calibration was conducted using the parameters listed in Table I-2. Coefficient of determination (r^2), Nash-Sutcliff efficiency coefficient (NSE), percentage bias (PBIAS) and RSR (RMSE-observation standard deviation ratio) were calculated and used as statistical indicators for the evaluation of model's performance and goodness-of-fit during model calibration and validation.

Coefficient of determination (r^2) obtained from regression analysis was used to evaluate the degree of collinearity between the simulated and measured data with r^2 ranging from zero to one (0 to 1). An r^2 value close to one indicates the least error variance between the simulated and measured data. Values greater than 0.50 are typically considered to be acceptable (Santhi et al., 2001; Van-Liew et al., 2007).

Nash-Sutcliff Efficiency coefficient is the dimensionless measure of the relative 'noise' (residual variance) compared to observed data variance ('information') (Nash and Sutcliffe, 1970). NSE can vary from -∞ to 1.0. NSE having a value close to or equal to 1.0 is ideal and it indicates how "well" the observed versus simulated plot fits with the line of 1:1 with zero y-intercept. An NSE value less than zero (NSE ≤ 0) indicates that the mean of the observed value is a better predictor than the simulated values. The NSE is calculated using Equation 23 (Nash and Sutcliffe, 1970):

$$NSE = 1 - \left[\frac{\sum_{i=1}^{n} (Y_i^{obs} - Y_i^{sim})^2}{\sum_{i=1}^{n} (Y_i^{obs} - Y_i^{sim})^2}\right] \quad (23)$$

where Y_i^{sim}, Y_i^{obs} and Y_i^{mean} are the i^{th} simulated, observed and mean data, respectively and n is total number of observations.

PBIAS and RSR were used as error indexes to evaluate model's goodness-of-fit. PBIAS or percent bias indicates the (average) tendency of deviation of simulated data from observed data (Gupta et al., 1999). Ideal value would be 0.0 for PBIAS, indicating that the simulated values are

accurate and unbiased. Positive and negative PBIAS values are indicative of under- and over-estimation bias, respectively. PBIAS was calculated according to Equation 24 (Gupta et al., 1999):

$$PBIAS = \left[\frac{\sum_{i=1}^{n}(Y_i^{obs} - Y_i^{sim}) \times 100}{\sum_{i=1}^{n}(Y_i^{obs})}\right] \quad (24)$$

RSR or the Root Mean Squares of Error's (RMSE) observation standard deviation ratio is a commonly used statistical error index (Shirmohammadi et al., 2004; Singh et al., 2004; Vazquez-Amabile et al., 2005). An RSR value of 0.0 is ideal and would indicate that there is zero residual variation or zero RMSE. RSR was calculated by the ratio of the standard deviation of observed data and RMSE using the Equation 25 (Moriasi et al., 2007) and Table I-6 provides the list of recommended statistics generally used in performance rating for a monthly time-step simulation.

$$RSR = \frac{RMSE}{StdDev_{.obs}} = \frac{\sqrt{\sum_{i=1}^{n}\left(Y_i^{obs} - Y_i^{sim}\right)^2}}{\sqrt{\sum_{i=1}^{n}\left(Y_i^{obs} - Y_i^{mean}\right)^2}} \quad (25)$$

Table I-6. Recommended statistics and general performance rating (Moriasi et al., 2007).

Performance rating	RSR	NSE	PBIAS (%)	
			Streamflow	N, P
very good	0.00≤RSR≤0.50	0.75≤NSE≤1.00	PBIAS <±10	PBIAS <±25
good	0.50≤RSR≤0.60	0.65≤NSE≤0.75	±10≤PBIAS <±15	+-25≤PBIAS <±40
satisfactory	0.60≤RSR≤0.70	0.50≤NSE≤0.65	±15≤PBIAS <±25	±40≤PBIAS <±70
unsatisfactory	RSR≥0.70	NSE≤0.50	PBIAS ≥ ±25	PBIAS ≥ ±70

The simulation period for Delft3D Flow-Wave was chosen from August 05th, 2016 to August 31st, 2020. Delft3D Flow-Wave and Delft3D WAQ model were calibrated from August 2016 to August 2018 and validated from September 2018 to August 2020. Since algal blooms occur over a short period of time and at exponential rates (Alosairi and Alsulaiman, 2019; Chen and Mynett, 2006; Lung and Paerl, 1988; Xu et al., 2017), to study the diurnal effects on algal growth, outputs from WAQ model were extracted at 60 minute intervals for the simulations conducted from September 25th, 2016 to November 30th, 2016. Providing approximately two months of warmup period, the models were calibrated from October 01st, 2016 to October 31st, 2016 and validated from November 01st, 2016 to November 30th, 2016, for water levels. The time

period of September 25th, 2016 through November 30th, 2016 was chosen based on the latest algal blooms reported in the Nueces Estuary by Texas Parks and Wildlife Department (TPWD, 2019a).

7.3 Sensitivity analyses of model input parameters

Sensitivity analysis of Delft3D models was performed based on Equation 26 (Xu et al., 2020):

$$S=\frac{\left(\frac{X_i - X_{base}}{X_{base}}\right)}{\left(\frac{P_i - P_{base}}{P_{base}}\right)} \quad (26)$$

where X_i is the simulated value of the output quantity corresponding to i^{th} parametric values (for example, output value of X at 120% or 150% or 50% of parametric base-value, P_{base}), X_{base} is the output value of the quantity corresponding to base parametric value (for example, output value of X at parametric base value, P_{base}). The parametric base values were the parameter values obtained from the model calibration.

Table I-7 lists the parameters and their corresponding calibrated parametric base values that were used in Delft3D Flow-Wave model and Delft3D-WAQ model, for sensitivity analyses. The bottom friction coefficient parameter and Manning's n were used for Delft3D Flow-Wave sensitivity analyses, as studies show that these parameters have the most impact on wave growth and water level outputs (Deltare, 2018; Garcia et al., 2015; Rahman and Venugopal, 2017; Roelvink and Banning, 1995; Xu et al., 2017). For Delft3D WAQ model, sensitivity analyses focused on maximum growth rate, respiration factor, nutrient limitation function and mortality rate. The sensitivity analyses were carried out by varying each individual parameter while keeping the rest of the parameter constant at their calibrated values.

Table I-7. Parameters and their base values used in sensitivity analyses.

Parameters	Calibrated parametric base values
Delft3D- Flow -Wave model	
Bottom friction coefficient, C_{jon} (m^2/s^3)	0.067
Manning's coefficient, n	0.02
Delft3D- WAQ model	
Maintenance respiration Green temp, 1/d	0.05
Maximum production rate Green, 1/d	1.2
Half-saturation value N Greens, gn/m^3	0.03
Half-saturation value P Greens, gp/m^3	0.002
Temperature coefficient for growth	1.04
Growth respiration factor Green, 1/d	0.085
Temperature coefficient for respiration	1.07
Mortality rate Greens, d^{-1}	0.085

7.4 Model Application

After calibration and sensitivity analysis, effects of extreme high/low inflows, wind speeds, and nutrient loads on hydrodynamics, nutrient and algal dynamics were evaluated using Delft3D Flow-Wave and WAQ models. Ten years (2011 to 2019) of available data from TCEQ station ID#12960, USGS station ID# 08211500 and USGS station ID#08211503 (Figure I-3) were collected, from which the maximum and minimum inflows, wind speeds, chlorophyll-a (chl-a), temperature and nutrients were used as model inputs (Table I-8).

Scenarios simulation to demonstrate the effect of high/low inflows, wind speeds, temperature, and nutrient and chlorophyll-a loads on algal growth at TCEQ station ID# 13422 (Figure I-3) were conducted using the extreme high and low historical data, as tabulated in Table I-8. TCEQ station ID#13422 was selected to study the effect of inflows from Nueces River. The inflows, that is, freshwater inflows, chlorophyll-a (chl-a) and total nitrogen (TN), through Nueces River to Nueces Bay, were added to the model through the discharge point (see 'inflow from Nueces River', Figure I-3). The simulation period was between October 2016 to November 2016, that is, during the HAB event. The meteorological data, that is, wind and water temperature, were imposed uniformly throughout Nueces Bay. The highest recorded wind speed and direction, from the whole simulation period, was uniformly applied as model input during the simulation period to demonstrate the effect of wind on algal growth. The effects of highest and lowest water

temperature were also simulated in the study. All the hypothetical scenarios' simulations were compared with the calibrated base model.

Table I-8. Freshwater inflows, total nitrogen, chlorophyll-a, wind speed and temperature values used in scenarios analysis to demonstrate their effects.

	Inflow, m^3/s	**Total nitrogen, mg/L**	**Chl-a, µg/L**	**Wind speed, mph**	**Temperature, ^oC**
High	80.0 (Oct. 2018)	3.0 (Jul. 2018)	134.0 (Jul. 2017)	60.0 (Mar. 2018)	32.4 (Aug. 2018)
Low	0.01 (Aug. 2016)	0.9 (Oct. 2016)	4.4 (Jan. 2019)	4.0 (Oct. 2018)	4.9 (Jan. 2018)

8. FIELD SAMPLING IN NUECES BAY

Water quality data were collected from Nueces Bay at 3-month intervals beginning in August 2019 and ending in August 2020, for a total of 5 sampling trips. These samples were collected to assist with ground-truthing the modeling efforts to understand the relationship between water quality and phytoplankton biomass, and especially the factors leading to rapid increases in phytoplankton biomass known as blooms. Samples and data were collected from an outboard motor boat at 6 stations (Station #1 - #6 shown in Figure I-3) within Nueces Bay, and water samples were collected at various depths using a Wildco Alpha Horizontal water bottle (2.2-liter capacity). Water samples were collected for analysis of inorganic nutrients (N, P, Si), extracted chlorophyll a (as a proxy for phytoplankton biomass) and whole water samples for analysis of biological oxygen demand (BOD). Nutrient concentration measurements were made using a Lachat QuikChem 8500 nutrient autoanalyzer, with duplicate samples collected at each location. Water quality parameters were also collected at various depths at each station using a YSI EXO water quality data sonde, with probes to measure water temperature, specific conductivity (salinity), pressure (depth), oxygen, pH, turbidity, and in vivo chlorophyll a.

Three of the stations were located in the western half of Nueces Bay, near the head of the estuary where the Nueces River enters (Stations 1, 2 and 5, Figure I-4) and the other three stations were located in the eastern half of Nueces Bay, further from the river and closer to the connection with Corpus Christi Bay (Stations 3, 4 and 6, Figure I-4). The mean depth over all sampling efforts at each station varied from 0.9 m at Station 5 to 1.8 m at Station 4. Water temperature and salinity measurement taken from the surface, mid depth and near bottom at each station all showed similar

values, indicating that this shallow water column was well mixed, and showed no indication of density stratification. Mean inorganic nutrient concentrations of phosphate ranged from 4.0 uM L^{-1} at Station 3 to 6.8 uM L^{-1} at Station 5, while combined inorganic nitrogen from ammonium, nitrate and nitrite ranged from 1.8 uM L^{-1} at Station 3, to 4.9 uM L^{-1} at Station 6. N:P ratios ranged from 0.32 at Station 2 to 0.73 at Station 6. All N:P ratios were less than one, which is well below the Redfield Ratio average for seawater of 16, which indicates potentially strong nitrogen limitation of primary production in Nueces Bay. It should be noted that organic forms of N were not measured, so organic N may have contributed to phytoplankton primary production in this system. Measurements of silicate were very high throughout this study at all stations and sampling seasons, with values ranging from 50 to over 400 uM L^{-1}. Silicate is required by diatoms, a common group of phytoplankton in marine environments. There is no indication that availability of silicate would limit diatom growth.

Measurements of extracted chlorophyll a were obtained by filtering a known volume of whole seawater onto a GF/F glass fiber filter in a darkened room and extracted in 10 ml of 90% acetone overnight in a refrigerator. Analysis was performed the next day using a Turner Designs Trilogy fluorometer. Mean values of chlorophyll a ranged from 10 ug L^{-1} at Station 4 to 20.3 ug L^{-1} at Station 6. These estimates of phytoplankton biomass are within the normal range for estuaries in South Texas, and do not indicate either eutrophication through excess nutrient loads or low productivity due to nutrient limitation.

Biological Oxygen Demand (BOD) is a bioassay procedure that measures the oxygen consumed by bacteria during the decomposition of organic matter at a constant temperature in the dark. Upon returning from the field, four BOD bottles were filled from each station; two from each of two replicate water samples. An initial oxygen reading was taken for each bottle using a Hach HQ30d oxygen meter. Bottles were then filled and sealed with the ground glass cap, ensuring there were no air bubbles trapped inside. Bottles were wrapped in aluminum foil to exclude light and were incubated in the dark for 5 days in an incubator set at 20 ^{o}C. At the end of the incubation period the oxygen concentration was measured again, and the difference between starting and ending concentrations of oxygen is the BOD.

The mean BOD for each station averaged over all the sampling dates ranged from 2.1 mg O_2 per liter at Station 4 to 3.7 mg O_2 per liter at Station 6, All of these measures of BOD fall within

the normal range of values for unimpacted estuarine waters, and show no evidence of a high load of dissolved or particulate organic matter in the water column during the course of this fieldwork.

Other measures of water quality were recorded in the field using the YSI EXO data sondes include dissolved oxygen, pH and turbidity. Mean oxygen concentrations measured throughout the year at each station ranges from 6.2 mg O_2 per liter to 6.9 mg O_2 per liter. This represents a percent oxygen saturation range of 89.7% to 97.2%, indicating that there was no evidence of hypoxia during our period of study. The mean values of pH varied little over the year we collected measurement, with the mean values for each station ranging from 8.0 to 8.2. This does not indicate that there is any issue related to ocean acidification in the Nueces estuary. Turbidity was measured at three depths at each station, and there was a consistent trend of slightly increasing turbidity with depth at each station. This indicates that turbidity was due in part to resuspension of fine sediments near the bottom by surface wave mixing and tidal currents. The mean values for surface turbidity ranged from 10.1 ntu at station 3 to 30.7 ntu at station 5.

In vivo measures of chlorophyll a fluorescence were also made with a chlorophyll probe on the YSI water quality sonde. This method measures the chlorophyll a contained within living phytoplankton cells within the seawater, rather than measuring the chlorophyll extracted from phytoplankton in the laboratory. These values ranged from 6.0 ug/L chlorophyll a from surface samples at station 4 to 13.5 ug/L chlorophyll a at Station1. These measures are lower than the values than those for extracted chlorophyll taken at the same location, as is often the case. Chlorophyll molecules within the chloroplasts of phytoplankton cells may be shaded to the UV light used to elicit their fluorescence, leading to lower values than when the chlorophyll molecules are extracted into solvents. There was only minor variance in chlorophyll a measurement with depth, again indicating that the shallow water column was well mixed.

There were clear seasonal patterns in water temperature, with minimum water temperatures of approximately 20 ^{o}C measured during sampling trips in November 2019 and February of 2020, and maximum temperatures of approximately 30 ^{o}C measured in August 2019 and August 2020. There was lower variability of salinity with season, with maximum salinity measured in November 2019 of about 32 psu at all stations and minimum salinity of about 24 psu at the three stations closest to the Nueces River (Stations 1, 2 and 5) and higher salinities of about 31 psu at Stations 3, 4 and 6 further from the river. No clear patterns of seasonal variation in inorganic nutrient concentrations or phytoplankton abundance were observed.

9. RESULTS

9.1 Wave growth and hydrodynamic mixing

Effects of wind, bottom friction and tidal forces were simulated for wave growth using Delft3D-Wave standalone model. Figure I-6 andFigure I-7 show the significant wave height produced at the NOAA station ID # 8775244 (Figure I-3) and the corresponding parametric effect on wave growths for different wind speeds, wind directions and parametric values.

The simulated significant wave height were higher for north wind than for south wind for the same wind speeds and bottom friction coefficient (Figure I-6). Also, higher wind speeds resulted in higher wave height for the same bottom friction coefficient. Figure I-7 shows that increase in bottom friction coefficient (C_{jon}) did not increase wave growth (significant wave height) for the same wind speed and direction. Also, there is no significant wave growth in the absence of wind. This shows that the wave growth in the shallow Nueces Bay is primarily dependent on wind.

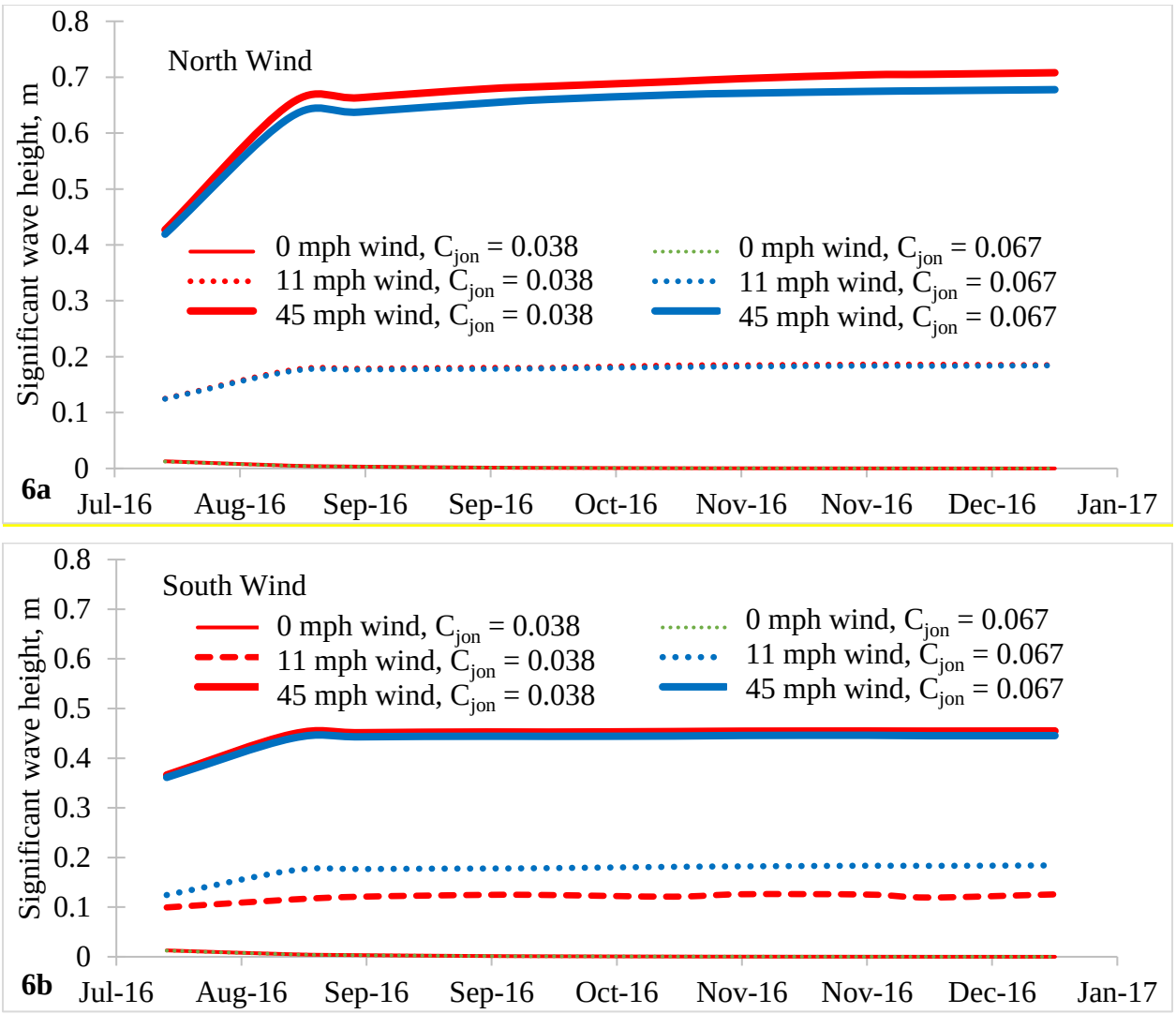

Figure I-6. Effect of wind direction on wave growth for different wind speeds for swell (C_{jon} = 0.038 m^2s^{-3}) and fully developed (C_{jon} = 0.067 m^2s^{-3}) wind conditions, (a) From north, (b) From south.

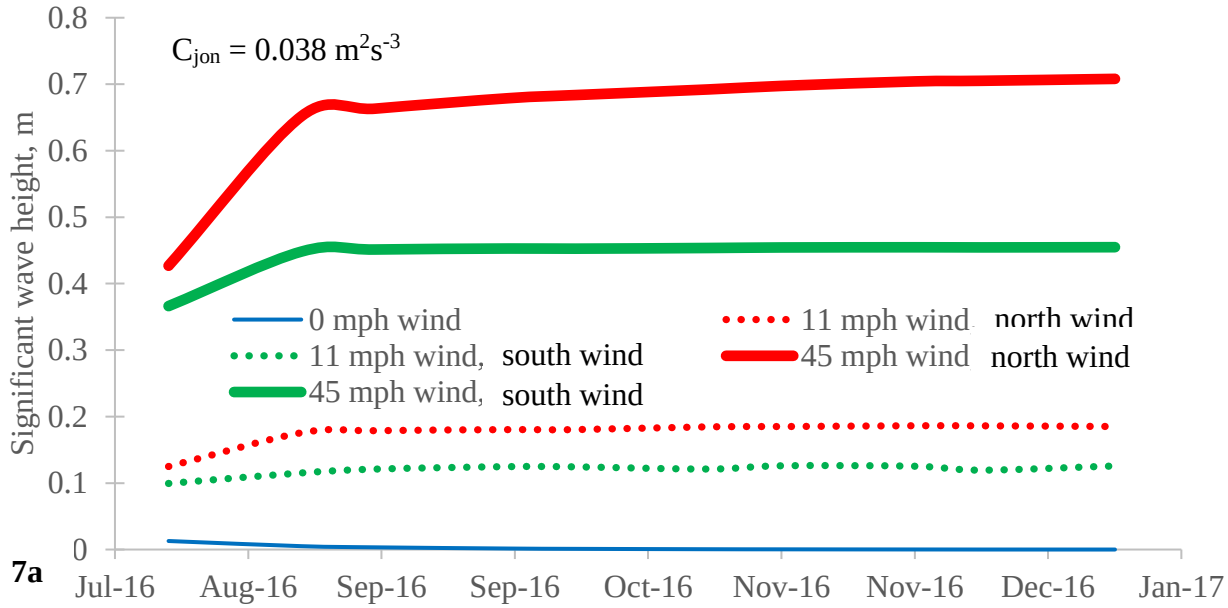

7a

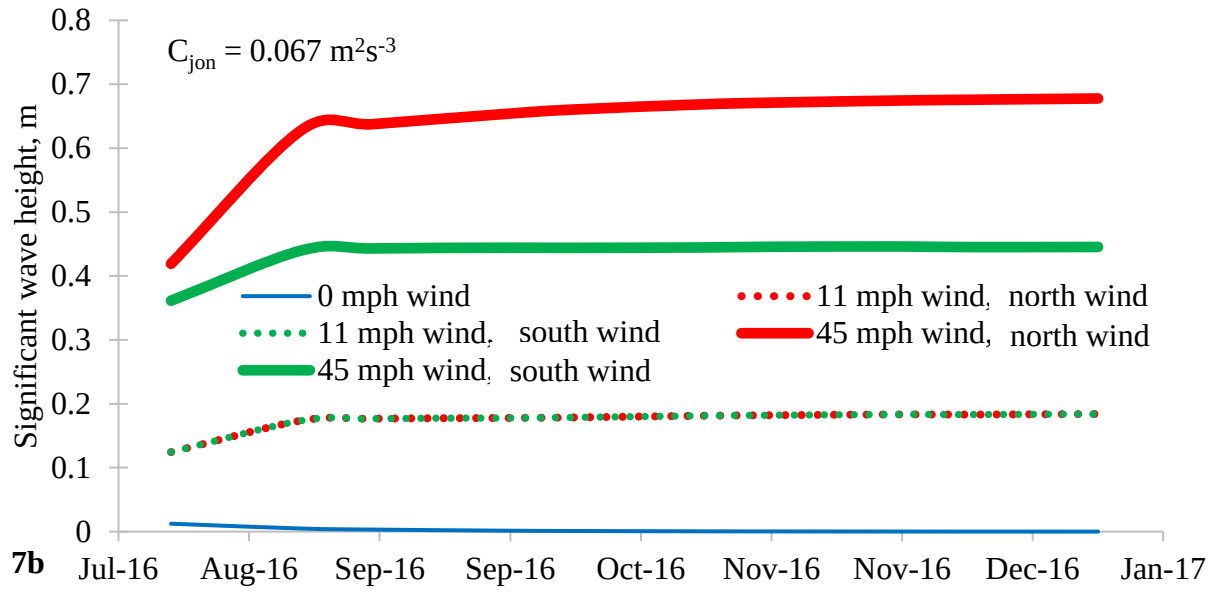

7b

Figure I-7. Effect of wind speeds and directions on wave growth for (a) Swell conditions (C_{jon} = 0.038 m^2s^{-3}) and (b) Fully developed wind conditions (C_{jon} = 0.067 m^2s^{-3}).

9.2 Model Calibration and Validation

9.2.1 For the period between August 2016 and August 2020

Delft3D Flow-Wave coupled model was calibrated and validated for water levels with daily simulated outputs at NOAA station ID#8775244 (Figure I-3), using historical water levels, from August 2016 to August 2020 (Figure I-8). During the calibration from August 2016 to August 2018, the statistical indicators NSE, r^2, PBIAS and RSR yielded values of 0.93, 0.68, 4.39% and 0.27, respectively. During validation, the statistical indicators NSE, r^2, PBIAS and RSR yielded values of 0.94, 0.86, 1.41% and 0.24, respectively. Figure I-8b shows the plot of simulated water levels versus the observed water levels during calibration and validation. The plot also shows that the regression line for calibration and validation passed through the origin with r^2 values of 0.68 and 0.86, respectively. Statistical analyses for model's goodness-of-fit and error indices showed 'very good' performance ratings (Table I-9).

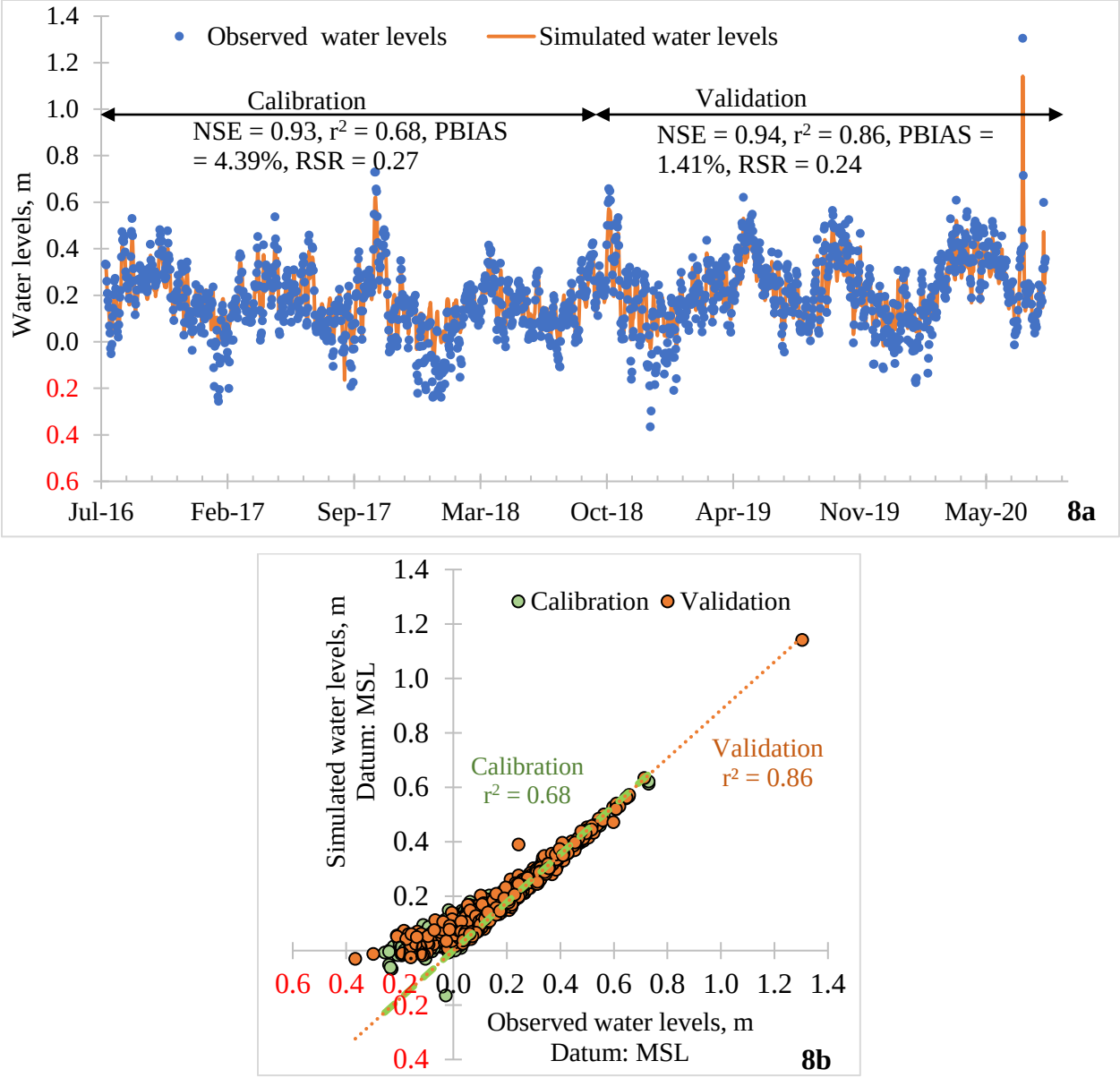

Figure I-8. a) Time plot of observed and simulated water levels at NOAA station (ID#8775244), and b) Plot of simulated and observed water levels during calibration and validation. Water level datum is the mean sea level (MSL).

Table I-9. Performance rating of Delft3D Flow-Wave coupled model's calibration and validation using simulated and observed water levels data at NOAA station ID # 8775244.

Statistical indicators	Calibration	Performance rating*	Validation	Performance rating*
NSE	0.93	very good	0.94	very good
r^2	0.68	very good	0.86	very good
PBIAS	4.39%	very good	1.41%	very good
RSR	0.27	very good	0.24	very good

*(Moriasi et al., 2007)

Figure I-9a shows that the simulated daily variations of TN provide more information for the time periods (on average, at 4 months intervals) in between the observed TN values. To allow for direct comparisons between the simulated and observed TN values, simulated TN values for the dates when the observed data were available were extracted from the daily simulated output (Figure I-9b). Data shown in Figure I-9b were then used in statistical analyses to quantify the calibration and validation performance. During calibration from August 2016 to August 2018, the statistical indicators NSE, r^2, PBIAS and RSR yielded values of 0.99, 0.92, 0.75% and 0.05, respectively. During validation from September 2018 to December 2019, the statistical indicators NSE, r^2, PBIAS and RSR yielded values of 0.99, 0.92, 4.05% and 0.08, respectively. Figure I-9c shows the plot of simulated TN versus the observed TN during calibration and validation periods. The plot also shows that the regression line for calibration and validation passed through the origin with r^2 values of 0.92 for both calibration and validation. Statistical analyses showed 'very good' performance ratings during calibration and validation (Table I-10).

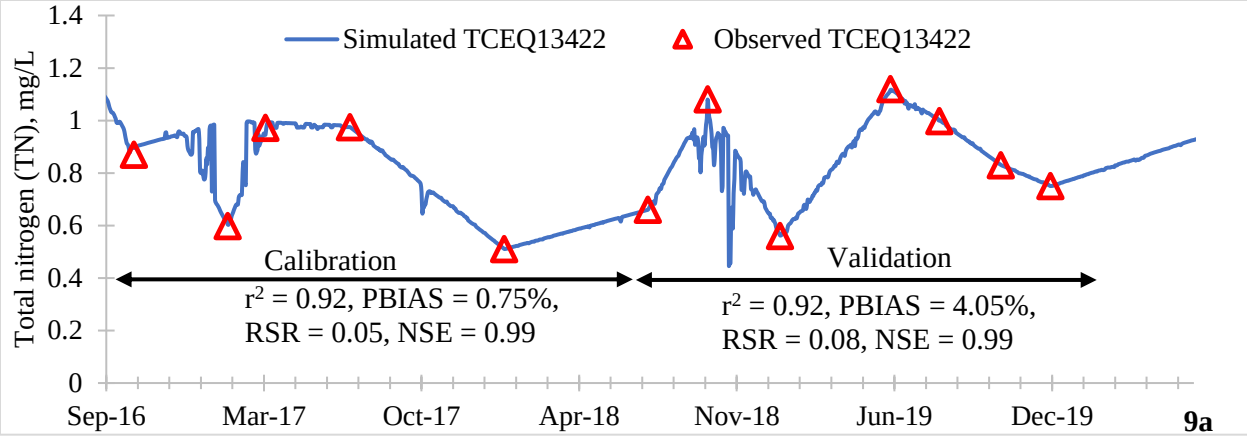

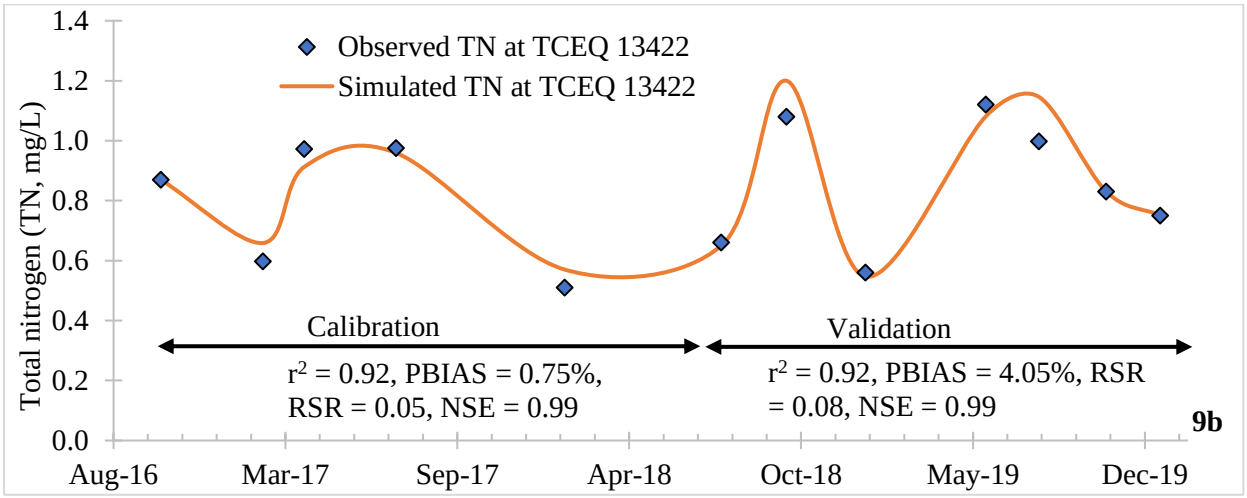

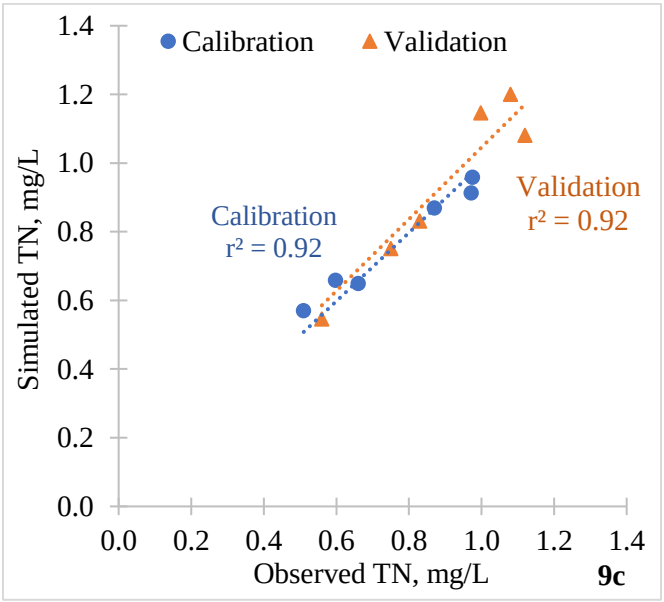

Figure I-9. a) Time-series plot of observed and simulated daily total nitrogen (TN, mg/L) at TCEQ station ID# 13422, b) Plot of observed and simulated TN at available historical dates, and c) Plot of simulated versus observed total nitrogen (TN, mg/L) during calibration and validation.

Table I-10. Performance rating of model calibration and validation for total nitrogen (mg/L).

Statistical indicators	Calibration	Performance rating*	Validation	Performance rating*
NSE	0.99	very good	0.99	very good
r^2	0.92	very good	0.92	very good
PBIAS	0.75%	very good	4.06%	very good
RSR	0.05	very good	0.08	very good

*****(Moriasi et al., 2007)

Similar to Figure I-9, Figure I-10a shows that the daily simulation output provides more variations of chl-a in between the chl-a measurement dates. The statistical analyses for the dataset extracted from daily simulations for the dates when the observed data were available indicate NSE, r^2 and PBIAS values of 0.75, 0.88 and 13.64%, respectively, during model calibration (Figure I-10b). During validation from September 2018 to August 2020, the statistical indicators NSE, r^2 and PBIAS yielded values of 0.72, 0.74 and 4.03%, respectively. Figure I-10c shows the plot of simulated versus observed chl-a, which showed that the regression line for calibration and validation passed through the origin with r^2 values of 0.88 and 0.74, respectively. Statistical analyses for goodness-of-fit and error indices showed ‘very good’ to ‘good’ performance ratings during calibration and ‘good’ to ‘satisfactory’ performance ratings during validation (Table I-11).

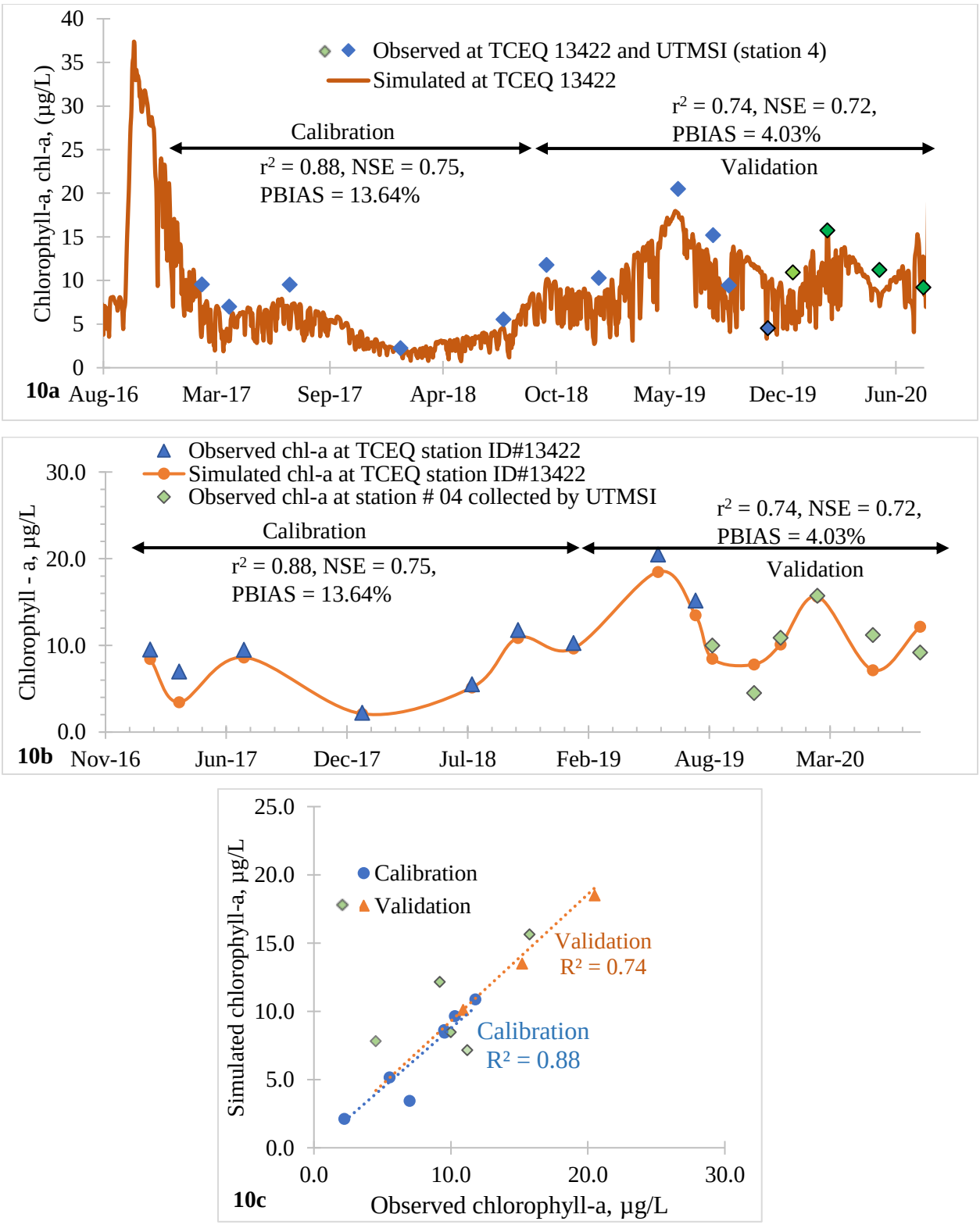

Figure I-10. a) Time-series plot of observed and simulated daily chlorophyll-a (µg/L) at TCEQ station ID # 13422, and station 4, b) Plot of observed and simulated chl-a at historical observed chl-a dates, and c) Plot of simulated versus observed chl-a (µg/L) during calibration and validation.

Table I-11. Performance rating of model calibration and validation for chlorophyll-a (µg/L).

Statistical indicators	Calibration	Performance rating*	Validation	Performance rating*
NSE	0.71	good	0.53	satisfactory
r^2	0.88	good	0.74	good
PBIAS	13.64%	very good	4.03%	very good

*(Moriasi et al., 2007)

9.2.2 For the period between October 01st, 2016 to November 30th, 2016

High temporal resolution data at 60 minutes interval were extracted for the period between October 01st, 2016 and November 30th, 2016 to account for the diurnal effects, hydrodynamics, and growth of algae in Nueces Bay. Figure I-11a shows the model calibration and validation results for water levels. The model was calibrated and validated with 'good' performance rating with r^2 values of 0.96 for both calibration and validation and NSE values of 0.67 and 0.87 for calibration and validation, respectively. Figure I-11b shows the regression line passed through the origin with r^2 values of 0.96 for both calibration and validation.

Figure I-12 shows the simulated 1-hour and 24-hour (daily) chlorophyll-a concentrations at TCEQ station ID#13422 (TCEQ 13422) and station # 06 from October to November 2016. The plots show the difference between the hourly and daily variations of algal concentrations during the algal blooms period. The 1-hour data outputs showed detailed variations in the algal concentrations within a day, where the variations of the algal concentrations are indicative of the diurnal patterns of algal growth, respiration, and mortality.

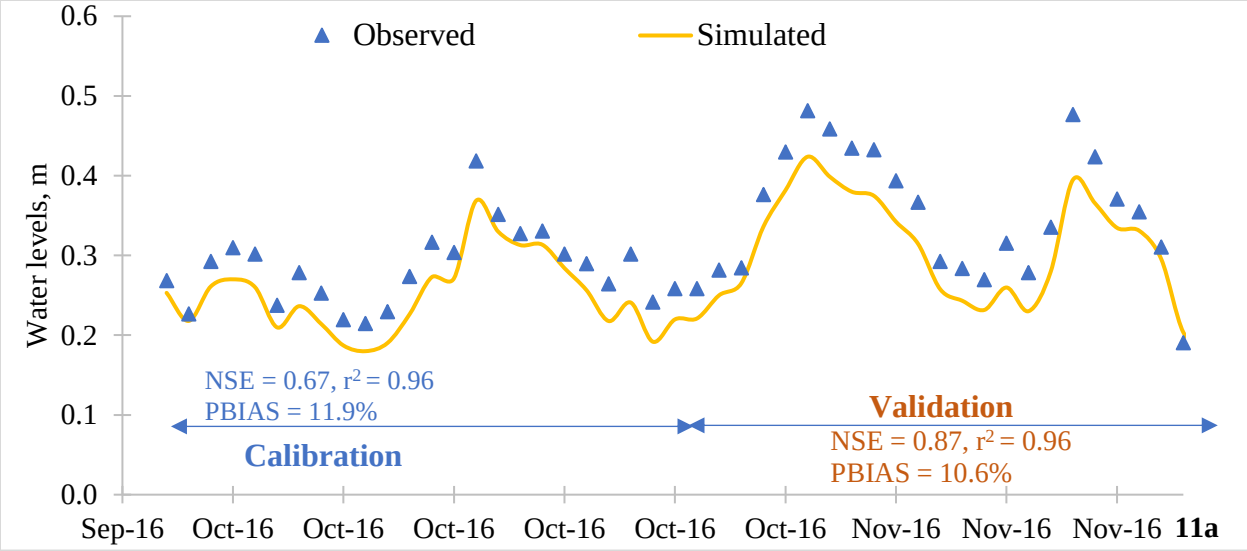

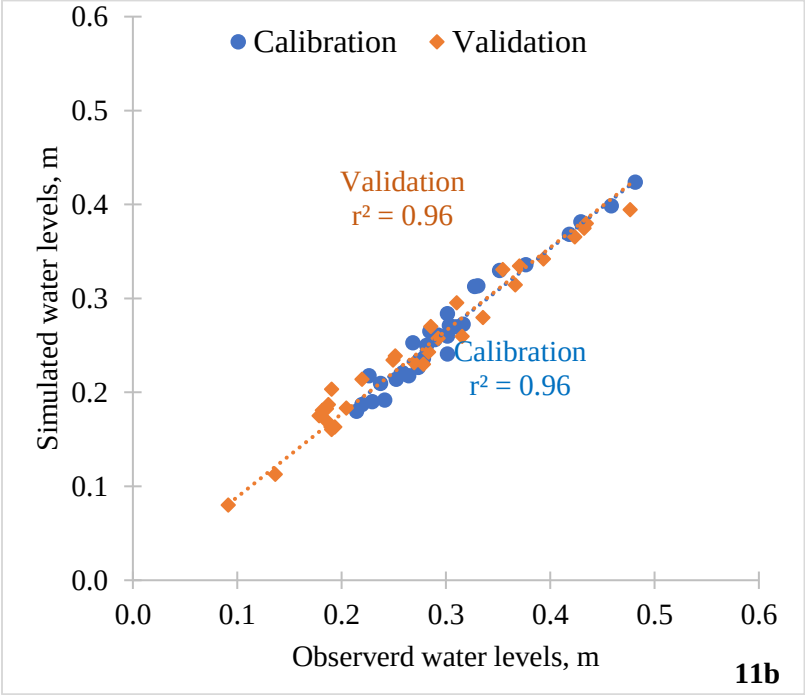

Figure I-11. a) Simulated and historic daily tide/water level at NOAA station ID#8775244, and b) Plot of simulated and observed water levels. Water level datum is mean sea level (MSL).

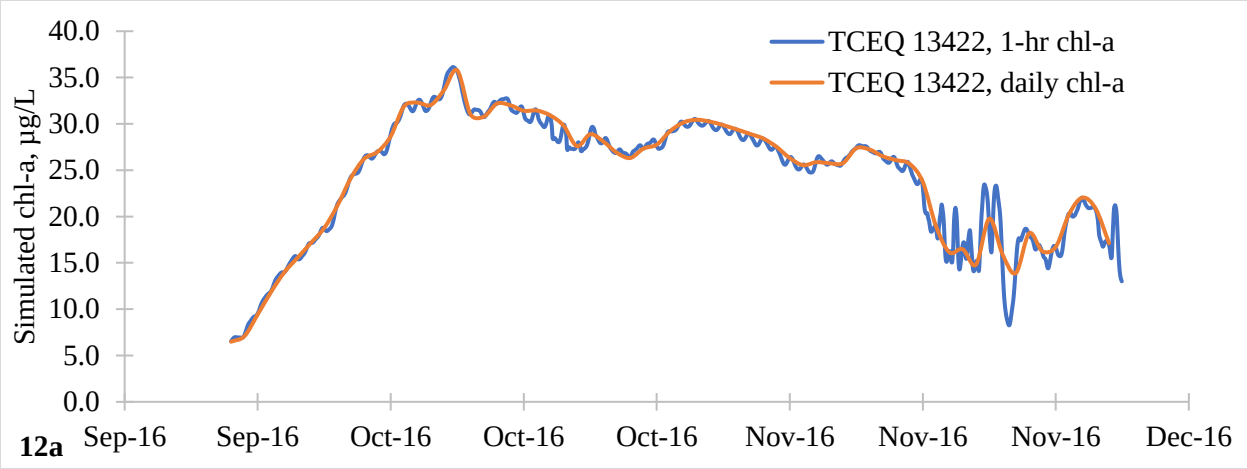

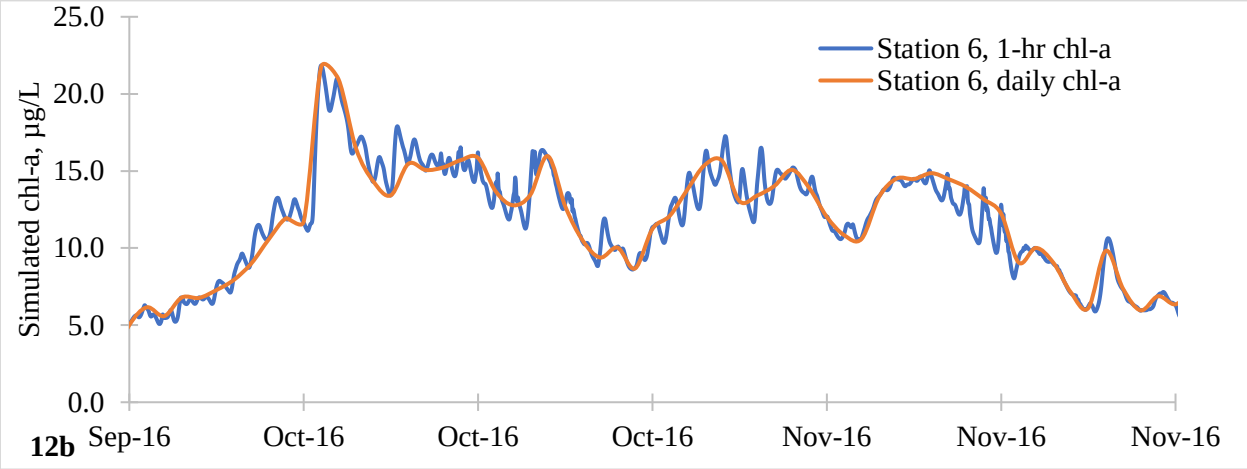

Figure I-12. Simulated 1-hour and daily (or 24-hr) chlorophyll-a (chl-a) concentration at a) TCEQ 13422, and b) Station 6.

9.3 Sensitivity Analyses

Figure I-13 shows the plot of sensitivity of different parameters in response to algal growth corresponding to different percentage changes of the input parameters from their base values (values of parameters after calibration). Table I-12 shows the numerical sensitivity of the model parameters on algal growth. Local sensitivity analyses were performed by changing one of the parameters to 120%, 150% and 180% from its calibrated base values, while keeping all the other parameters constant. Results show that temperature (T) and maximum production rate (MPR) are the most sensitive parameters with average sensitivities of 105 and 74, respectively. Temperature of the water impacts the rate of reactions and reaction kinetics, growth of algae and respiration. The maximum production rate (MPR) is dependent on factors such as sunlight and heat flux or

exchange, temperature, pH and salinity. The respiration rates depend on the availability of dissolved oxygen as well (Alosairi and Alsulaiman, 2019; Deltares, 2018c; Jian et al., 2014; Mao et al., 2015; Schladow and Hamilton, 1997; Xu et al., 2017).

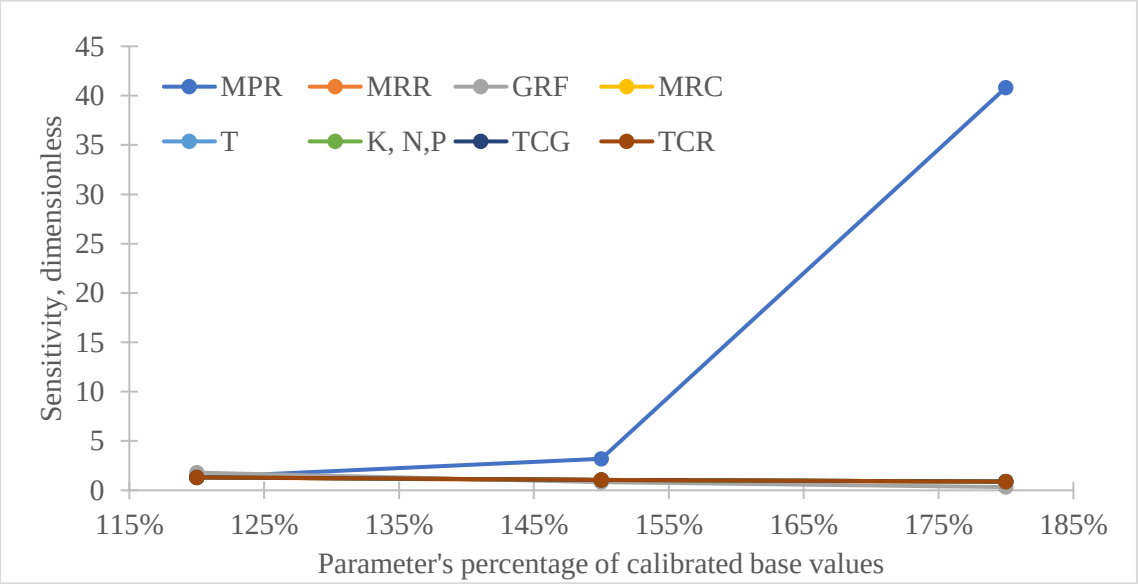

Figure I-13. Sensitivity of different parameters of high temporal resolution algal model.

Table I-12. Sensitivities of the Delft3D WAQ model parameters at high temporal resolution.

		% of base value			
Rank	**Description of Parameters**	**120%**	**150%**	**180%**	**Average**
1.	Temperature, T	2.38	3.99	308.39	104.92
2.	Maximum Production Rate, MPR	2.38	8.71	217.43	76.17
3.	Half-saturation constant, $K_{N,P}$	4.83	1.98	1.24	2.68
4.	Mortality Rate Constant, MRC	2.38	1.90	1.22	1.83
5.	Maintenance Respiration Rate, MRR	2.38	1.89	1.22	1.83
6.	Growth Respiration Factor, GRF	3.10	1.37	0.59	1.69
7.	Temperature coefficient for growth, TCG	2.38	0.95	0.59	1.31
8.	Temperature coefficient for respiration, TCR	2.38	0.95	0.59	1.31

9.4 Model application

9.4.1 Spatial variations of algal growth and total nitrogen concentrations during an algal blooms event

Figure I-14 shows the simulated daily algal concentration (chl-a, µg/L) at the six monitoring stations between October 2016 and August 2020. The algal concentrations near the stations # 5 and # 6 were around and/or below 20 µg/L during October 2016 and for the whole simulation period (August 2016 to August 2020). 20 µg/L is the average threshold chlorophyll-a concentration for eutrophication (Sheldon & Alber, 2011). Station 6 is in the vicinity of the confluence of Nueces Bay and Corpus Christi Bay where there are tidal exchanges, hydrodynamics and mixing with Corpus Christi Bay (Figure I-3). Station 5 is to the west end of the model domain (Figure I-3) enclosed by land-water boundaries and a small open boundary (Nueces River-Bay confluence) to its south. The depth averaged velocity vectors plots showed that there was relatively higher mixing at station 5 (Figure I-15), which yielded in lesser algal growth. Stations 1 to 4 showed increased growth of algae, and crossed the threshold concentration for eutrophication, during the HAB event in October 2016 (TPWD, 2019a). As the location of the station moves towards the confluence of Nueces and Corpus Christi Bay, the overall algal growth decreases from station 1 to station 4 (Figure I-14a). At the confluence (station 6) the algal growth/concentration was limited by the relatively higher hydrodynamics activities and mixing as observed from Figure I-15. Thus, at stations 5 and 6, the velocity vectors were in haphazard/random motion (Figure I-15), that is, there has been mixing and momentum exchanges within the waters which limited algal growth and yielded lower algal concentrations. Whereas stations 1 through 4 exhibited uniform motion, lower mixing and yielded in higher algal concentrations.

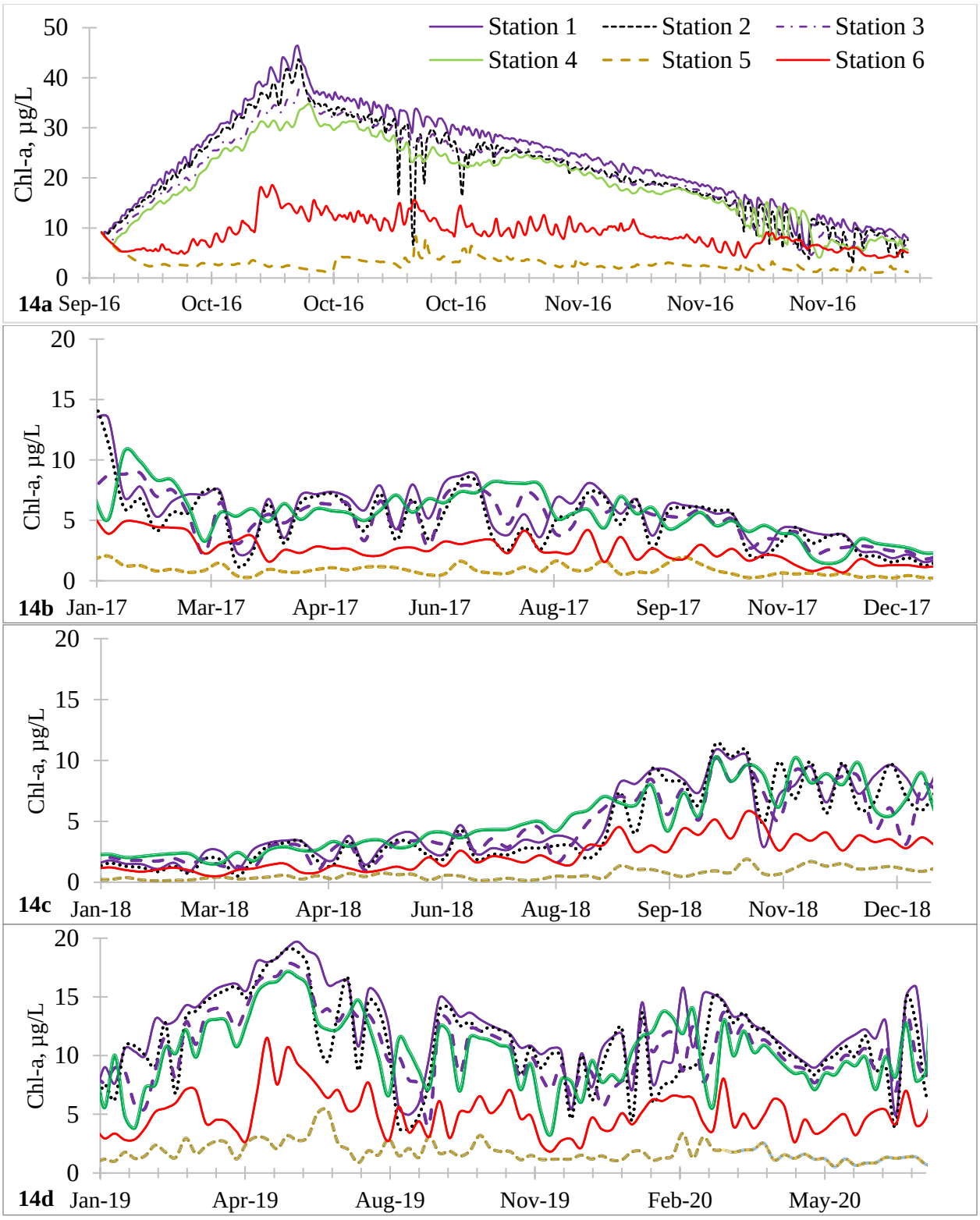

Figure I-14. Simulated daily algal concentration (chlorophyll-a, chl-a, µg/L) at stations # 01 - # 06, a) from October 2016 to November 2016, and b) from January 2017 to December 2017, c) January 2018 to December 2018, d) January 2019 to August 2020.

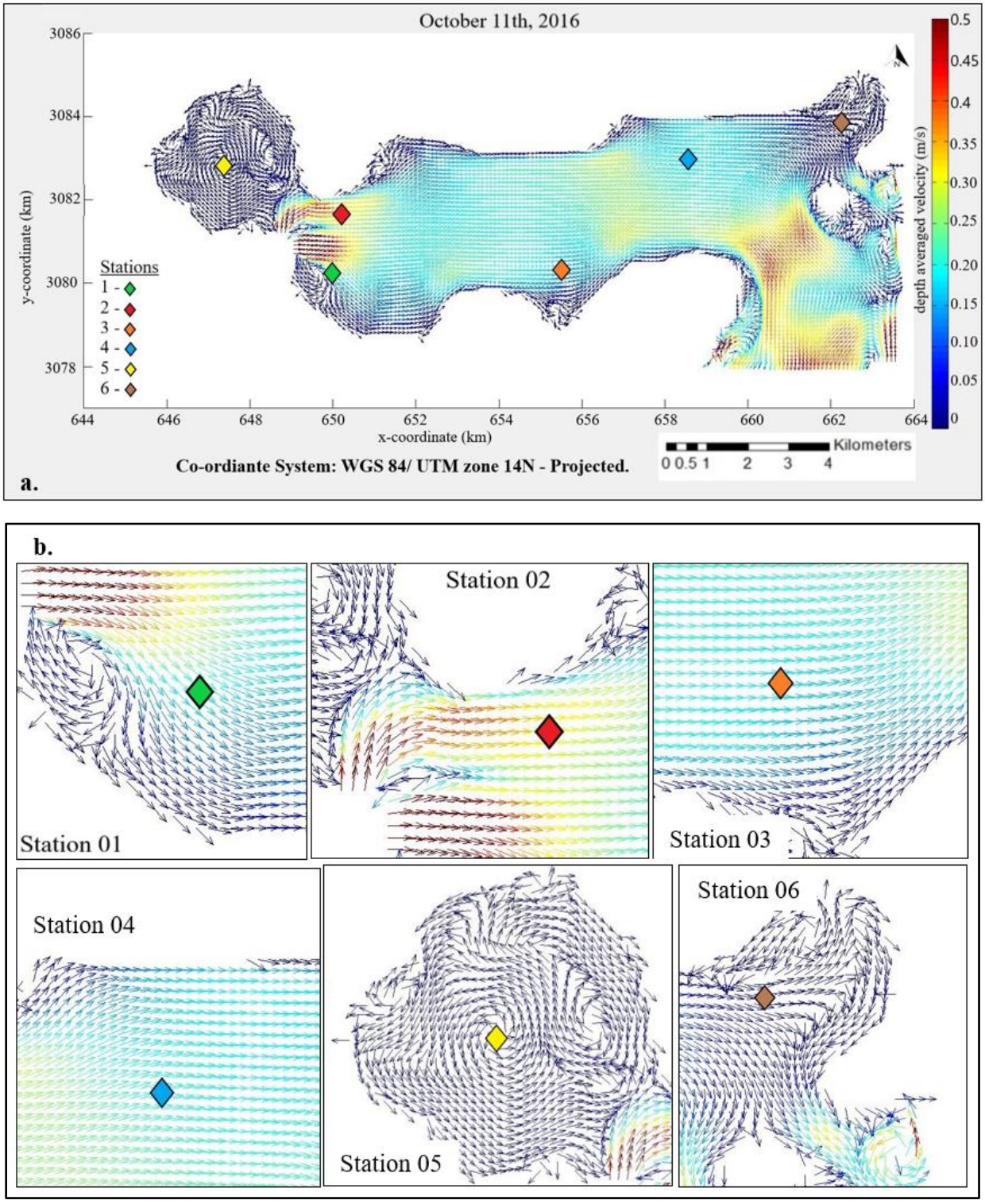

Figure I-15. Depth averaged water velocity variations simulated for Oct 11, 2016 at 12:00 am for a) all six stations, and b) magnified velocity vectors at each station.

Figure I-16 and I-17, shows the spatial variations of total nitrogen (mg/L) and chlorophyll-a (µg/L) concentrations throughout Nueces Bay, before (October 05th, 2016), during (October 13th, 2016) and after (October 22nd, 2016) the algal blooms event. Stations with high hydrodynamics and mixing conditions (stations 5 and 6) had lower chlorophyll-a concentration than stations that experienced lower hydrodynamics and mixing (stations 1-4). The insignificant changes in chlorophyll-a concentrations (Figure I-167b and I-17c) were suggestive of low hydrodynamics and mixing at station 1 (at the confluence of Nueces River and Nueces Bay). During the month of October 2016, the maximum inflow was 19.7 m^3/s (October 05th 2016) and a minimum of 0 m^3/s, with an average of 5.4 m^3/s. During HAB event (October 09 to 11) the daily inflow rate was about 5.0 m^3/s on average. From Figures I-16-17, it is evident that the inflows from Nueces River had little impact on the hydrodynamics activities at the confluence or at the discharge point of Nueces River into Nueces Bay and facilitated the growth of algae during the algal blooms event in October 2016.

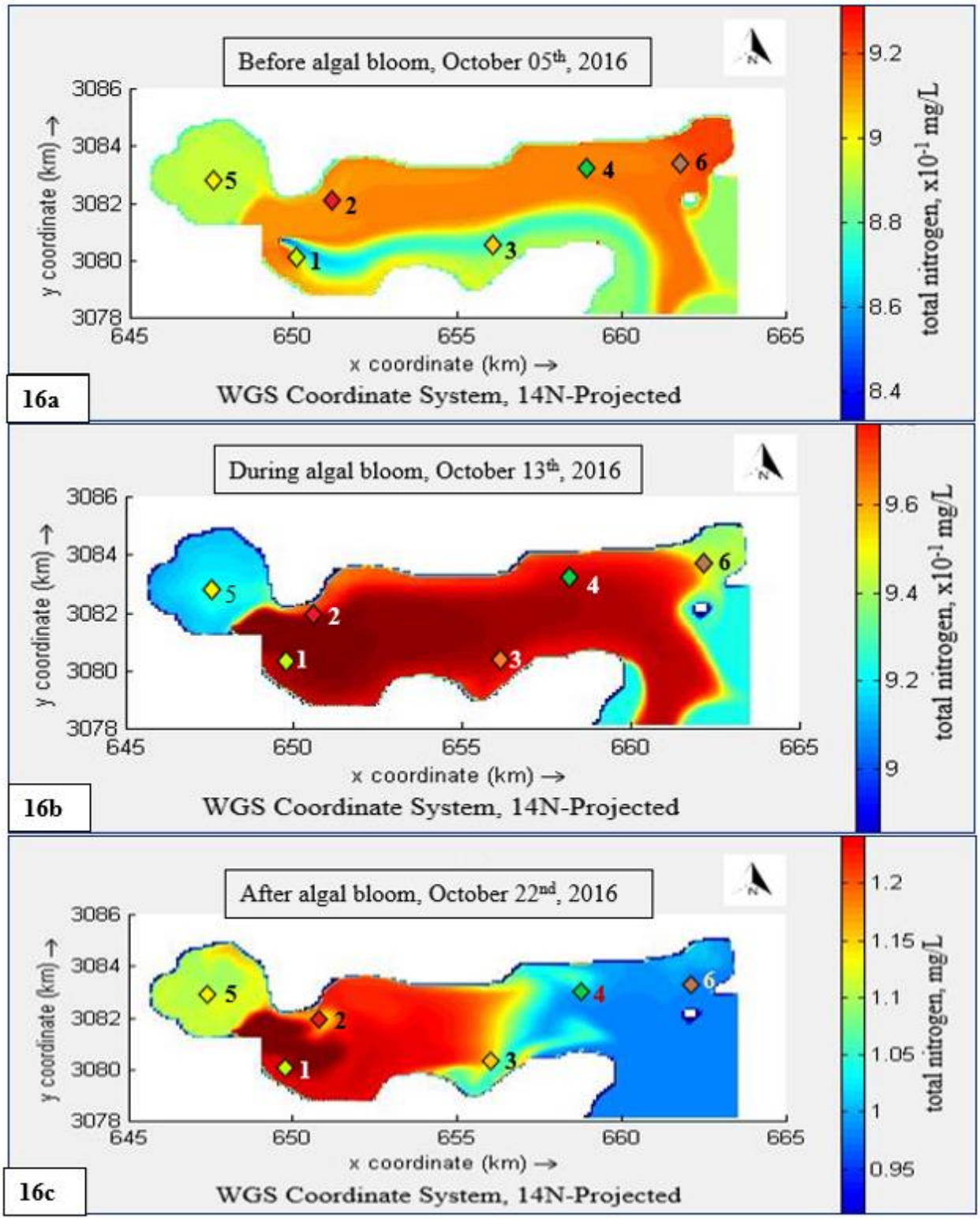

Figure I-16. Spatial variations of total nitrogen concentration, a) before algal blooms, b) during algal blooms, and c) after agal blooms.

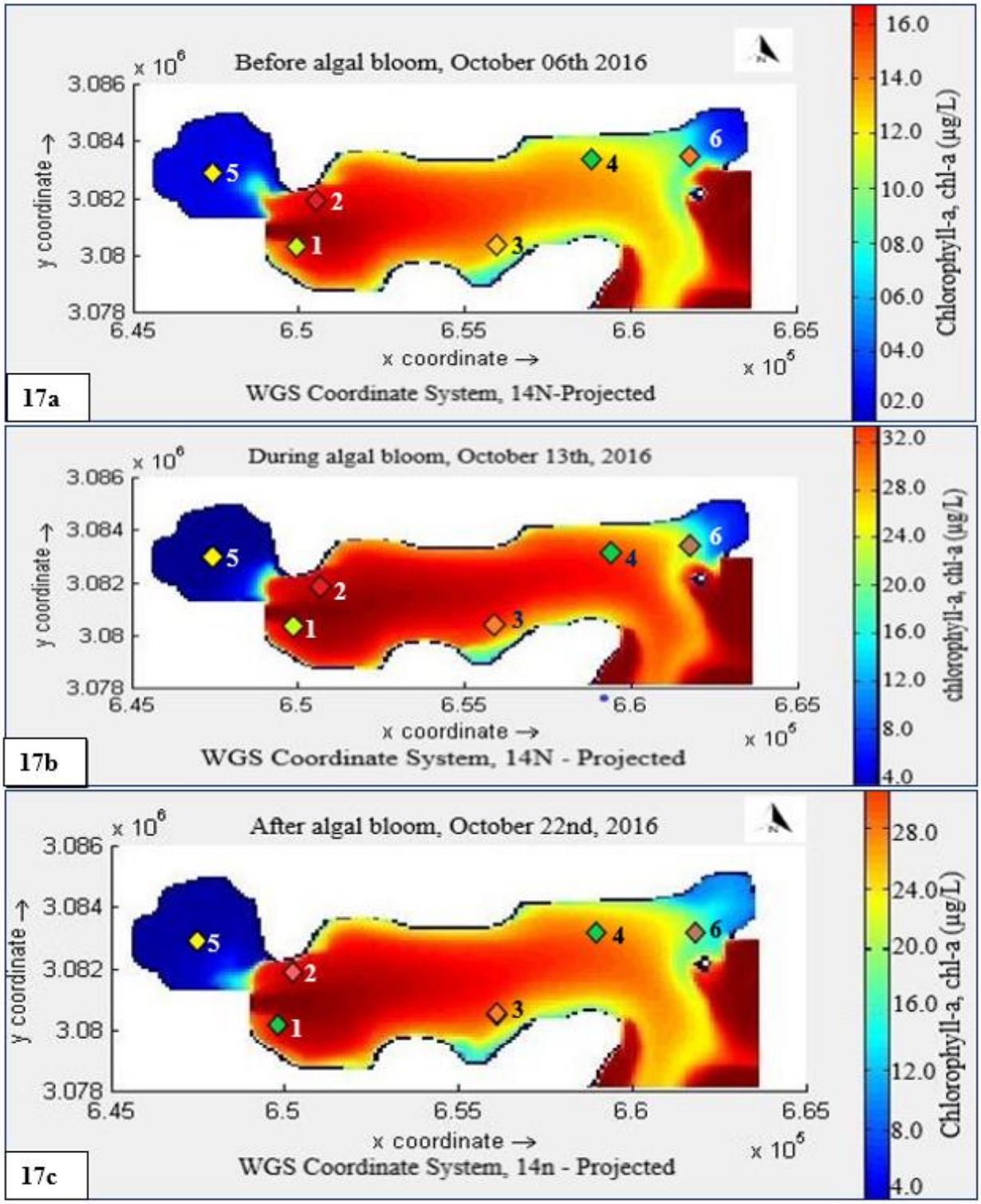

Figure I-17. Spatial variations of chlorophyll-a concentration, a) before algal blooms, b) during algal blooms, and c) after agal blooms.

Figure I-18a shows that as algal growth increased, the total nitrogen concentration decreased, which can be indicative of the use of nitrogen during the growth of algae and conversely, as total nitrogen increases the algal growth decreases (indication of addition of nutrients from detrital organic matter) (Deltares, 2018c; Vaz et al., 2019). Figure I-18b showed high correlation between the total nitrogen and algal concentration at stations 1-4 while weak correlations were observed at stations 5 and 6. Recalling that stations 1-4 have low hydrodynamic activities while stations 5-6 have higher hydrodynamic activities as shown in Figure I-15. Thus, the correlations between the total nitrogen and algal concentration are closely related to the hydrodynamic conditions at the observation/monitoring locations.

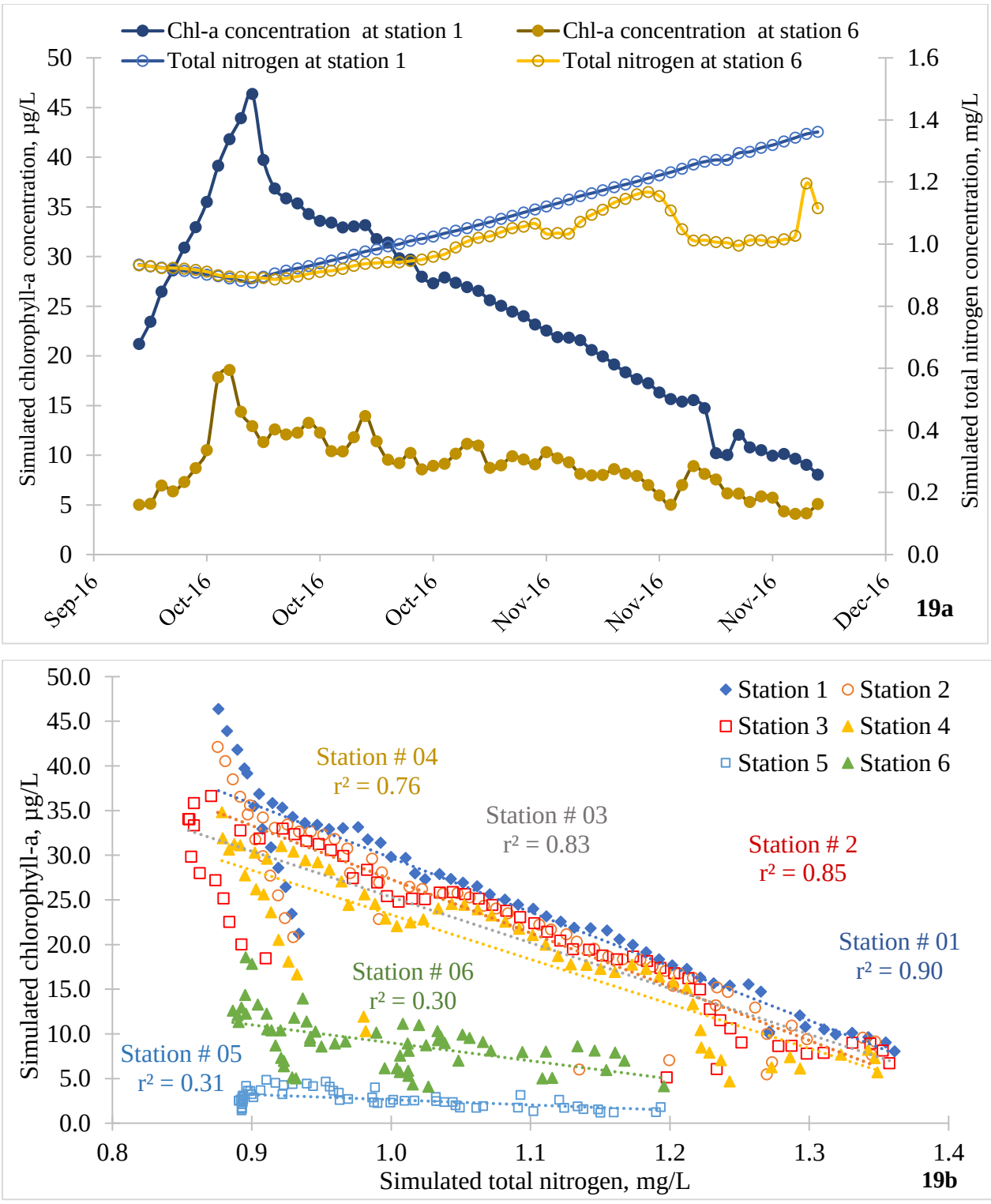

Figure I-18. a) Correlations of simulated algal concentration and available total nitrogen, and b) plot of algal (µg/L) and total nitrogen concentration (mg/L).

9.4.2 Scenario analysis on effects of inflows, wind speeds, temperature and nutrient loads

Figure I-19a shows that high inflows (with high total nitrogen and high chlorophyll-a inflows) reduced the algal growth in the Bay. Figure I-19b shows that with low flow and high chlorophyll-a concentration, there were no change on the algal growth. Figure I-19c shows that high inflows (with low total nitrogen and low chlorophyll-a) significantly reduce the algal concentration in the bay. Figure I-19d shows that algal growth increases due to high nutrient and chlorophyll-a loads at base inflows. This indicates that high nutrient and/or chlorophyll-a concentration can increase the algal growth and induce greater diversity (Yamamoto and Hatta, 2004). Figure I-19e shows that at low temperatures the algal growth is significantly reduced while at high temperatures the algal growth increases. Figure I-19f show that at high wind speed the algal growth is significantly reduced while at low wind speed the algal growth increases. The base model is the calibrated model. From October to November 2016 there was a maximum and minimum inflow of 19.7 (October 05th) and 0.0 m^3/s, respectively, and a mean of 2.7 m^3/s. The high/low values of inflows, total nitrogen, chlorophyll-a, wind speed and temperature, used in scenario simulations, are tabulated in Table I-8.

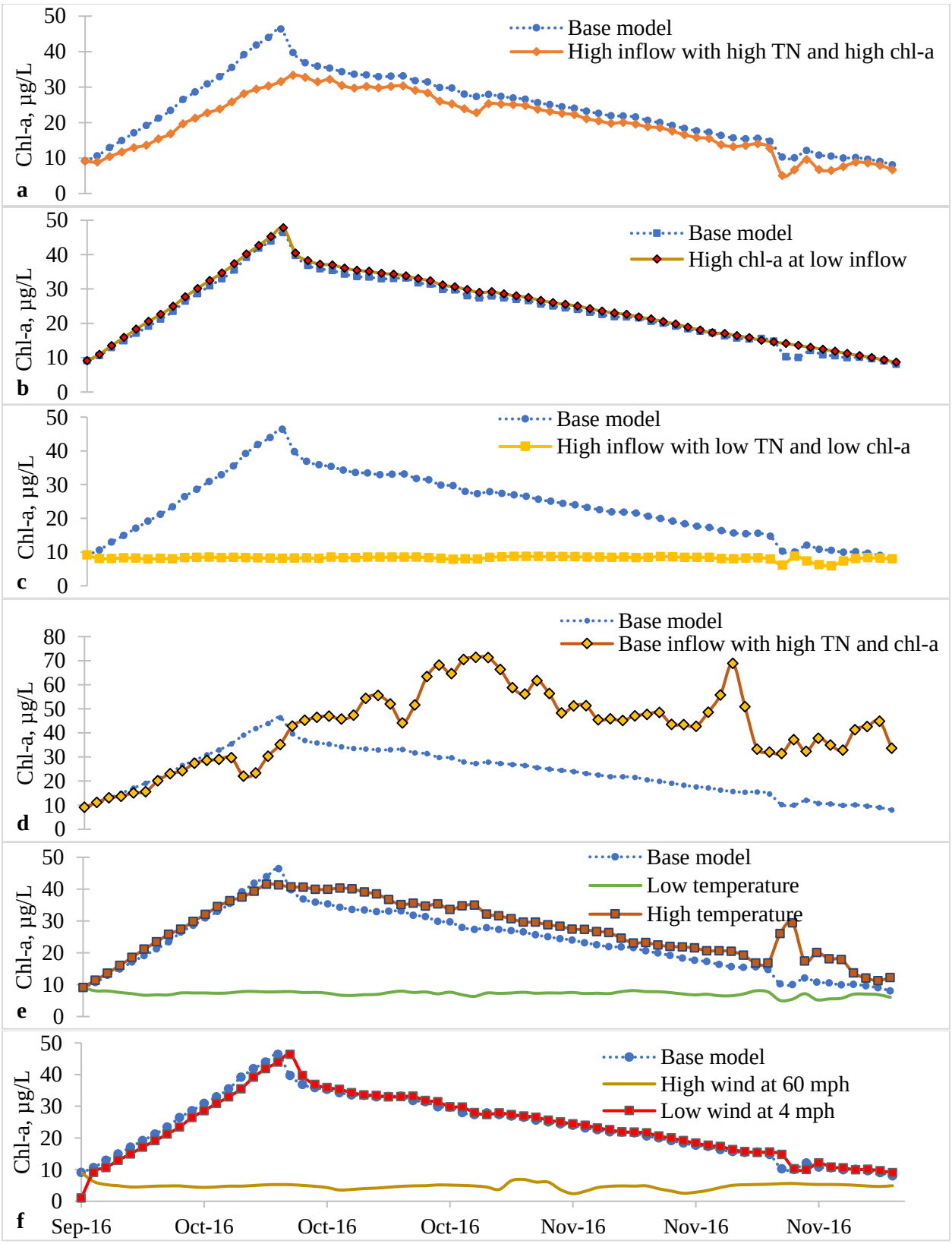

Figure I-19. a to f) Effect of various factors on algal growth (chl-a, µg/L).

10. CONCLUSIONS AND DISCUSSION

10.1 Summary and Conclusions

This study focused on setting up a model to simulate algal growth in Nueces Bay. The model showed very good performance ratings during calibration and validation of water levels, total nitrogen concentration and algal concentrations (Figure I-8-Figure I-10) with NSE and r^2 > 0.75 and PBIAS < 15%. The model was able to simulate the algal blooms event (Figure I-14a and 19a).

From the Delft3D-Wave standalone simulations, it was found that wave growths in Nueces Bay were dominated by wind and not by tidal forces (Figure I-7), that is, less than one foot of waves were formed with tidal forcing in the absence of wind.

Figure I-20a shows the wind-rose diagram for wind speed and wind directions during the month of October 2016, expressed as a percentage of all wind speeds for the whole month.

Figure I-20b shows the wind-rose diagram for wind speeds from August 2016 to August 2020 expressed as a percentage of all wind speeds during the whole period. Table I-13 shows the statistics for the wind speeds for October 2016 (during the HAB event) and for the whole simulation period. From

Figure I-20a and Table I-13, it can be seen that the wind speeds were < 6 mph (during October 2016) which is relative low, compared to wind speeds of other periods where average wind speed is around 10 mph (August 2016-2020). This indicates that there was little wave growth due to wind and thus lower hydrodynamics and mixing in the Nueces Bay during the HAB event. From Figure I-19f, it is evident that low wind speed (< 4 mph) facilitated algal blooms than high winds speed.

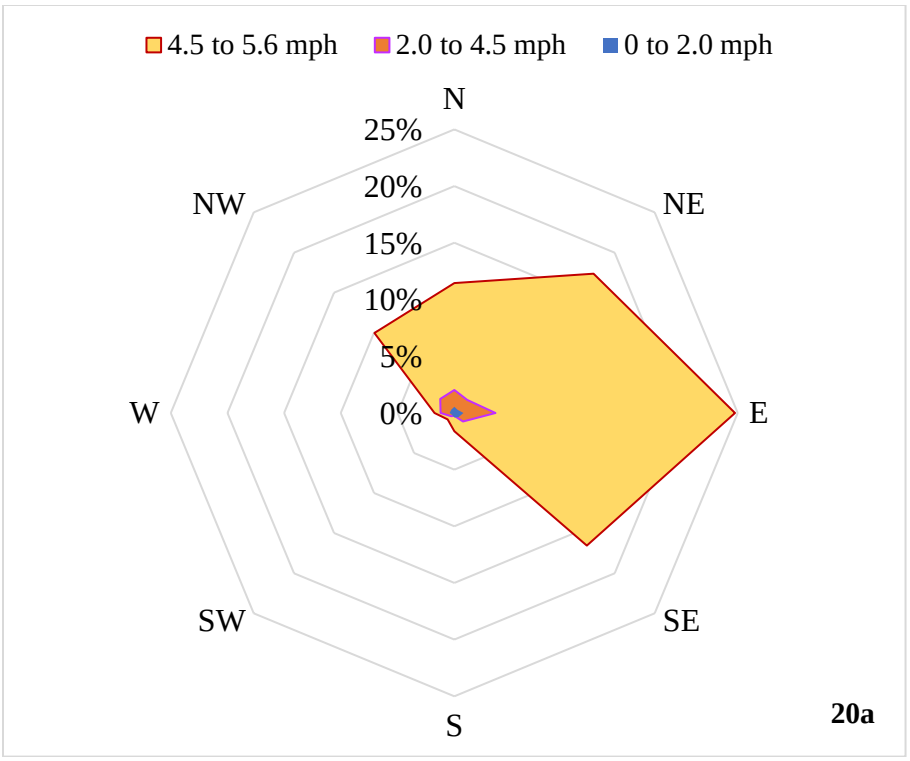

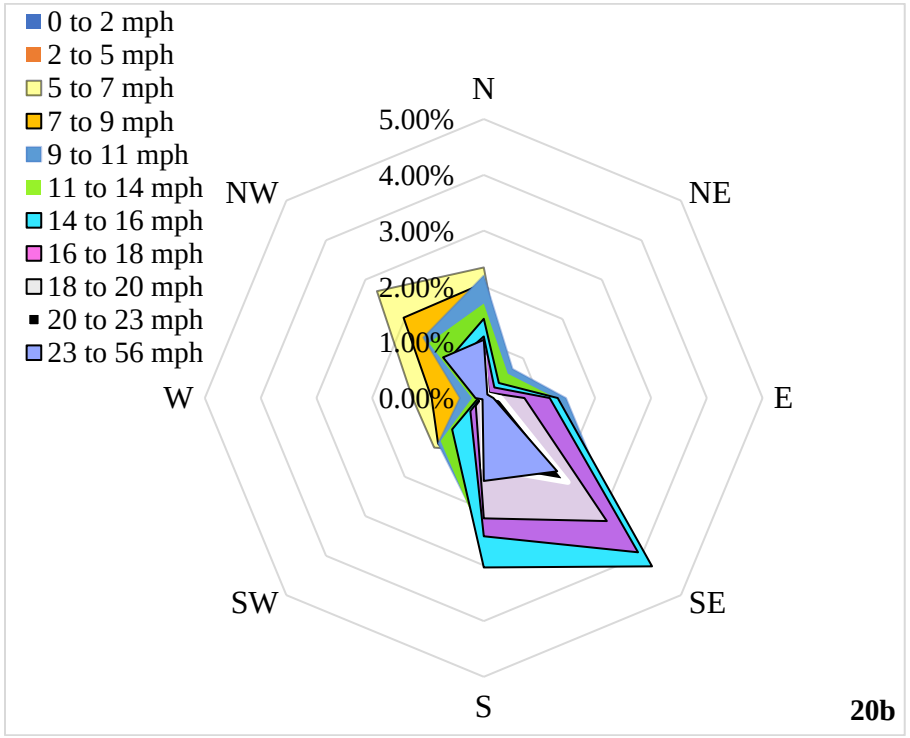

Figure I-20. a) Wind speed (as a percentage of all wind speeds) and wind directions for the month of October 2016, and b) Wind speeds (as a percentage of all wind speed) and wind directions between August 2016 to August 2020.

Table I-13. Wind speed statistics for whole simulation period of August 2016 to August 2020 and during HAB, October 2016

Wind speeds, mph	August 2016-2020	October 2016
Average speed, mph	10.42	4.46
Maximum speed, mph	58.69	5.60
Minimum speed, mph	0.00	0.00

Simulated hourly algal concentrations showed variations within a day reflecting the effect of sunlight, temperatures and other factors, on algal growths, mortality and respirations (Figure I-12). Sensitivity analyses showed that water temperature had the most impact on the simulated algal concentrations followed by the maximum production rate of algae (Sensitivity ≥ 50) (Figure I-13, Table I-12). This indicates that with the current global warming trends, that is, increasing temperatures, HABs are likely to occur at higher concentrations and frequencies in coming years. The maximum production rate is a function of nutrient availability, dissolved oxygen, radiation flux, temperature, pH and salinity (Vaz et al., 2019). This cycles back to temperature rise, which can affect the dissolved oxygen concentrations, pH, and the maximum production rate of algae.

From spatial variations it was observed that as the monitoring stations moved from the confluence of Nueces River and Nueces Bay (NR-NB) to the confluence of Nueces Bay and Corpus Christi Bay (NB-CCB), the hydrodynamic activities and mixing relatively increased, with high activities at NB-CCB confluence (Figure I-14). The Nueces Bay exhibited uniform behavioral pattern except at the vicinity of the confluences of NR-NB and NB-CCB. Higher algal (≥ 100 µg/L) and total nitrogen concentration (3.0 mg/L) inflows from Nueces River increased the algal concentration in Nueces Bay and have the potential to induce algal blooms (Figure I-19). Simulations at high wind speed of about 60 mph showed that the algal growth and concentrations decreased (≤ 10.0 µg/L) (Figure I-19). Except during the HAB event in October 2016, the algal concentrations remained below 20 µg/L throughout the simulation period, indicating that Nueces Bay was not eutrophic other than in October 2016 (Figure I-14). High freshwater inflows (≥ 80 m^3/s) increased hydrodynamics and mixing and reduced the algal growth. Thus, it is evident that freshwater inflow rates are an essential component in the health of the ecosystem of the bay and prevention of algal blooms (Figure I-19). Simulations also showed that chlorophyll-a or algal inflows from Nueces River increased algal concentrations in the bay (Figure I-19).

Algal growth is a complex dynamic process which is dependent on many biotic and abiotic factors, which in turn is dependent on each other (Blevins, 1997; Powley et al., 2017b; Vaz et al., 2019). For example, algal growth is dependent on sunlight, production rates, respiration rates, which in turn is dependent on water temperatures and dissolved oxygen as well. This study made an effort to incorporate the key processes identified based on literature reviews and focused on freshwater inflows and nitrogen as the limiting nutrient in relation to algal growths. Although there are rooms for improvement to the model, this model can serve as a reconnaissance study or as a tool to assess the algal biomass in the Nueces Bay using the sparingly available water quality data for Nueces Bay. This model can also be used to simulate algal growths in Nueces Bay for different environmental conditions which can be anticipated to be onset by anthropogenic activities and climate changes. This in turn can help coastal managers to take necessary actions to mitigate or prevent any environmental hazards.

10.2 Discussion

This study included a range of factors and processes to investigate the hydro-, nitrogen and algal dynamics in relation to algal blooms in Nueces Bay. Algal growth is a complex and dynamic process (Blevins, 1997; USGS, 2004) with many factors governing its growth. There is room for improvements to this model since there are few processes which this study did not investigate. For example, the current model did not investigate the different species of algae responsible for HAB but rather focused on overall algal biomass. The advantage of this approach is to provide a reconnaissance study to allow the evaluation of factors underlying algal growth. Thus, the model developed in this study can be used to set guidelines to evaluate the criteria of algal growth in estuarine, for example, nutrient loads, temperature, and freshwater inflows. The disadvantage of this approach is that, not all algae produces toxins responsible for harmful effects caused during blooms. There are certain species of algae, for example, K. Brevis, which is predominant during “red tides” and releases harmful toxins (Magaña et al., 2003). Apart from the presence of harmful species/toxins, algal blooms or eutrophication itself (in the absence of toxic species) can cause environmental damage, by exerting more oxygen demands (during and after blooms), reducing light penetration, and taking up nutrients during blooms (EPA, 2000; Katin et al., 2019; Kristin, 2011; Ritter and Montagna, 1999). Therefore, looking into different species during algal blooms

can add further knowledge of the key species responsible for toxin releases, toxin concentrations and their impacts on the environment and human health.

From scenarios analyses (Figure I-19), it was observed that high nutrient (3.0 mg/L) inflows increased algal growth. High algal inflows (or chlorophyll-a ≥ 100 µg/L) from Nueces River to the Nueces Bay also increased the algal growth in Nueces Bay. High nutrient inflows are the results of anthropogenic activities, for example, chemical fertilizers in agricultural runoffs and farm applications, which is expected to increase in the future to meet food demands (Alexandratos, 2012). This increase in nutrients in the surface runoff eventually reaches the streams and rivers. Stream and rivers are primarily phosphorous limited (Turner and Chislock, 2010; Turner et al., 2015) and can lead to increased algal growth from these nutrients. This high concentration of algae in the river is carried to the bay, together with nutrients, act as a pulse input to the bay which can promote diversity and growth in phytoplankton or algae (Bowman et al., 2008; Ciampitti and Vyn, 2014; Ruddy et al., 2006; Smil, 1999; Stewart, et al., 2005, 2005; Yamamoto and Hatta, 2004). Thus, continuous high freshwater inflows are vital to estuarine health, as it can reduce the concentration of nitrogen algae reaching the bay. This, in turn, can diminish the effect of pulse-input and reduce the biodiversity and algal growth. Also, floating surface "skimming" barriers could be installed at the Nueces River at the upstream of confluence (Nueces River – Nueces Bay) and also along the Nueces Bay causeway to remove and harvest algae from the surface and preventing algal inflows in Nueces Bay and Corpus Christi Bay. This could potentially reduce the induction of algal growth/blooms in the bays. The harvested algae can also be utilized in the production of biofuels using this process. "No Harm" solutions (Levy, 2020) can be used to remove algae and nutrients from water bodies, where the algae harvested for biofuel production as well. These methods could be utilized in rivers to prevent HABs in bays, and in lakes, bays, and estuaries to remove surface algae in existing HABs region.

Algal growth near station 6 exhibited large fluctuations and low algal concentration due to the hydrodynamics and mixing with the Corpus Christi Bay (Figure I-14-18). Stations 1-4 showed lower hydrodynamics activities and high algal growth or concentrations, indicating that higher hydrodynamics and mixing is also essential to prevent potential algal blooms and avoid environmental hazards. The tidal exchange of algae from Nueces to Corpus Christi Bay can also act as a nutrient and algal pulsed input for Corpus Christi Bay, which can favor diversity in algal species and promote growth of algae in Corpus Christi Bay (Yamamoto and Hatta, 2004). Since

Nueces Bay is relatively shallow, the mixing in the waterbodies can be increased by promoting recreational activities, for example, speed-boat riding, jet skiing and other similar activities, especially from September to December (since, historically, algal blooms were observed during this period). This can potentially prevent algal blooms in the bay.

Station 5 showed trends of high mixing with low algal concentrations. Since station 5 is near the model's enclosed land-water boundaries, where there are marshes in the proximity, the velocity vector lines exhibited that there were intermixing within the waters causing mixing and resulting in lower algal concentrations (Figure I-15). Marshes can affect the hydrodynamics and algal growth due to its shallow depth and high thermal stratification. Due to the presence of high concentrations of aquatic species in marshes, the dissolved oxygen is usually low (Blevins, 1997). The deficiency of dissolved oxygen is met by denitrification of nitrate for respiration and maintenance of the species. Nitrogen through atmospheric deposition (dry and wet) has the potential to induce algal growth in the marshes as well. Thus, the processes and compartments of nitrogen in marshes and/or wetlands are complex (Blevins, 1997; USGS, 2004). The effect of the marshes and its nutrient cycling were not studied in the current model. Thus, marshes and its effect on nitrogen cycling can be added to the model to further improve its performance in simulating algal concentrations and blooms.

The model can also be refined by including sediments and nutrients transported through sediments, which can also be responsible for algal blooms. Nitrification, denitrification, and nutrient transport through sediment is important in coastal water algal blooms (Chen and Mynett, 2006). Algae prefers ammonia over nitrate (Deltares, 2018a) during growth. Since, this study focused on the total nitrogen concentrations, the nitrogen species and its factor in algal growth were not investigated. Addition of nitrogen through atmospheric deposition and tidal exchanges with Corpus Christi Bay were not studied. About 25 to 33% of net tidal entrainments and inflows occur through the adjacent bays and almost 8% of total nitrogen is deposited through dry and wet atmospheric deposition in the Nueces Estuary, although, about 40% of the nutrient is lost through denitrification from Nueces Bay (Brock, 2001). Thus, the integration of atmospheric deposition and speciation of total nitrogen can also improve the model's accuracy in simulating algal growth.

The model could be improved if more data, for example, nutrients and chlorophyll-a, were available at a finer temporal resolution, especially before, during and after an algal bloom was observed. Also, data at different points in space of Nueces Bay and Corpus Christi Bay could help

further refine the model in both space and time. These could be achieved if remote sensing devices could be employed to measure/record different water quality quantities. Observed data points for total nitrogen and chlorophyll-a were sparingly available (in terms of temporal resolution). Since collection and laboratory testing for nutrients and chlorophyll-a could be economically unfeasible, application of Bootstrap method using sample/learning data and accounting for uncertainties, can generate large datasets which can be used in calibration and validation, in situations where few data points are available (Jones et al., 1996; Lee et al., 2019). The high temporal resolution data is desirable because algal growth is a dynamic and exponential process happening within minutes, and to understand this process in-depth, large dataset would facilitate in greater accuracy of models and understanding. Thus, implementation of Bootstrap method using historical data to generate (estimate) large dataset and using it in model simulation and calibration can have significant impact on model's refinements and improvements, as well as understanding the processes.

PART II. MODELING NITROGEN LOADING AND ITS RELATIONSHIPS TO FRESHWATER INFLOWS FROM NUECES RIVER BASIN

To better understand the relationships between anthropogenic activities, hydrologic processes and water quality changes under a changing climate, this part of the project focused on the examination of the relationship between freshwater inflows and nitrogen loadings, nitrogen species and DO concentrations. The SWAT (Soil and Water Assessment Tool) model was employed to simulate the hydrological and transport processes in the Nueces River Basin (NRB). The sensitivity of the input parameters of the model for simulating stream flow and total nitrogen loadings was also examined.

1. MODEL DESCRIPTION

The SWAT model was set up using the integrated ArcGIS geodatabase, Digital Elevation Models (DEM), raster store master database and ArcSWAT based on work conducted by fellow researcher (Mr. Siavash Bassam, PhD candidate at Texas A&M University-Kingsville) and funded by the City of Corpus Christi (Bassam and Ren, 2018). A DEM model of 100 m x 100 m grid was used. Automatic watershed delineation via ArcSWAT was used for the NRB. The total area of the watershed simulated is 1,029,071 km^2 (Figure II-1). A total of 129 sub-basins with 3387 hydrologic response units (HRUs) covering the entire watershed (Figure II-2) were used. Each HRU is approximately gridded as 17.5 km x 17.5 km.

Figure II-1. Nueces Watershed (Source: ArcSWAT and Google Pro).

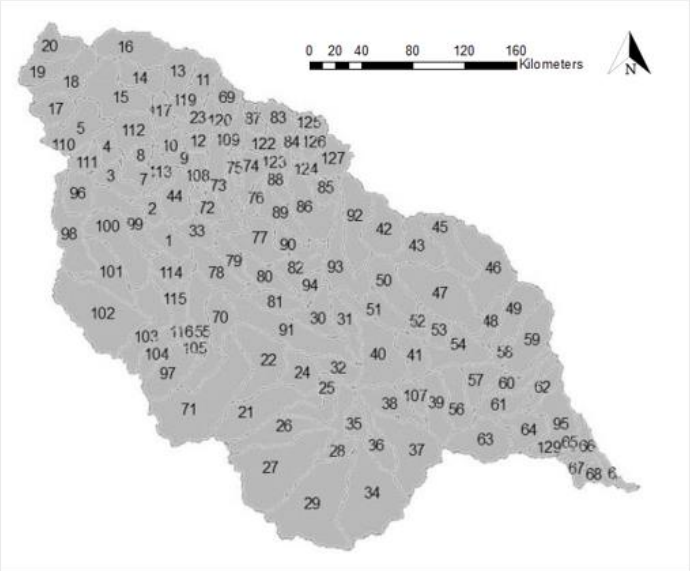

Figure II-2. Nueces Watershed showing sub-basins (Source: ArcSWAT).

"WGEN_CFSR_World_1979_2014" Global weather database was integrated in the statistical "Weather Generator Data" of the SWAT model to allow statistical forecasting of the model up to the year 2100. The CFSR was designed and executed as a global, high resolution, coupled atmosphere-ocean-land surface-sea ice system to provide the best estimate of the state of these coupled domains over the period 1979-2014 (global weather, TAMU, http:\\globalweather.tamu.edu).

To simulate the recent events and years (2011 -2019), the weather data including wind speed, rainfall, temperature, relative humidity, and solar radiations were obtained from existing datasets from 14 different stations (Table II-1, Figure II-3). The datasets were collected from NCEI (National Centers for Environmental Information) of NOAA (National Oceanic and Atmospheric Administration) and distributed among the sub-basins using Theissen polygon method (Figure II-4). Atmospheric deposition, soil data, land use data, sub-basin and drainage data, groundwater data, water use data, soil water quality data, discharge data, fertilizer application, and stream water quality data were used to simulate flows and nutrients in the surface runoff.

Table II-1. List of stations used in SWAT model for collecting weather data.

SL NO	STATION_ID (NCEI)	STATION NAME
1	WBAN:12932	ALICE INTERNATIONAL AIRPORT, TX US
2	WBAN:00127	BEEVILLE MUNICIPAL AIRPORT, TX US
3	WBAN:12947	COTULLA LA SALLE CO AIRPORT, TX US
4	WBAN:00270	FAITH RANCH AIRPORT, TX US
5	WBAN:12985	GARNER FIELD AIRPORT, TX US
6	WBAN:12962	HONDO MUNICIPAL AIRPORT, TX US
7	WBAN:12907	LAREDO INTERNATIONAL AIRPORT, TX US
8	WBAN:12974	ORANGE GROVE, TX US
9	WBAN:00130	PLEASANTON MUNICIPAL AIRPORT, TX US
10	WBAN:12984	ROBSTOWN NUECES CO AIRPORT, TX US
11	WBAN:12909	SAN ANTONIO KELLY FIELD AFB, TX US
12	WBAN:12970	SAN ANTONIO STINSON MUNICIPAL AIRPORT, TX US
13	USW00012924	CORPUS CHRISTI INTERNATIONAL AIRPORT, TX, US
14	72236323098	ROCKSPRINGS, TX, US

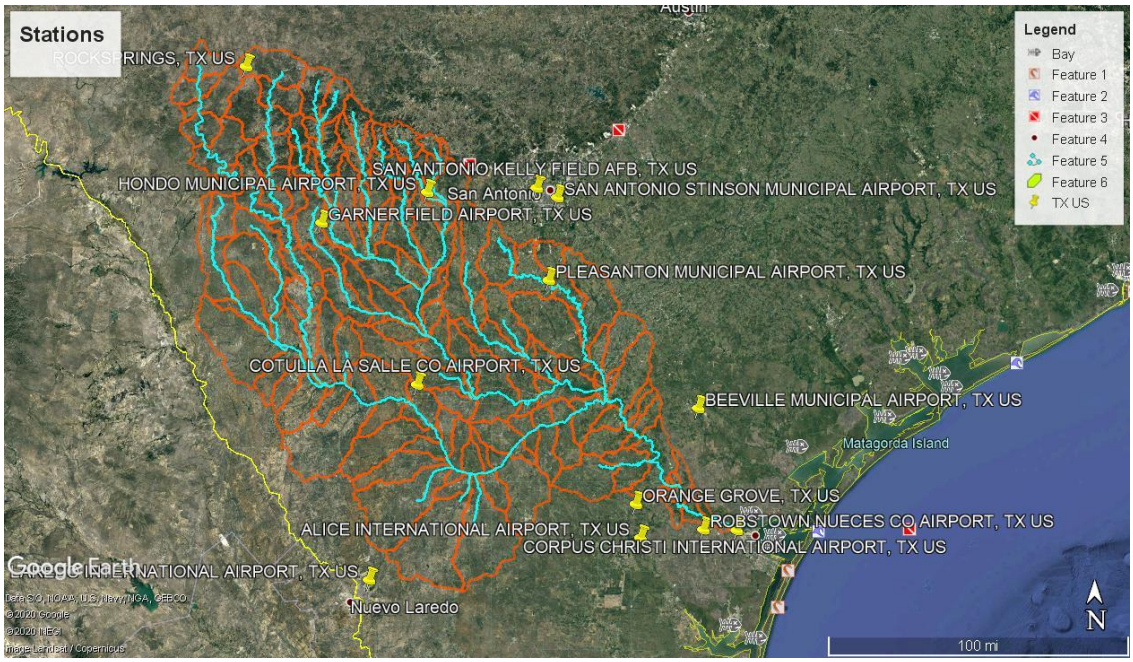

Figure II-3. Nueces watershed with dropped pins showing the NCEI stations used (Source: ArcSWAT, NCEI and Google Pro).

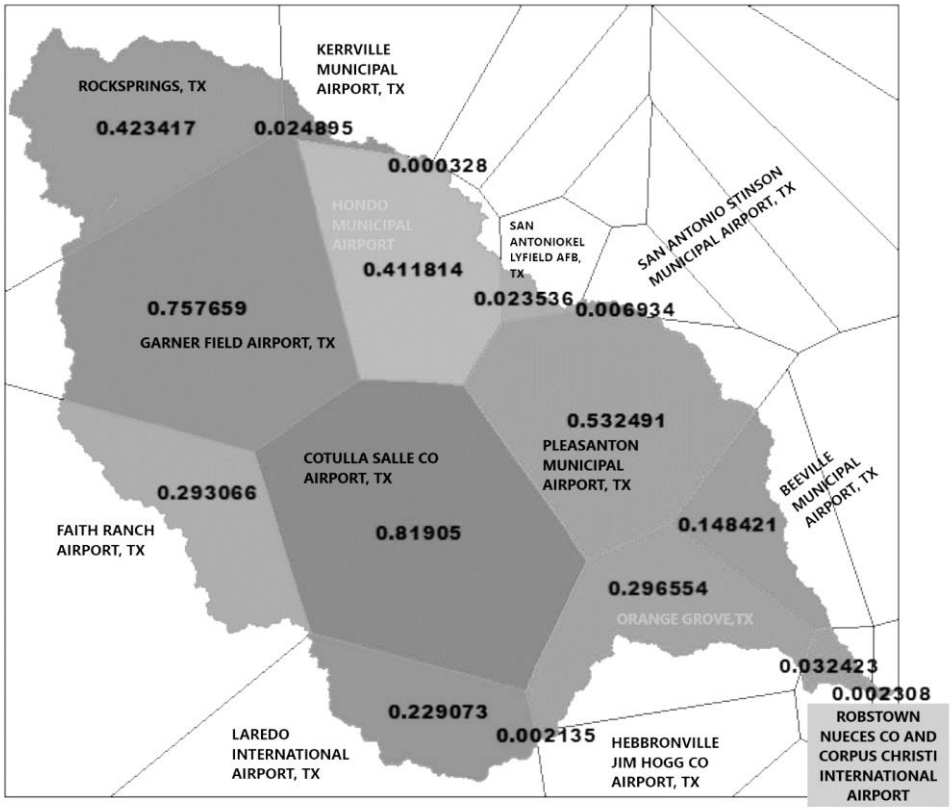

Figure II-4. Nueces watershed showing contribution of different weather station after Theisen polygon distribution.

Table II-2 tabulates the key model input parameters and their initial values used in SWAT to simulate monthly average flow and monthly average total nitrogen from the NRB. The model included inflows from different points along the Nueces river. It also incorporated the two reservoirs of the watershed as shown in Figure II- 5.

Table II-2. Key model input parameters for simulation and calibration of flow and total nitrogen.

No.	Input Parameters	Description of Parameters	Initial Values	References and Sources
1	CN2	SCS runoff curve number. SCS defines three antecendent moisture conditions. i. dry (wilting point), ii. Average moisture, iii. Wet (field capacity). CN2 is the moisture condition II curve number	0.1	(Abbaspour et al., 2015a; Arnold et al., 2011; Brouziyne et al., 2017)
2	SURLAG	Surface runoff lag coefficient (days)	5.00	
3	OV_n	Mannings 'n' value for overland flow	0.02	
4	EPCO	Soil evaporation compensation factor. It is used to meet the potential water uptake compensated by the lower layers of soil	0.50	
5	ESCO	Plant uptake compensation factor. This coefficient is used to modify depth distribution used to meet the soil evaporative demand.	0.50	
6	ALPHA_BF	Baseflow alpha factor (days) relating to goundwater flow.	0.01	
7	GW_DELAY	Groundwater delays (days)	5.00	
8	GWQMN	Threshold depth of water in the shallow aquifer required for return flow to occur (mm)	10.00	
9	SOL_AWC	Available water capacity of the soil layer (mm H_20/mm soil)	0.25	
10	SOL_K	Saturated hydraulic conductivity (mm/hr)	5.00	
11	RCN	Concentration of nitrogen in rainfall (mg N/L)	1.00	(Abbaspour et al., 2015b; Arnold et al., 2011; Jung & Kim, 2017; Wu & Chen, 2009)
12	CDN	Denitrification exponential rate coefficient; to control the rate of denitrification.	1.4	
13	CMN	Rate factor for humus mineralization of active organic nutrients (N & P)	0.0003	
14	N_UPDIS	Nitrogen uptake distribution parameter.	20.00	
15	NPERCO	Nitrate percolation coefficient; controls the amount of nitrate removed from the surface layer in runoff relative to the amount removed via percolation. NPERCO of 0.0 means that the concentration of nitrate in the runoff approaches 0 & 1.0 means that the surface runoff has the same conc. of nitrate as the percolate. Default = 0.20	0.20	
16	RSDCO	Residue decomposition coefficient; the fraction of residue which will decompose in a day assuming optimal moisture, temperature, C:N ratio and C:P ratio. Default = 0.05.	0.05	
17	BC1	Rate constant for biological oxidation of NH_4 to NO_2 in the reach (day^{-1})	0.10	
18	BC2	Rate constant for biological oxidation of NO_2 to NO_3 in the reach (day^{-1})	0.10	
19	BC3	Rate constant for hydrolysis of organic N to NH4 in the reach (day^{-1})	0.02	
20	BC4	Rate constant for organic phosphorous mineralization at 20 C (day^{-1})	0.35	

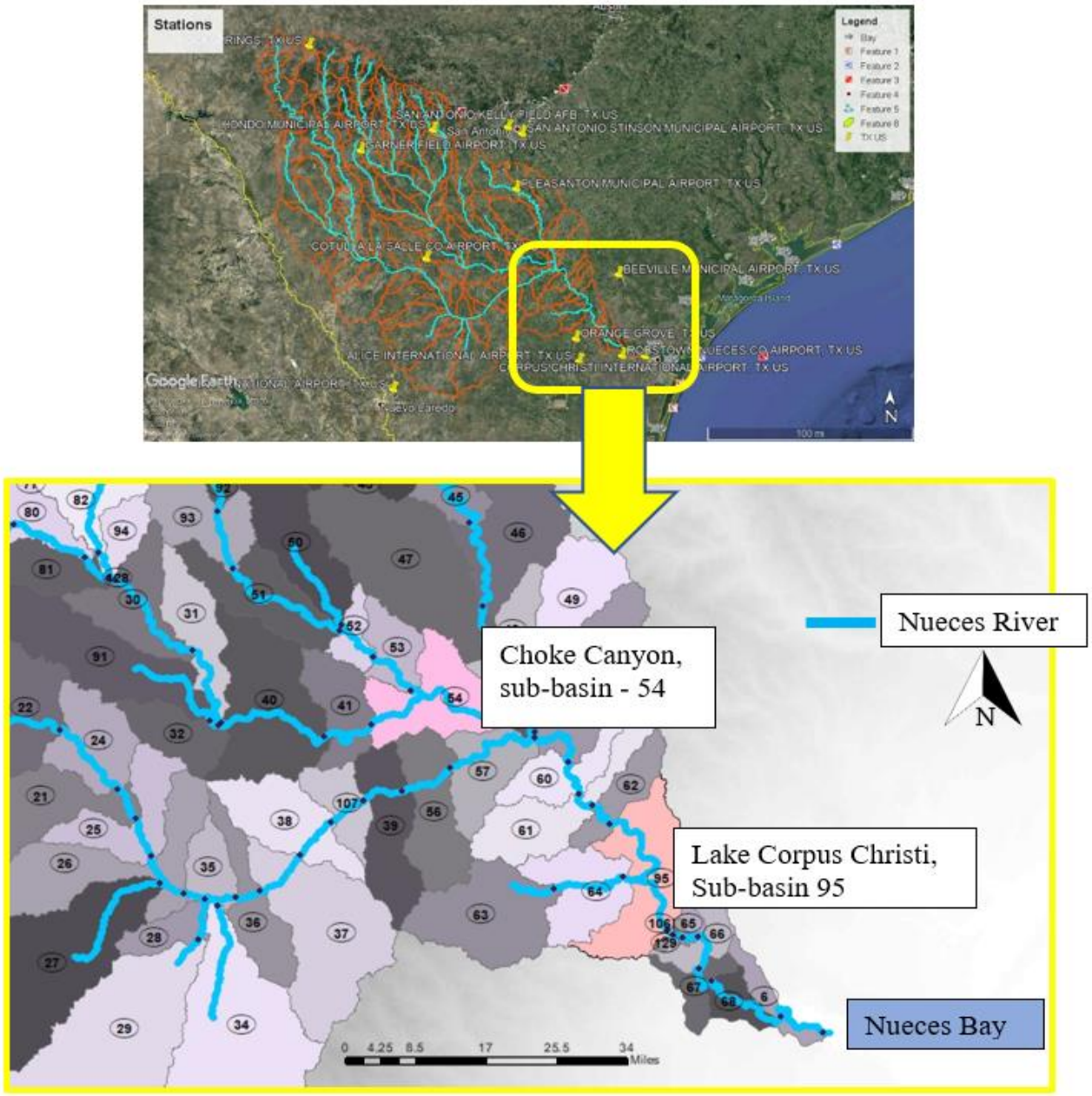

Figure II-5. Location of the two reservoirs (sub-basins 54 and 95, respectively as highlighted).

The model inputs also include weather data, that is, rainfall, temperature, and wind speed, obtained from available stations and the relative humidity and solar radiation obtained using the weather generator. Average monthly flow recorded at the USGS station ID # 08211500 was used to represent the average flow coming from the entire watershed. Average monthly nutrient load discharge recorded at the TCEQ station ID # 12960 was used to represent the average monthly nutrient load discharge input from the entire watershed. TCEQ station 12960 (near the confluence

of Nueces Bay and Nueces River) is 11.6 km downstream of USGS station 08211500 (Figure II-6). Both these stations were used because they are at the most downstream points of the watershed. Geographically, the entire Nueces watershed converged into a single stream, after Calallen Dam, and these stations are located on that single stream. Thus, data from these points were assumed to be representative of the flow and nutrient loads of the entire watershed before they are discharged into Nueces Bay. These stations were chosen because USGS 08211500 did not have any nutrient data (thus flow data was used) and TCEQ 12960 did not have any flow data (thus nutrient data was used). Thus, a combination of data from these two stations were used for calibration and validation of the model. It was also assumed that from USGS 08211500 to TCEQ 12960, there were little to no contribution of additional flow and nutrients to the Nueces River.

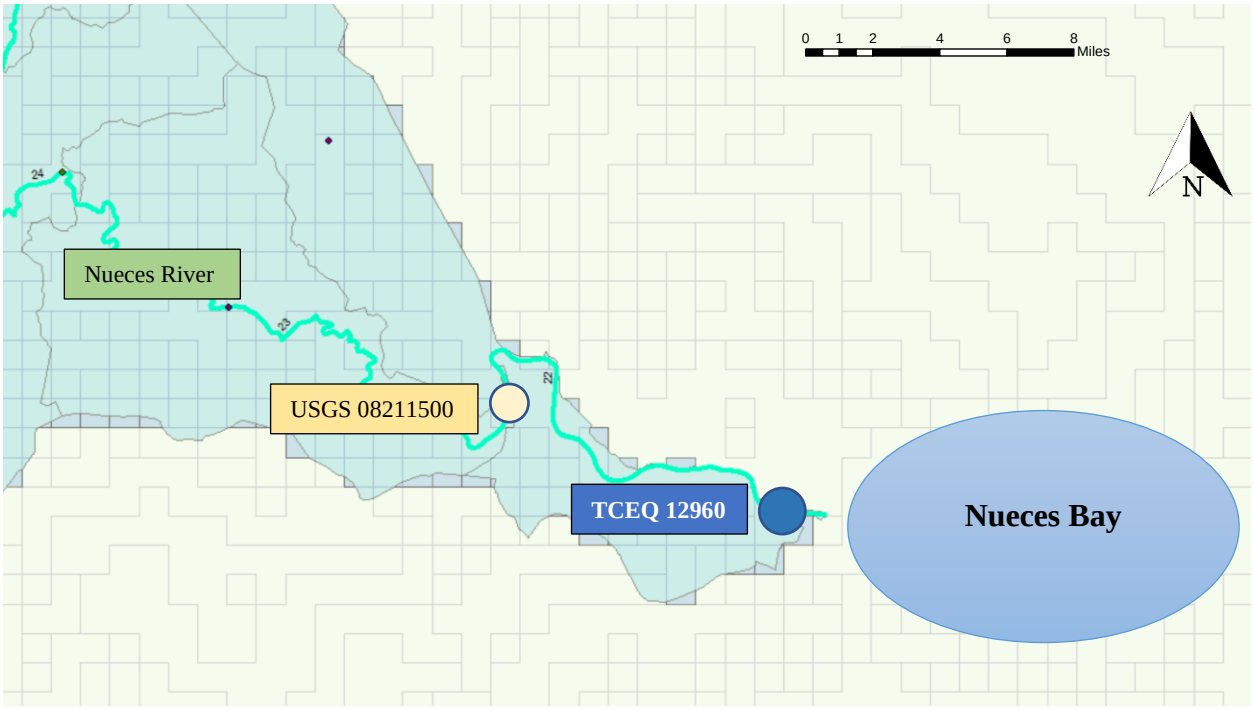

Figure II-6. Section of Nueces watershed showing the two stations USGS 08211500 and TCEQ 12960 used for this study.

2. MODEL CALIBRATION, VALIDATION, AND APPLICATION

Performance of model calibration for flow is evaluated using Nash-Sutcliff Efficiency (NSE) coefficient and coefficient of determination (r^2) as goal functions as described in Part I. Guidelines to test model performance using NSE are from Moriasi et al. (2007) (see Table I-6). For total nitrogen calibration and validation, coefficient of determination (r^2) was used as goal function. After model calibration, the calibrated model was run to obtain inflows and total nitrogen data for the period of January 2011 to December 2019. The data were plotted to examine the relationship between freshwater inflows and nitrogen loadings, nitrogen species and dissolved oxygen loadings/concentrations.

3. SENSITIVITY ANALYSIS

Global Sensitivity analysis was conducted via multiple regression analysis on input parameters to observe model's response and parameter sensitivity. t-stat which measures the precision with which the regression coefficient is measured (coefficient of parameter/standard error) was calculated. Large t-stat values indicate that the parameter is sensitive to the model. A large t-stat corresponding to a low p-value ($p<0.05$) indicates that the variable is having an effect on the model's response with 95% or more probability of correctness. t-stat and p-values were extracted using SWAT-CUP (SWAT-Calibration and Uncertainty Program). Parameters were ranked according to the t-stat and p-values.

Local Sensitivity analysis was conducted by changing each parameter with respect to the calibrated values while keeping all other parameters constant, using Equation 26 (see Section 7.3 of Part I). Relative impacts of each parameter on total sensitivity (percentage S) were calculated to rank the local sensitivities.

3. RESULTS

3.1 Model calibration and validation of stream flow

From Figures II-7 and 8, it was observed that the NSE and r^2 for flow were found to be 0.79 and 0.72, respectively, during calibration. Calibration period was from January 2011 to May 2015 and validation period was from June 2015 to December 2018. For NSE value of 0.79, a "very good" performance can be rated for the model. During validation, NSE and r^2 values of 0.72 and 0.73, respectively, were observed which showed "very good" performance rating as well. CN2 was found to be the most sensitive parameter during the peak flow calibration.

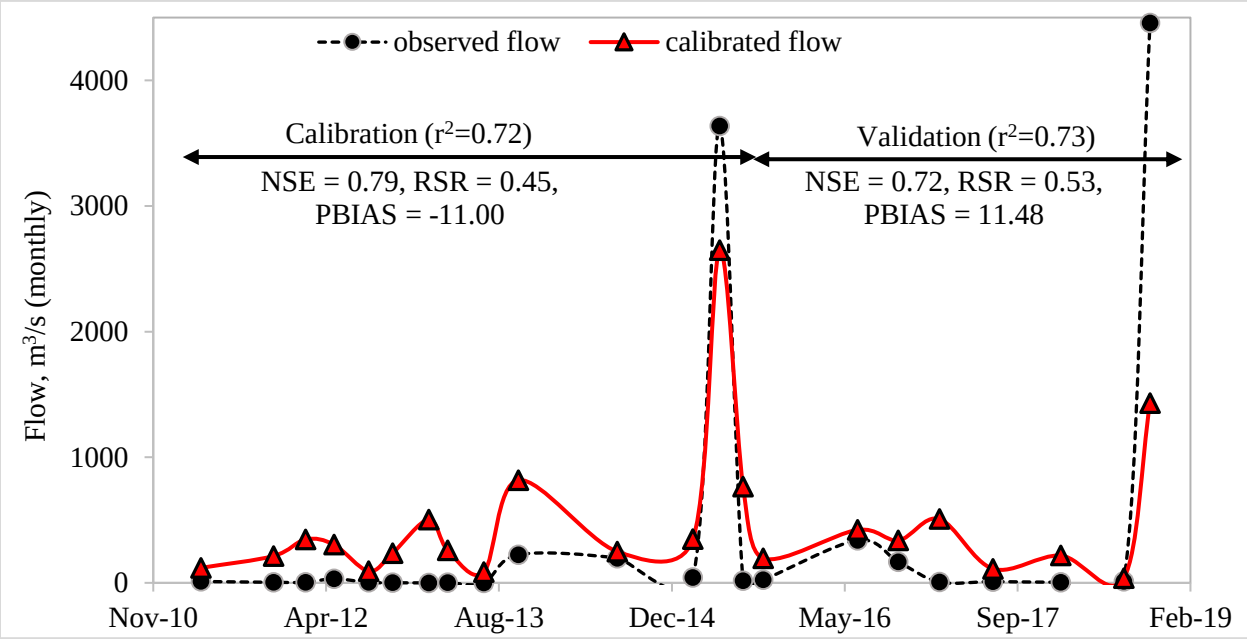

Figure II-7. Time series of observed and simulated flows.

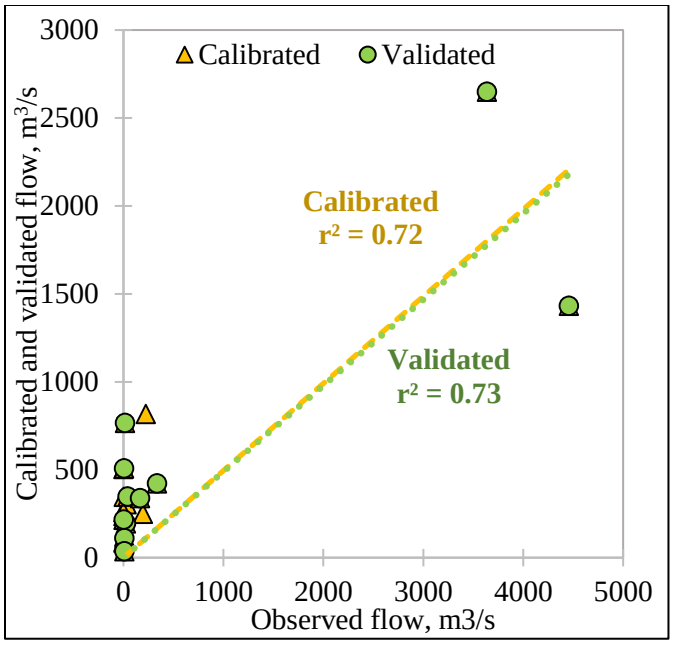

Figure II-8. Relationships between observed, calibrated, and validated flows.

3.2 Model calibration and validation for total nitrogen

From Figures II-9 and 10, it was observed that the NSE and r^2 for total nitrogen were found to be 0.80 and 0.63, respectively, during calibration. Calibration period was from January 2011 to May 2015 and validation period was from June 2015 to December 2018. During validation, the NSE and r^2 were 0.93 and 0.87, respectively. In both calibration and validation, the model showed "very good" performance ratings.

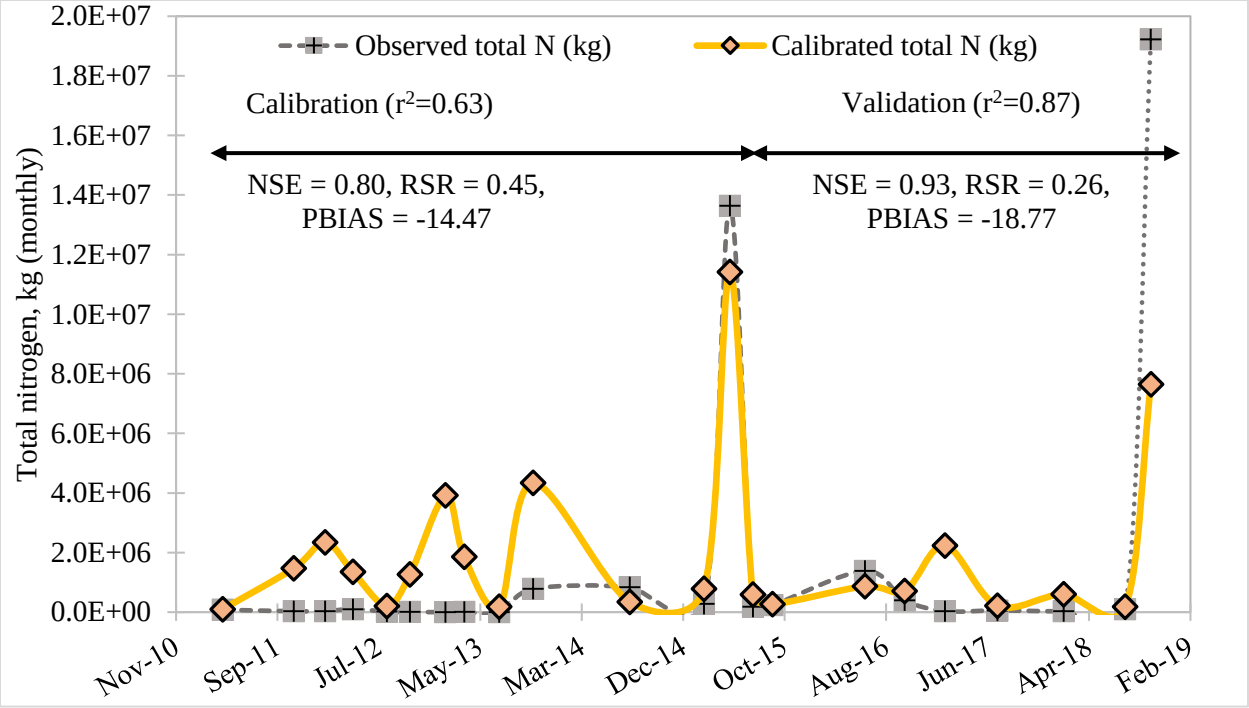

Figure II-9. Time series plot of observed and simulated total nitrogen.

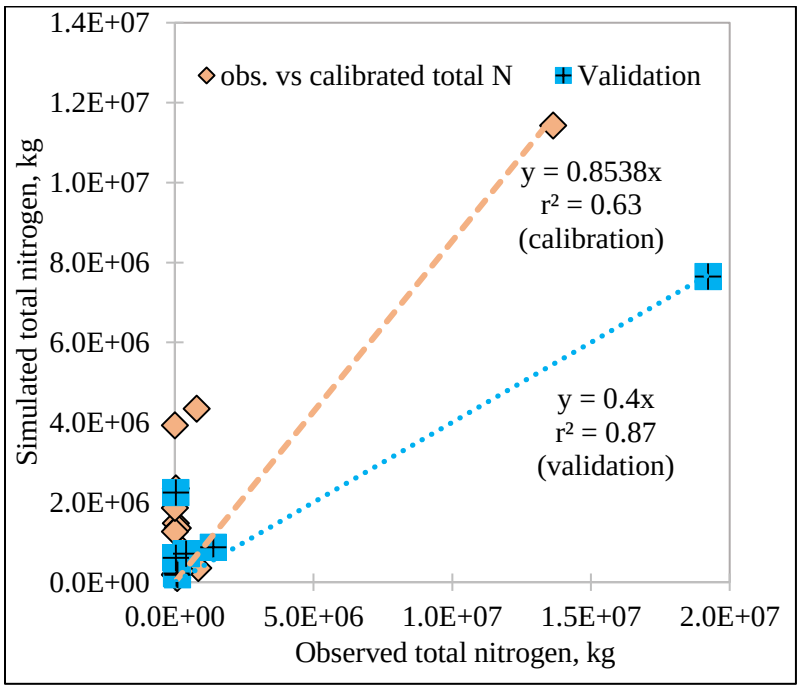

Figure II-10. Correlation between observed and simulated total nitrogen.

3.3 Effects of freshwater inflows on total nitrogen.

Figure II-11 shows the time series plot of freshwater inflows with simulated total nitrogen loading and total nitrogen concentration. The alternative grey areas in the plot mark the ‘wet’ and ‘dry’ seasons, where the lighter area represents ‘dry’ season and darker area represents the ‘wet’ season. It is observed that the total nitrogen loading increases with freshwater inflows. The total nitrogen concentration shows a seasonal variation where it increases during the ‘dry’ seasons and decreases during the ‘wet’ seasons.

Figure II-12 shows the time series plot of total nitrogen, total Kjeldahl nitrogen (TKN), inorganic nitrate and nitrite and dissolved oxygen. The alternate grey and light areas represent the wet and dry seasons as in Figure II-11. It is observed that the TKN concentration increases with increase in total nitrogen and total nitrogen constitutes mostly of TKN. Also, TKN is higher during dry seasons than during wet seasons. Dissolved oxygen varied from 6.5 to 9.0 mg/L and it increased during wet seasons and decreased during dry seasons, indicating oxygen demands during the dry seasons.

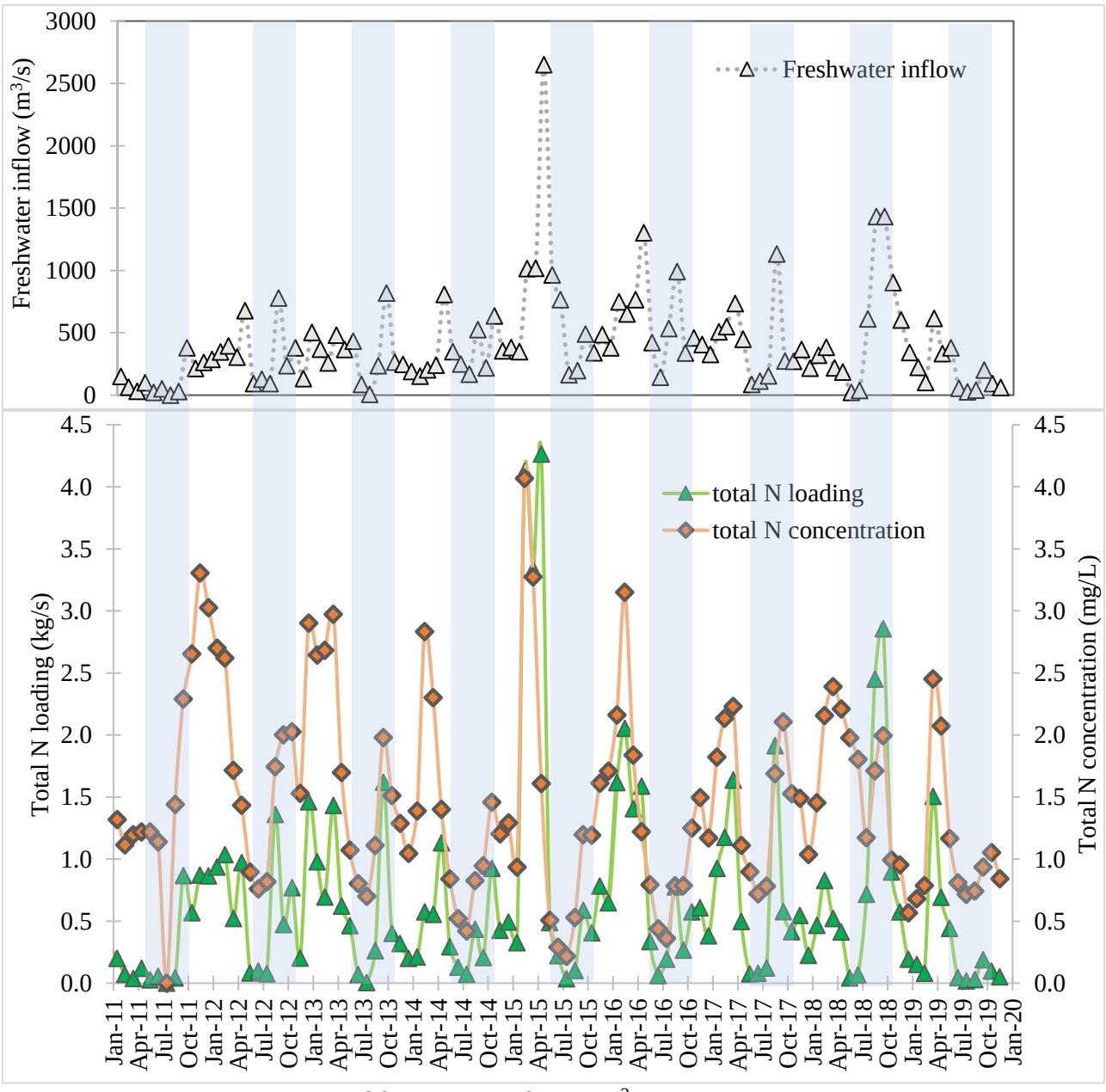

Figure II-11. Time series plot of freshwater inflows (m^3/s), total nitrogen loading (kg) and total nitrogen concentration (mg/L).

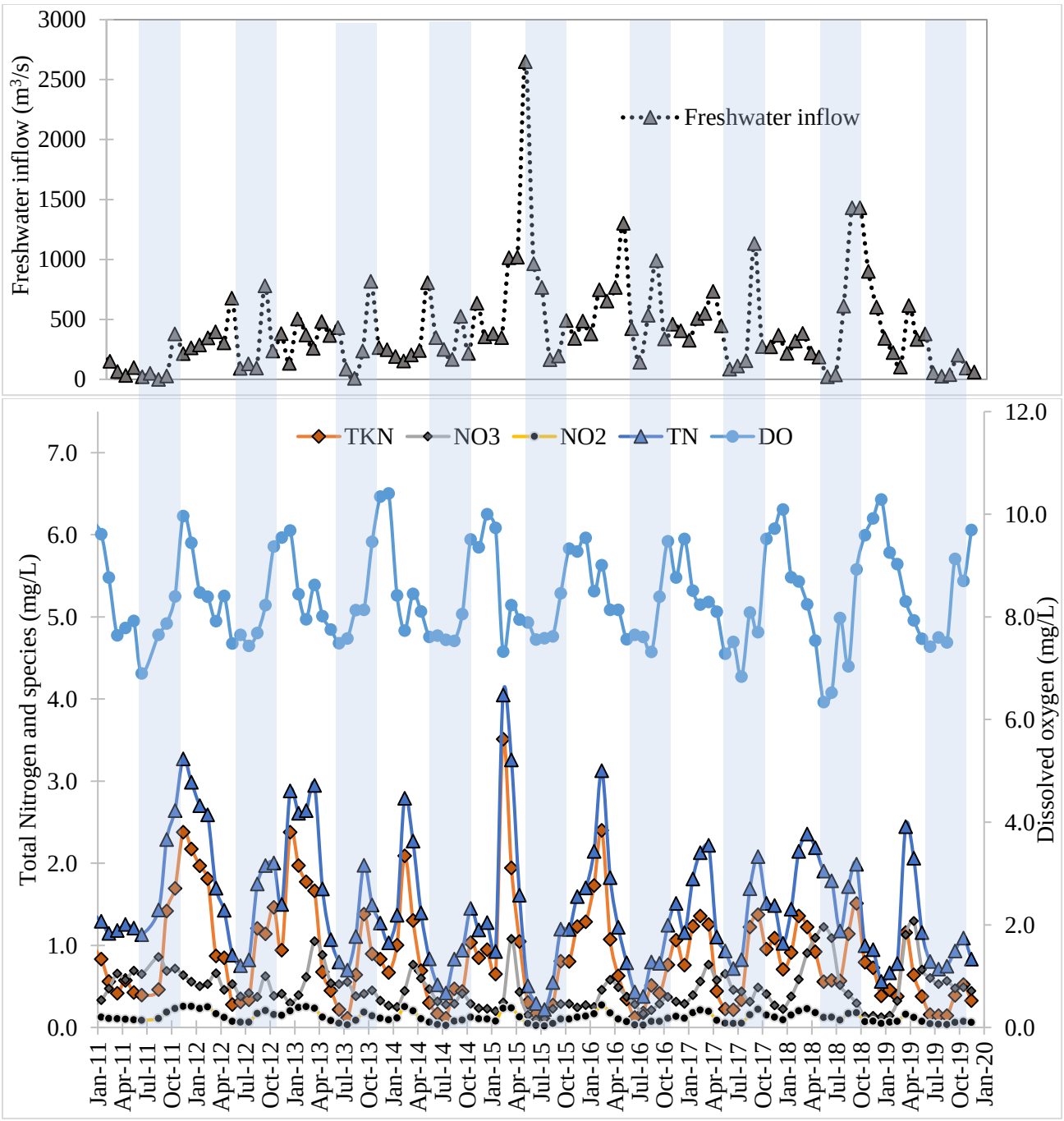

Figure II-12. Time series plot of freshwater inflows (m^3/s) and seasonal variation of dissolved oxygen (DO, mg/L), total nitrogen (mg/L), total Kjeldahl nitrogen (mg/L), inorganic nitrate and nitrite (mg/L).

Figure II-13 shows the time series plot of freshwater inflows, total Kjeldahl nitrogen (TKN) and inorganic nitrogen (nitrate + nitrite). The TKN and inorganic nitrogen are expressed as percentage of total nitrogen. Similar to Figures II-11 and II-12, the alternate grey and light areas

represent the dry and wet seasons. The two parts of total nitrogen, TKN and inorganic nitrogen, show seasonal variations in composition. During dry seasons, the TKN increases while the inorganic nitrogen decreases and vice-versa. Figure II-14 shows the relationship between freshwater inflows and TKN and inorganic nitrogen.

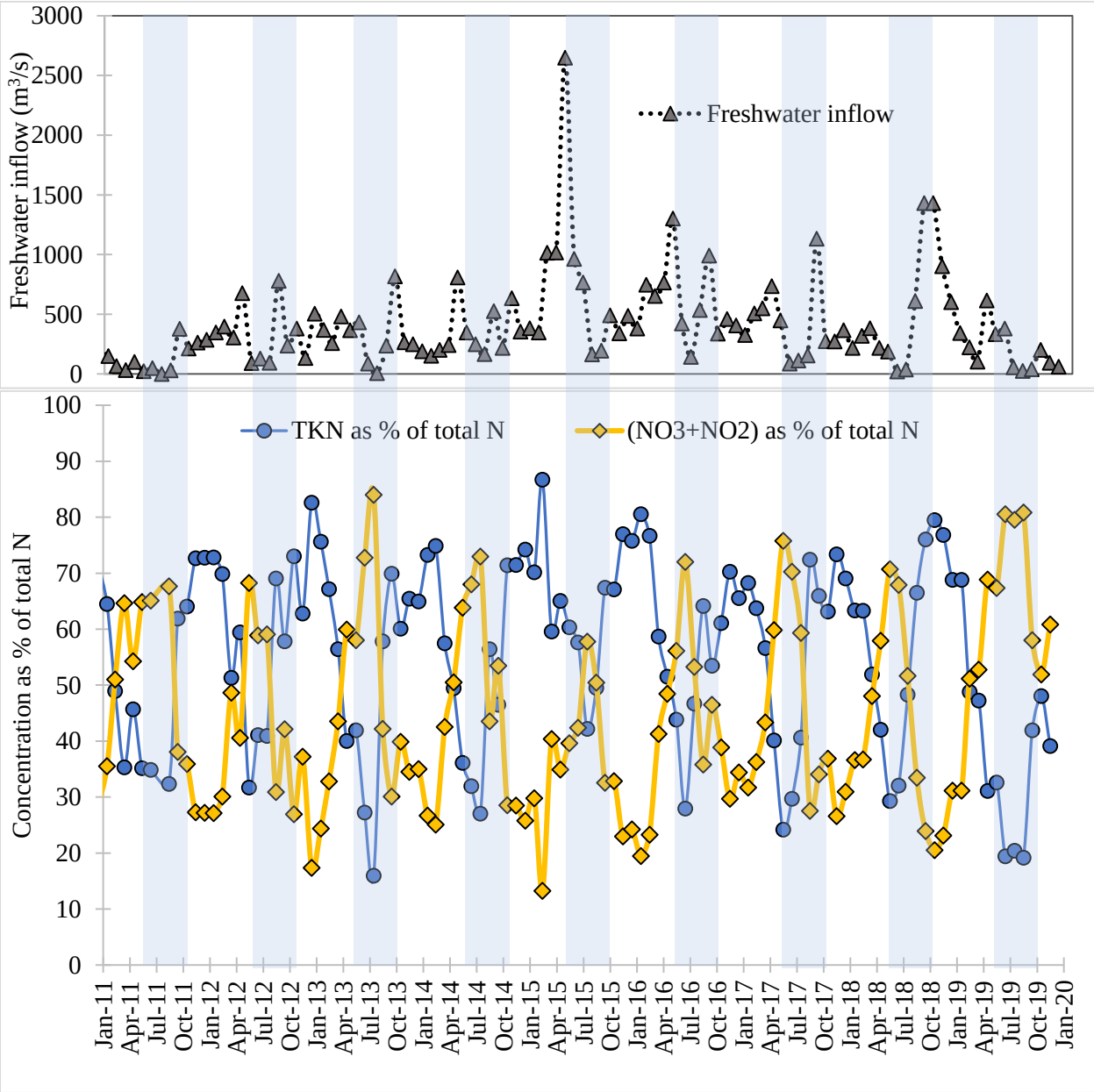

Figure II-13. Time series plot of freshwater inflows (m^3/s) and seasonal variation of total Kjeldahl nitrogen as percentage of total nitrogen and inorganic nitrogen (nitrate + nitrite) as percentage of total nitrogen.

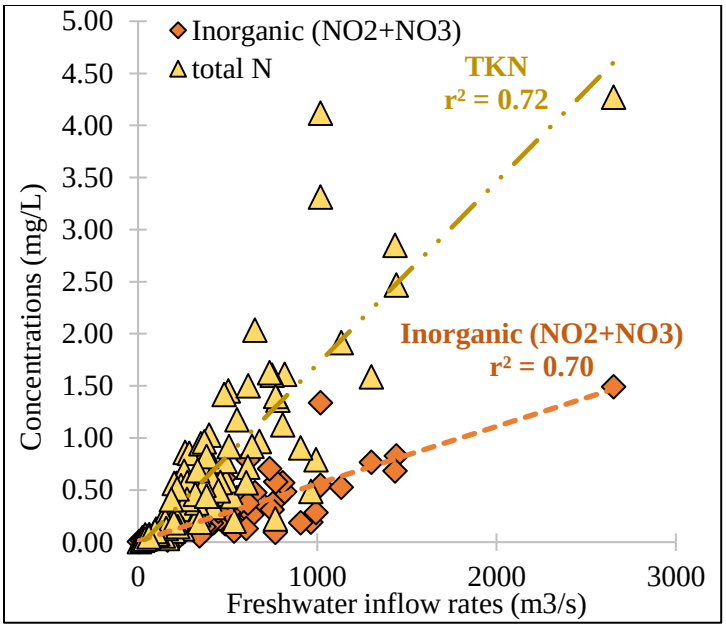

Figure II-14. Relationship between freshwater inflows and TKN and inorganic nitrogen.

3.4 Sensitivity analysis results for stream flow simulation

From global sensitivity analyses for average monthly flow, the parameters: SURLAG (surface runoff lag coefficient), GWQMN (ground water discharge minimum) and SOL_K (saturated hydraulic conductivity) were found to be most sensitive (Table II-3).

Table II-3. Global sensitivity analysis for flow.

	Flow	Global Sensitivity	
Rank	Parameters	t-Stat	p-value
1	SURLAG.bsn	1.8291	0.1006
2	GWQMN.gw	-1.7909	0.1069
3	SOL_K(..).sol	1.5415	0.1576
4	OV_N.hru	-1.4032	0.1941
5	CN2.mgt	1.3890	0.1982
6	ALPHA_BF.gw	1.3745	0.2025
7	EPCO.bsn	-1.1108	0.2954
8	SOL_AWC(..).sol	0.9807	0.3524
9	ESCO.bsn	0.8595	0.4124
10	GW_DELAY.gw	0.6810	0.5130

From local sensitivity analyses (Table II-4) for average monthly flow, the parameters: CN2 (SCS runoff curve number), OV_n (Manning's n value for overland flow) and AWC (available water capacity of the soil layer) were found to be most sensitive (Table II-4).

Table II-4. Sensitivity analysis for flow.

	Flow	Local Sensitivity	
Rank	Parameters	avg. S	% S
1	CN2	1.02E+00	67.18
2	OV_n	3.06E-01	20.13
3	AWC	1.36E-01	8.93
4	SOL_K	5.33E-02	3.50
5	GW_DELAY	2.00E-03	0.13
6	GWQMN	1.91E-03	0.13
7	ESCO	2.15E-05	0.00
8	EPCO	1.89E-05	0.00
9	ALPHA_BF	1.89E-05	0.00
10	SURLAG	1.89E-05	0.00

3.5 Sensitivity analysis results for total nitrogen simulation

From global sensitivity and local sensitivity analysis (Tables II-5 and 6) for average monthly total nitrogen, the parameter NPERCO (nitrate, as nitrogen, percolation coefficient) was found to be the most sensitive (Tables II-5 and 6).

Table II-5. Global sensitivity analysis for total nitrogen.

	Total Nitrogen	Global Sensitivity	
Rank	Parameters	t-Stat	P-Value
1	NPERCO.bsn	8.02455	0.00002
2	RSDCO.bsn	-1.34127	0.21270
3	BC3.swq	0.46042	0.65614
4	CMN.bsn	0.44794	0.66479
5	RCN.bsn	0.43546	0.67348
6	BC4.swq	-0.41508	0.68780
7	N_UPDIS.bsn	0.37777	0.71436
8	CDN.bsn	0.09044	0.92992
9	BC1.swq	0.07140	0.94464
10	BC2.swq	-0.01220	0.99053

Table II-6. Local sensitivity analysis for total nitrogen.

	Total Nitrogen	Local Sensitivity	
Rank	Parameters	Sum S	% S
1	NPERCO	6.04E-03	41.98
2	N_UPDIS	5.80E-03	40.29
3	CDN	2.16E-03	14.98
4	BC2	1.73E-04	1.20
5	RSDCO	3.68E-05	0.26
6	BC2	3.68E-05	0.26
7	CMN	3.68E-05	0.26
8	RCN	3.68E-05	0.26
9	BC3	3.68E-05	0.26
10	BC4	3.68E-05	0.26

4. SUMMARY OF FINDINGS

The surface runoff (CN2, SURLAG) and overland Manning's coefficient for flow (OV_n) were found to be the most sensitive parameters for the streamflow simulations. Nitrogen uptake, denitrification, nitrogen percolation and residual nitrogen coefficients (NUPDIS, CDN, NPERCO and RSDCO) are the most sensitive parameters for nitrogen loads. Total nitrogen transported through Nueces River increases with total freshwater flow and vice versa (r^2 = 0.72). From September to February (dry season), proportion of TKN increased and inorganic (NO_3^-+NO_2^-) decreased, and the converse is true during wet season. Total nitrogen and inorganic (NO_2^-+NO_3^-) nitrogen increased with freshwater inflows (r^2 = 0.72 and 0.70, respectively). The dissolved oxygen increased during wet seasons while it decreased during the dry seasons.

PART III. PUBLIC EDUCATION AND OUTREACH

Due to COVID-19, public education and outreach activities were limited. The following is a summary of the activities conduced:

1) Presentations at the professional conferences:

   Two presentations were conducted at the AWRA 2020 Geospatial Water Technology Conference in August 2020. One focused on the SWAT model and one focused on the Delft3D model. The details are:

   - Rony, S.M.S.M., J. Ren, T. Sinha, E. Buskey, and T. Lynn, Nitrogen Loading and its Relationship to Freshwater Inflows and Algal "Blooms" from a Large Semi-Arid Watershed: A Modeling Study, AWRA 2020 Geospatial Water Technology Conference on "Complex Systems.", Austin, Texas, August 4-13, 2020.
   - Rony, S.M.S.M., J. Ren, E. Buskey, T. Sinha, and T. Lynn, Modeling Nutrient and Algal Blooms Dynamics in Coastal Bays: A Case Study of Nueces Bay, Texas, AWRA 2020 Geospatial Water Technology Conference on "Complex Systems.", Austin, Texas, August 4-13, 2020.

2) A 2-minute video for K-12 outreach was prepared. This short video will be posted in social media through TAMUK Department of Environmental Engineering.

3) A recorded presentation about Part I of the project will be distributed through the South Texas Water Center group, which includes representatives from academic institutions, government agencies, regional/local communities, private industries, and NGOs in the South Texas region. The presentation video will also be posted on the Water Center website at http://www.tamuk.edu/engineering/departments/even/research/watercenter.html.

Part IV. SUMMARY OF FUTURE WORKS AND RECOMMENDATIONS

1. The NB Delft3D model could be improved if more data, for example, nutrients and chlorophyll-a, were available at a finer temporal resolution, especially before, during and after algal blooms. Also, data at different points of Nueces Bay and Corpus Christi Bay could help further refine the model in both space and time.
2. Remote sensing for collecting continuous data of water quality and inflows and integrating the data with online models can be developed and/or implemented to obtain real time status of algal concentrations and other parameters of water quality needed in the model simulation.
3. Since wave development in Nueces Bay is dominated by wind, wind and wave data can be collected for future model calibration and validation at different points and regions within the Nueces Bay.
4. The current NB Delft3D model focused on the overall production of the phytoplankton biomass, thus, different algal species were not investigated. Since toxins are released by certain species, which are often the dominant ones during an HABs, investigating algal species growth during HABs and species responsible for toxin releases would provide further understanding of the algal blooms.
5. Freshwater inflows from Nueces River to Nueces Bay, not only bring in nutrients from Nueces River Basin, but also transport sediments. Since morphology and sediment transport were not included in the current model, nutrients transported through sediments and associated with sediment depositions were not investigated. Study of sediment transport and nutrient transport through sediments can also unlock new knowledges for algal blooms.
6. An integrated model of the Nueces River Basin, Nueces Bay and Corpus Christi Bay would provide an in-depth insight of the nutrient transport and mechanisms of HABs.
7. The bathymetric data used in this study was collected in 2008. Updated bathymetry data will be needed to further reduce the model uncertainty.

ACKNOWLEDGEMENTS

This study would not have been possible without the funding by Texas General Land Office (Texas-GLO), Contract: 19-45-000-B079. The contribution of Siavash Bassam, Ph.D. candidate, Department of Environmental Engineering, TAMUK, to the second part of the study is unparallel. His meticulous modeling techniques and efforts resulted in a versatile model that was used as a basis to carry out the second part of the modeling work. The collaborative effort and coordination among the team members and the institutions, TAMUK and The University of Texas at Austin Marine Science Institute (UTMSI), have led to the successful completion of the project within its timelines.

REFERENCES

Abbaspour, K. C., Rouholahnejad, E., Vaghefi, S., Srinivasan, R., Yang, H., & Kløve, B. (2015a). A continental-scale hydrology and water quality model for Europe: Calibration and uncertainty of a high-resolution large-scale SWAT model. *Journal of Hydrology*, *524*, 733–752. https://doi.org/10.1016/j.jhydrol.2015.03.027

Abbaspour, K. C., Rouholahnejad, E., Vaghefi, S., Srinivasan, R., Yang, H., & Kløve, B. (2015b). A continental-scale hydrology and water quality model for Europe: Calibration and uncertainty of a high-resolution large-scale SWAT model. *Journal of Hydrology*, *524*, 733–752. https://doi.org/10.1016/j.jhydrol.2015.03.027

Alexandratos, N. (2012). *World Agriculture towards 2030/2050: The 2012 revision*. 154.

Alosairi, Y., & Alsulaiman, N. (2019). Hydro-environmental processes governing the formation of hypoxic parcels in an inverse estuarine water body: Model validation and discussion. *Marine Pollution Bulletin*, *144*, 92–104. https://doi.org/10.1016/j.marpolbul.2019.04.067

Anderson, A. A. (1960). Marine resources of the Corpus christi are. Austin: Bureau of Business Research. *The University of Texas*, *21*, 1–49.

Arnold, J. R., Neitsch, S. L., Kiniry, J. R., & Williams, J. R. (2011). *Swat2009-theoritical-documentations.pdf*. Texas Water Resources Institute.

Bassam, S., & Ren, J. (2018). *A Decision Support Modeling System for Managing the Water Resources around the Region of Choke Canyon Reservoir of the Nueces River Basin. A Report on integrated SWAT-MODFLOW Model System.* (Contract No. 15-0101). City of Corpus Christi.

Bastidas, L. A., Knighton, J., & Kline, S. W. (2015). *Parameter sensitivity and uncertainty analysis for a storm surge and wave model 2197*. https://doi.org/10.5194/nhessd-3-6491-2015

Begin, R., Cluis, D., Couture, R., & Visser, S. A. (1988). Potential eutrophication assessment in rivers; relationship between produced and exported loads. *Schweiz. Z. Hydrology*, *50*, 166–181.

Blevins, D. W. (1997). *Hydrology and Cycling of Nitrogen and Phosphorus in Little Bean Marsh: A Remnant Riparian Wetland along the Missouri River in Platte County, Missouri, 1996-97*. 87.

Bouws, E., & Komen, G. (1983). On the Balance Between Growth and Dissipation in an Extreme Depth-Limited Wind-Sea in the Southern North Sea. *Journal of Physical Oceanography - J PHYS OCEANOGR*, *13*, 1653–1658. https://doi.org/10.1175/1520-0485(1983)013<1653:OTBBGA>2.0.CO;2

Bowman, W. D., Cleveland, C. C., Halada, Ĺ., Hreško, J., & Baron, J. S. (2008). Negative impact of nitrogen deposition on soil buffering capacity. *Nature Geoscience*, *1*(11), 767–770. https://doi.org/10.1038/ngeo339

Bricker, S. B., Clement, C. G., & Pirhalla, D. E. (1999). National Estuarine Eutrophication Assessment: Effects of Nutrient Enrichment in the Nation's Estuaries. *NOAA*, 84.

Brock, D. A. (2001). *Nitrogen budget for low and high freshwater inflows, Nueces Estuary, Texas | SpringerLink*. https://link.springer.com/article/10.2307/1353253

Broomans. (2003). *Numerical Accuracy in Solutions of the Shallow-Water Equations*. 101.

Brouziyne, Y., Abouabdillah, A., Bouabid, R., Benaabidate, L., & Oueslati, O. (2017). SWAT manual calibration and parameters sensitivity analysis in a semi-arid watershed in North-

western Morocco. *Arabian Journal of Geosciences*, *10*(19), 427. https://doi.org/10.1007/s12517-017-3220-9

Buskey, E. J. (1993). Annual pattern of micro- and mesozooplankton abundance and biomass in a subtropical estuary. *Journal of Plankton Research*, *15*(8), 907–924. https://doi.org/10.1093/plankt/15.8.907

Buskey, E. J. (1998). *Current Status and Historical Trends of Brown Tide and Red Tide Phytoplankton Blooms in the Corpus Christi Bay National Estuary Program Study Area Corpus*.

Cao, P., Lu, C., & Yu, Z. (2018). Historical nitrogen fertilizer use in agricultural ecosystems of the contiguous United States during 1850–2015: Application rate, timing, and fertilizer types. *Earth System Science Data*, *10*(2), 969–984. https://doi.org/10.5194/essd-10-969-2018

Chai, Z. Y., Wang, H., Deng, Y., Hu, Z., & Zhong Tang, Y. (2020). Harmful algal blooms significantly reduce the resource use efficiency in a coastal plankton community. *Science of The Total Environment*, *704*, 135381. https://doi.org/10.1016/j.scitotenv.2019.135381

Chen, Huang, P., & Zhang, Z. (2019). Interaction between carbon dioxide emissions and eutrophication in a drinking water reservoir: A three-dimensional ecological modeling approach. *Science of The Total Environment*, *663*, 369–379. https://doi.org/10.1016/j.scitotenv.2019.01.336

Chen, & Mynett, A. E. (2006). Modelling algal blooms in the Dutch coastal waters by integrated numerical and fuzzy cellular automata approaches. *Ecological Modelling*, *199*(1), 73–81. https://doi.org/10.1016/j.ecolmodel.2006.06.014

Chu, T. W., & Shirmohammadi, A. (2004). Evaluation of the SWAT model's hydrology component in the piedmont physiographic region of Maryland. *Transactions of the ASAE*, *47*((4)), 1057–1073.

Ciampitti, I. A., & Vyn, T. J. (2014). Understanding Global and Historical Nutrient Use Efficiencies for Closing Maize Yield Gaps. *Agronomy Journal*, *106*(6), AGJ2AGRONJ140025. https://doi.org/10.2134/agronj14.0025

Cira, E. K., & Wetz, M. S. (2019). Spatial-temporal distribution of Aureoumbra lagunensis ("brown tide") in Baffin Bay, Texas. *Harmful Algae*, *89*, 101669. https://doi.org/10.1016/j.hal.2019.101669

Cunningham, A. M. (1999). *Corpus Christi water supply:documented history 1852-1997, 2nd ed. Corpus Christi (TX)*. Texas A&M University - Corpus Christi.

Deltare, N. (2018). *Delft3D-FLOW User Manual*. 694.

Deltares. (2018a). *D-Water_Quality_Processes_Technical_Reference_Manual.pdf*.

Deltares. (2018b). *Delft3D-WAVE User Manual*. 214.

Deltares, N. (2016). *Archive 2016*. TU Delft. https://www.tudelft.nl/en/eemcs/the-faculty/departments/applied-mathematics/applied-probability/events/seminars/archive-2016/

Deltares, N. (2018c). *D-Water_Quality_User_Manual.pdf*. Deltares.

Dingemans, M. W. (1997). Water Wave Propagation over Uneven Bottoms. *World Scientific*, *13*(Vol 1 & 2).

Dodds, W. K., Bouska, W. W., Eitzmann, J. L., Pilger, T. J., Pitts, K. L., Riley, A. J., Schloesser, J. T., & Thornbrugh, D. J. (2009). Eutrophication of U.S. Freshwaters: Analysis of

Potential Economic Damages. *Environmental Science & Technology*, *43*(1), 12–19. https://doi.org/10.1021/es801217q

EPA. (2000). *Nutrient Criteria Technical Guidance Manual: Rivers and Streams*. 253.

EPA. (2015). *Nutrient-economics-report-2015.pdf*. EPA.

Fasham, M. J. R., Ducklow H.W, H. W., & McKelvie, S. M. (1990). A nitrogen-based model of plankton dynamics in the oceanic mixed layer. *Journal of Marine Research*, *48*, 591–639.

Felip, M., & Catalan, J. (2000). The relationship between phytoplankton biovolume and chlorophyll in a deep oligotrophic lake: Decoupling in their spatial and temporal maxima. *Journal of Plankton Research*, *22*(1), 91–106. https://doi.org/10.1093/plankt/22.1.91

Ferreira, J. G., Andersen, J. H., Borja, A., Bricker, S. B., & Camp, J. (2011). Overview of eutrophication indicators to assess environmental status within the European Marine Strategy Gramework Directive. *Estuarine, Coastal and Shelf Science, 93(2)*, 117–131. https://doi.org/10.1016

Fondriest. (2014, October). *Algae, Phytoplankton and Chlorophyll*. Environmental Measurement Systems. https://www.fondriest.com/environmental-measurements/parameters/water-quality/algae-phytoplankton-chlorophyll/

Garcia, M., Ramirez, I., Verlaan, M., & Castillo, J. (2015). Application of a three-dimensional hydrodynamic model for San Quintin Bay, B.C., Mexico. Validation and calibration using OpenDA. *Journal of Computational and Applied Mathematics*, *273*, 428–437. https://doi.org/10.1016/j.cam.2014.05.003

Glé, C., Del Amo, Y., Sautour, B., Laborde, P., & Chardy, P. (2008). Variability of nutrients and phytoplankton primary production in a shallow macrotidal coastal ecosystem (Arcachon

Bay, France). *Estuarine, Coastal and Shelf Science*, *76*(3), 642–656. https://doi.org/10.1016/j.ecss.2007.07.043

Griffith, A. W., & Gobler, C. J. (2019). Harmful algal blooms: A climate change co-stressor in marine and freshwater ecosystems. *Harmful Algae*, 101590. https://doi.org/10.1016/j.hal.2019.03.008

Gupta, H. V., Sorooshian, S., & Yapo, P. O. (1999). Status of automatic calibration for hydrologic models: Comparison with multilevel expert calibration. *Journal of Hydrology*, *192*((1)), 81–103.

Hasselmann, K., Barnett, T. P., Bouws, E., & Carlson, H. (1973). Measurements of wind-wave growth and swell decay during the Joint North Sea Wave Project (JONSWAP). *Deutsche Hydrographische Zeitschrift*, *8*(12). https://repository.tudelft.nl/islandora/object/uuid%3Af204e188-13b9-49d8-a6dc-4fb7c20562fc

Hill, E. M., Nicolau, B. A., & Zimba, P. V. (2011). History-of-Water-and-Habitat-Improvement-in-the-Nueces-Estuary-Texas-USA.pdf. *Texas Water Resource Institute*, *2*, 97–111.

"Hurricanes." World Book Encyclopedia. (Vols. 452-456.). (1998). Chicago, IL: World Book, 1998.

Islam, M. s, Bonner, J., Edge, B., & Page, C. (2014). Hydrodynamic characterization of Corpus Christi Bay through modeling and observation. *Environmental Monitoring and Assessment*, *186*. https://doi.org/10.1007/s10661-014-3973-5

Janssen, A. B., Janse, J. H., Beusen, A. H., Chang, M., Harrison, J. A., Huttunen, I., Kong, X., Rost, J., Teurlincx, S., Troost, T. A., van Wijk, D., & Mooij, W. M. (2019). How to

model algal blooms in any lake on earth. *Current Opinion in Environmental Sustainability*, *36*, 1–10. https://doi.org/10.1016/j.cosust.2018.09.001

Jian, L., Zhongwu, J., & Wenjun, Y. (2014). Numerical modeling of the Xiangxi River algal bloom and sediment-related process in China. *Ecological Informatics*, *22*, 23–35. https://doi.org/10.1016/j.ecoinf.2014.03.002

Jones, G., Wortberg, M., Kreissig, S. B., Hammock, B. D., & Rocke, D. M. (1996). Application of the Bootstrap to Calibration Experiments. *Analytical Chemistry*, *68*(5), 763–770. https://doi.org/10.1021/ac950985g

Jung, C.-G., & Kim, S.-J. (2017). SWAT Modeling of Nitrogen Dynamics Considering Atmospheric Deposition and Nitrogen Fixation in a Watershed Scale. *Agricultural Sciences*, *08*(04), 326–340. https://doi.org/10.4236/as.2017.84024

Katin, A., Del Giudice, D., & Obenour, D. R. (2019). Modeling biophysical controls on hypoxia in a shallow estuary using a Bayesian mechanistic approach. *Environmental Modelling & Software*, *120*, 104491. https://doi.org/10.1016/j.envsoft.2019.07.016

Khan, F. A., & Ansari, A. A. (2005). Eutrophication: An Ecological Vision. *The Botanical Review*, *71*(4), 449–482. https://doi.org/10.1663/0006-8101(2005)071[0449:EAEV]2.0.CO;2

Kiedrzyńska, E., Kiedrzyński, M., Urbaniak, M., Magnuszewski, A., Skłodowski, M., Wyrwicka, A., & Zalewski, M. (2014). Point sources of nutrient pollution in the lowland river catchment in the context of the Baltic Sea eutrophication. *Ecological Engineering*, *70*, 337–348. https://doi.org/10.1016/j.ecoleng.2014.06.010

Kim, H.-C., & Montagna, P. A. (2012). Effects of climate-driven freshwater inflow variability on macrobenthic secondary production in Texas lagoonal estuaries: A modeling study. *Ecological Modelling*, *235–236*, 67–80. https://doi.org/10.1016/j.ecolmodel.2012.03.022

Kingsford, R. (2000). Ecological impacts of dam, water diversions and river management of floodplain wetlands in Australia. *Austral Ecology*, *252(2)*, 109–127.

Kristin, K. A. (2011). Seasonal and interannual effects of hypoxia on fish habitat quality in central Lake Erie. *Freshwater Biology*, *56*(2). https://doi.org/10.1111

Kumar, Kumaraswami, M., Rao, G. D., Ezhilarasan, P., Sivasankar, R., Rao, V. R., & Ramu, K. (2018). Influence of nutrient fluxes on phytoplankton community and harmful algal blooms along the coastal waters of southeastern Arabian Sea. *Continental Shelf Research*, *161*, 20–28. https://doi.org/10.1016/j.csr.2018.04.012

Lee, G., Kim, W., Oh, H., Youn, B. D., & Kim, N. H. (2019). Review of statistical model calibration and validation—From the perspective of uncertainty structures. *Structural and Multidisciplinary Optimization*, *60*(4), 1619–1644. https://doi.org/10.1007/s00158-019-02270-2

Levy, D. (2020). *Mitigating Harmful Algal Blooms*. AWRA Annual Water Resources Conference. https://www.conferenceharvester.com/uploads/harvester/VirtualBooths/13668/WSOIXHXG-PDF-1-421743.pdf

Li, Z., Chen, Q., & Xu, Q. (2015). Modeling algae dynamics in Meiliang Bay of Taihu Lake and parameter sensitivity analysis. *Journal of Hydro-Environment Research*, *9*(2), 216–225. https://doi.org/10.1016/j.jher.2014.10.001

Longley. (1994). *FreshwaterInflows- Ecological Relationships and Methods for Determination of Needs—1994.pdf*.

Longley, K. R., Huang, W., Clark, C., & Johnson, E. (2019). Effects of nutrient load from St. Jones River on water quality and eutrophication in Lake George, Florida. *Limnologica*, *77*, 125687. https://doi.org/10.1016/j.limno.2019.125687

Luijendijk, A. (2001). *Validation, calibration and evaluation of a Delft3D-FLOW model with ferry measurements*. 93.

Lung, W.-S., & Paerl, H. W. (1988). Modeling blue-green algal blooms in the lower neuse river. *Water Research*, *22*(7), 895–905. https://doi.org/10.1016/0043-1354(88)90027-9

Magaña, H. A., Contreras, C., & Villareal, T. A. (2003). A historical assessment of Karenia brevis in the western Gulf of Mexico. *Harmful Algae*, *2*(3), 163–171. https://doi.org/10.1016/S1568-9883(03)00026-X

Mao, J., Jiang, D., & Dai, H. (2015). Spatial–temporal hydrodynamic and algal bloom modelling analysis of a reservoir tributary embayment. *Journal of Hydro-Environment Research*, *9*(2), 200–215. https://doi.org/10.1016/j.jher.2014.09.005

Mei, C. (1983). *The applied dynamics of ocean surface waves*. Wiley.

Moriasi, D. N., J. G. Arnold, M. W. Van Liew, R. L. Bingner, R. D. Harmel, & T. L. Veith. (2007). Model Evaluation Guidelines for Systematic Quantification of Accuracy in Watershed Simulations. *Transactions of the ASABE*, *50*(3), 885–900. https://doi.org/10.13031/2013.23153

Murgulet, D., Murgulet, V., Spalt, N., Douglas, A., & Hay, R. G. (2016). Impact of hydrological alterations on river-groundwater exchange and water quality in a semi-arid area: Nueces

River, Texas. *Science of The Total Environment*, *572*, 595–607. https://doi.org/10.1016/j.scitotenv.2016.07.198

Nash, J. E., & Sutcliffe, J. V. (1970). River flow forecasting through conceptual models: Part 1. A discussion of principles. *Journal of Hydrology*, *10*(3), 282–290.

NOAA. (2016). *What is a harmful algal bloom? | National Oceanic and Atmospheric Administration*. https://www.noaa.gov/what-is-harmful-algal-bloom

NOAA. (2019). *Harmonic Constituents—NOAA Tides & Currents.pdf*.

Novotny, V. (1994). Water Quality: Prevention, Identification and Management of Diffuse Pollution. *NY: Van Nostrand-Reinhold Publishers*.

O'Neil, J. M. (2011). International Journal on Algae. *Begell House*. https://doi.org/10.1016

Paudel, B., Montagna, P. A., & Adams, L. (2019). The relationship between suspended solids and nutrients with variable hydrologic flow regimes. *Regional Studies in Marine Science*, *29*, 100657. https://doi.org/10.1016/j.rsma.2019.100657

Powell, G. L., Matsumoto, J., & Brock, D. A. (2002). Methods for determining minimum freshwater inflow needs of Texas bays and estuaries. *Estuaries*, *25*(6), 1262–1274. https://doi.org/10.1007/BF02692223

Powley, H. R., Cappellen, P. V., & Krom, M. D. (2017a). Nutrient Cycling in the Mediterranean Sea: The Key to Understanding How the Unique Marine Ecosystem Functions and Responds to Anthropogenic Pressures. In B. Fuerst-Bjelis (Ed.), *Mediterranean Identities—Environment, Society, Culture*. InTech. https://doi.org/10.5772/intechopen.70878

Powley, H. R., Cappellen, P. V., & Krom, M. D. (2017b). Nutrient Cycling in the Mediterranean Sea: The Key to Understanding How the Unique Marine Ecosystem Functions and

Responds to Anthropogenic Pressures. In B. Fuerst-Bjelis (Ed.), *Mediterranean Identities—Environment, Society, Culture*. InTech. https://doi.org/10.5772/intechopen.70878

Rahman, A., & Venugopal, V. (2017). Parametric analysis of three dimensional flow models applied to tidal energy sites in Scotland. *Estuarine, Coastal and Shelf Science, 189*, 17–32. https://doi.org/10.1016/j.ecss.2017.02.027

Raven, J. A., Gobler, C. J., & Hansen, P. J. (2020). Dynamic CO2 and pH levels in coastal, estuarine, and inland waters: Theoretical and observed effects on harmful algal blooms. *Harmful Algae, 91*, 101594. https://doi.org/10.1016/j.hal.2019.03.012

Rebich, R. A., Houston, N. A., Mize, S. V., Pearson, D. K., Ging, P. B., & Evan Hornig, C. (2011). Sources and Delivery of Nutrients to the Northwestern Gulf of Mexico from Streams in the South-Central United States. *Journal of the American Water Resources Association, 47*(5), 1061–1086. https://doi.org/10.1111/j.1752-1688.2011.00583.x

Ritter, C. (2005). Short-term succession dynamics of macrobenthos in a salinity-stressed estuary. *Journal of Experimental Marine Biology and Ecology, 323)1)*, 57–69. https://doi.org/323(1) : 57-69

Ritter, & Montagna, P. A. (1999). Seasonal hypoxia and models of benthic response in a Texas Bay. *Estuaries*, *22*(1), 7–20. https://doi.org/10.2307/1352922

Roelke, D. L., Cifuentes, L. A., & Eldridge, P. M. (1997). Nutrient and Phytoplankton Dynamics in a Sewage-Impacted Gulf Coast Estuary: A Field Test of the PEG-Model and Equilibrium Resource Competition Theory. *Estuaries, 20*(4), 725. https://doi.org/10.2307/1352247

Roelvink, J. A., & Banning, G. K. F. M. V. (1995). Design and development of DELFT3D and application to coastal morphodynamics. *Oceanographic Literature Review*, *11*(42), 925.

Ruddy, B. C., Lorenz, D. L., & Muller, D. K. (2006). *Country-level estimates of nutrient inputs to the land surface of the conterminous United States, 1982-2001* (No. 2006–5012; p. 17).

Santhi, C., Arnold, J. R., Williams, J. R., Dugas, A., Srinivasan, R., & Hauck, L. M. (2001). Validation of the SWAT model on a large river basin with point and nonpoint sources. *J. American Water Resources Association*, *37(5)*, 1169–1188.

Schindler, D. W. (1974). Eutrophication and recovery in experimental lakes: Implications for lake management. *Science*, 897–899.

Schladow, S. G., & Hamilton, D. P. (1997). Prediction of water quality in lakes and reservoirs: PartII - Model calibration, sensitivity analysis and application. *Ecological Modelling*, *96*, 111–123.

Schoenbaechler, C., & Guthrie, C. (2011). *TWDB_TxBLEND_Nueces_20110726.pdf* (Bays and Estuaries Program Surface Water Resources Division). Texas Water Development Board.

Sheldon, J. E., & Alber, M. (2011). *RECOMMENDED INDICATORS OF ESTUARINE WATER QUALITY FOR GEORGIA*. 6.

Shen, J., Qin, Q., Wang, Y., & Sisson, M. (2019). A data-driven modeling approach for simulating algal blooms in the tidal freshwater of James River in response to riverine nutrient loading. *Ecological Modelling*, *398*, 44–54. https://doi.org/10.1016/j.ecolmodel.2019.02.005

Singh, J., Knapp, V., & Demissie, M. (2004). Hydrologic modeling of the Iroquois River waterhsed using HSPF and SWAT. *ISWS CR 2004-08, Champaign, III: Illinoi State Water Survey*. www.sws.uiuc.edu/pubdoc/CR/ ISWSCR2004-08.pdf

Smayda, T. J. (1997). What is a bloom? A commentary. *Limnology and Oceanography*, *42*(5part2), 1132–1136. https://doi.org/10.4319/lo.1997.42.5_part_2.1132

Smil, V. (1999). Nitrogen in Crop production: An account of global flows. *Global Biogeochemistry Cy.*, *13*, 647–662.

Smith, V. H. (2003). Eutrophication of freshwater and coastal marine ecosystems a global problem. *Environmental Science and Pollution Research*, *10*(2), 126–139. https://doi.org/10.1065/espr2002.12.142

Steele, J. H., & Henderson, E. W. (1981). A simple plankton model. *American Naturalist*, *117*, 676–691.

Stewart, W. M., Dibb, D. W., Johnston, A. E., & Smyth, T. J. (2005). The Contribution of Commercial Fertilizer Nutrients to Food Production. *Agron J.*, *97*, 1–6.

TCEQ, T. 2014. (2014). *2012_303d.pdf*. https://www.tceq.texas.gov/assets/public/waterquality/swqm/assess/12twqi/2012_303d.pdf

Tian, R., Lin, Q., Li, D., Zhang, W., & Zhao, X. (2020). Atmospheric transport of nutrients during a harmful algal bloom event. *Regional Studies in Marine Science*, *34*, 101007. https://doi.org/10.1016/j.rsma.2019.101007

TPWD. (1974). *An analysis of Texas waterways. A report on the physical characteristics of rivers, streams and bayous in Texas*. Texas Parks and Wildlife Department.

TPWD. (2019a). *Red Tide Index*. https://tpwd.texas.gov/landwater/water/environconcerns/hab/redtide/

TPWD. (2019b). *Red Tide Index*. https://tpwd.texas.gov/landwater/water/environconcerns/hab/redtide/

Turner. (2014). *Modeling nutrient_coast_Turner_'14.pdf*.

Turner, & Chislock, M. F. (2010). Blinded by the stink: Nutrient enrichment impairs the perception of predation risk by freshwater snails. *Ecological Applications: A Publication of the Ecological Society of America*, *20*(8), 2089–2095. https://doi.org/10.1890/10-0208.1

Turner, E. L., Bruesewitz, D. A., Mooney, R. F., Montagna, P. A., McClelland, J. W., Sadovski, A., & Buskey, E. J. (2014). Comparing performance of five nutrient phytoplankton zooplankton (NPZ) models in coastal lagoons. *Ecological Modelling*, *277*, 13–26. https://doi.org/10.1016/j.ecolmodel.2014.01.007

Turner, E. L., Paudel, B., & Montagna, P. A. (2015). Baseline nutrient dynamics in shallow well mixed coastal lagoon with seasonal harmful algal blooms and hypoxia formation. *Marine Pollution Bulletin*, *96*(1–2), 456–462. https://doi.org/10.1016/j.marpolbul.2015.05.005

USGS. (2004). *Hydrology and Cycling of Nitrogen and Phosphorous in Little Bean Marsh: A Remnant Riparian Wetland along the Missouri River in Platte County, Missouri*. https://pubs.usgs.gov/sir/2004/5171/pdf/complete.pdf

Van-Liew, M. W., Vieth, T. L., & Arnold, J. G. (2007). Suitability of SWAT for the conservation effects assessment project: A comparison on USDA-ARS experimental watersheds. *Journal Og Hydrologic Engineering*, *12*(2), 173–189.

Vaz, L., Frankenbach, S., Serôdio, J., & Dias, J. M. (2019). New insights about the primary production dependence on abiotic factors: Ria de Aveiro case study. *Ecological Indicators*, *106*, 105555. https://doi.org/10.1016/j.ecolind.2019.105555

Vazquez-Amabile, G. G., & Engel, B. A. (2005). Use of SWAT to compute groundwater table depth and streamflow in the Muscatatuck River watershed. *Trans. ASAE*, *48*((3)), 991–1003.

Vybernaite-Lubiene, I., Zilius, M., Giordani, G., Petkuviene, J., Vaiciute, D., Bukaveckas, P. A., & Bartoli, M. (2017). Effect of algal blooms on retention of N, Si and P in Europe's largest coastal lagoon. *Estuarine, Coastal and Shelf Science*, *194*, 217–228. https://doi.org/10.1016/j.ecss.2017.06.020

Wang, Liang, B., Wu, G., & Borsje, B. W. (2019). Modeling the formation and migration of sand waves: The role of tidal forcing, sediment size and bed slope effects. *Continental Shelf Research*, *190*, 103986. https://doi.org/10.1016/j.csr.2019.103986

Wang, Wang, Y.-N., Dao, G.-H., Du, J.-S., Han, Y.-P., & Hu, H.-Y. (2020). Decade-long meteorological and water quality dynamics of northern Lake Dianchi and recommendations on algal bloom mitigation via key influencing factors identification. *Ecological Indicators*, *115*, 106425. https://doi.org/10.1016/j.ecolind.2020.106425

Wetz, M. S., Cira, E. K., Sterba-Boatwright, B., Montagna, P. A., Palmer, T. A., & Hayes, K. C. (2017). Exceptionally high organic nitrogen concentrations in a semi-arid South Texas estuary susceptible to brown tide blooms. *Estuarine, Coastal and Shelf Science*, *188*, 27–37. https://doi.org/10.1016/j.ecss.2017.02.001

WGS 84 / UTM zone 14N. (2020). https://georepository.com/crs_32614/WGS-84-UTM-zone-14N.html

Whitham, G. (1974). *Linear and Non-Linear Waves*. Wiley.

Wu, Y., & Chen, J. (2009). Simulation of nitrogen and phosphorus loads in the Dongjiang River basin in South China using SWAT. *Frontiers of Earth Science in China*, *3*(3), 273–278. https://doi.org/10.1007/s11707-009-0032-6

Xu, C., Zhang, J., Bi, X., Xu, Z., He, Y., & Gin, K. Y.-H. (2017). Developing an integrated 3D-hydrodynamic and emerging contaminant model for assessing water quality in a Yangtze Estuary Reservoir. *Chemosphere*, *188*, 218–230. https://doi.org/10.1016/j.chemosphere.2017.08.121

Xu, Zhang, J., Xu, Y., Ying, W., Wang, Y. P., Che, Z., & Zhu, Y. (2020). Analysis of the spatial and temporal sensitivities of key parameters in the SWAN model: An example using Chan-hom typhoon waves. *Estuarine, Coastal and Shelf Science*, *232*, 106489. https://doi.org/10.1016/j.ecss.2019.106489

Yamamoto, T., & Hatta, G. (2004). Pulsed nutrient supply as a factor inducing phytoplankton diversity. *Ecological Modelling*, *171*(3), 247–270. https://doi.org/10.1016/j.ecolmodel.2003.08.011

Zhang, Liang, J., Zeng, G., Tang, W., Lu, Y., Luo, Y., Xing, W., Tang, N., Ye, S., Li, X., & Huang, W. (2020). How climate change and eutrophication interact with microplastic pollution and sediment resuspension in shallow lakes: A review. *Science of The Total Environment*, *705*, 135979. https://doi.org/10.1016/j.scitotenv.2019.135979